The PHILOSOPHICAL MAGAZINE

FIRST PUBLISHED IN 1798

1 Eighth Series No. 2 February 1956

A Journal of Theoretical Experimental and Applied Physics

PRICE 15s. 0d.
Annual Subscription £8 0s. 0d. payable in advance

ALERE FLAMMAM.
Printed and Published by
TAYLOR & FRANCIS LTD.
RED LION COURT, FLEET STREET, LONDON, E.C.4

CONTENTS OF No. 2.

****All communications for the Philosophical Magazine should be addressed, post-paid, to the Editors, c/o Messrs. TAYLOR AND FRANCIS, LTD., Red Lion Court, Fleet Street, London, England.

XI. *The Origin of Fatigue Fracture in Copper*

By N. Thompson, N. Wadsworth* and N. Louat†
H. H. Wills Physical Laboratory, University of Bristol‡

[Received December 12, 1955]

Summary

The paper describes metallographic observations of the development of fatigue cracks in copper. The specimens (polycrystal and single crystals) were tested in push-pull at 1000 c.p.s. It was shown that the fatigue crack started in a slip band inside a single grain. An electropolishing technique showed changes in the character of the slip band after 5% of the life had expired. Cracks more than one grain long were present when half the life had expired. It was confirmed that the fatigue life could be increased by preventing access of oxygen to the surface. The bearing of these observations on the problem of the origin of a fatigue crack is discussed.

§ 1. Introduction

The fundamental problem of the nature of fatigue failure in metals may conveniently be divided into two parts—although the division between the two may prove to be somewhat nebulous. Firstly, we must ask by what process an alternating stress can give rise to a singularity in the medium which can be called a crack ; and, secondly, we must investigate the laws governing the growth of such a crack. The final stages of crack propagation are undoubtedly very rapid and are also accelerated and complicated by the accompanying macroscopic re-distribution of stress. This phase is of little fundamental interest. There is a growing body of evidence, however, that the rate of growth of a small crack may in fact be very small. A recent paper by Head (1953) has dealt with this question. To obtain further evidence on the matter, and to make the most useful kind of observation on the origin of the crack, it is clearly necessary to detect the incipient fatigue crack as early as possible. Ideally, one would like to observe the point at which the crack will form, before it has in fact appeared. It is possible to restrict the area of search by deliberately introducing local stress-raisers (e.g. notches or grooves) but in so doing the conditions are necessarily made non-representative.

In the experiments to be described in this paper, it was possible to single out a very few places on the surface of a specimen from which fatigue cracks would grow, when less than half of the fatigue life had expired ; and of the few sites thus chosen, one would almost certainly give rise to the

* Now at R.A.E., Farnborough.
† Now at A.R.L., Melbourne.
‡ Communicated by the Authors.

eventual fatigue failure. In some early, exploratory work, use was made of artificial stress-raisers to localize the phenomena, but in almost all the results to be described, this was not done. It is not claimed that the methods or results have any validity outside the particular material on which observations have so far been carried out. Nor have the conclusions any status more than that of a working hypothesis. But it has been thought worth while to publish the results of such experiments and speculations as have so far been made, in case they may stimulate other workers to confirm or refute them.

§ 2. Apparatus and Techniques

When embarking on experiments on the mechanism of fatigue, it was considered essential that the stresses be macroscopically uniform over the gauge length, so as to avoid at least one of the factors which complicate the interpretation of results. For this reason a direct stress push-pull machine was favoured. Such a one was designed, built and tested by one of us (N. L.) and has been used for all the subsequent work. It is similar to the Amsler ' Vibrophore ' but has sufficient points of difference to merit a brief description. The specimen is, typically, of the form shown at S in fig. 1. It is supported vertically from the top, and carries at its lower end a massive coil holder (M, fig. 1) and a formerless coil, C. The coil lies in the annular gap G of a permanent magnet, PM, and provides the driving force to excite the oscillations. In order to obtain sufficiently large forces from this arrangement, it is run at the resonant frequency determined by the inertia of the coil holder and associated parts, and the compliance of the specimen itself. This frequency is of the order of 1000 cycles per second : by altering the mass of the coil holder and the dimensions of the specimen, it is possible to increase or decrease this by almost a factor of two.

In view of the sharpness of the resonance peak, such a system must be self-excited, rather than driven by an independent oscillator. The controlling signal is obtained from a piezo-electric crystal (quartz) incorporated in the top grip (SM, fig. 1). Part of the same signal is fed into a valve voltmeter, and is used to measure, continuously, the stress in the specimen. The amplitude of the oscillations is fixed by a limiting device, which automatically adjusts the gain of the system so that the output signal from the quartz crystal has a pre-determined value. The specimen is thus driven at constant stress throughout the test, after having taken one or two seconds to stabilize itself at the pre-set level on first switching on. When fatigue failure is imminent, the power needed to maintain the oscillations rises sharply : this increase in demand is made to operate a cut-out, which switches off the machine. This usually happens when the crack has spread along $\frac{1}{3}$–$\frac{1}{2}$ of the circumference. The endurance is calculated from the known frequency of the oscillations and the duration of the test, as measured by a mains-driven electric clock.

The degree of axiality of loading is believed to be good. The driving coil and its holder are axially symmetrical and are laterally unconstrained

in any way. In addition, the shape of the specimen lends itself to accurate aligning, since, during its production, all four conical bearing surfaces, and the gauge length itself, can be turned between centres without removing the work from the lathe. Finally, the method of driving the system at its resonant frequency for longitudinal vibrations—which will be different from the resonances corresponding to other modes—tends to improve the degree of axiality. Tests using resistance strain gauges have failed to show any asymmetry greater than the errors of the method of test, and the position of the origin of fatigue fracture has shown a gratifying randomness in azimuth.

Fig. 1

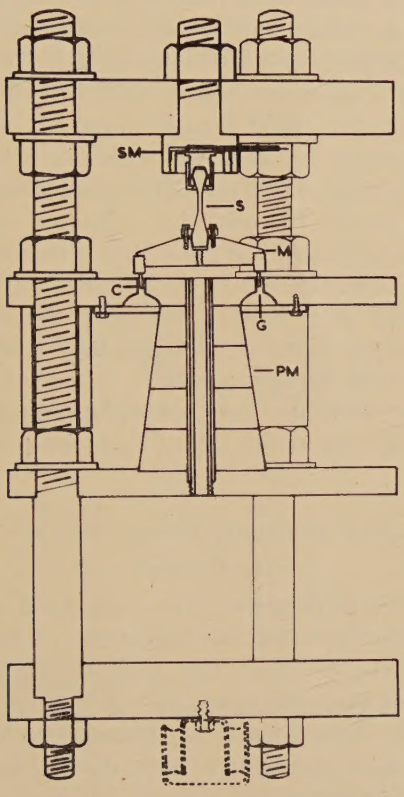

Diagram of fatigue machine.

The fracture always occurs within the gauge length and usually near the centre of it. This is taken as indicating that the radius of curvature of the ' fillets ' is so large that no important stress-concentration effects are to be found there, and as justifying the use of the nominal stress at the centre of the gauge length as the actual maximum stress. Before this can be given in absolute units, however, the quartz-crystal and valve-voltmeter assembly must be calibrated. The most satisfactory method yet devised of doing this has been to observe the peak-to-peak amplitude of the

excursion of the coil holder when the machine is running, using a microscope with an eyepiece scale. A knowledge of the mass of the moving parts, and the frequency of the oscillation, then gives the peak force immediately. The absolute accuracy of this method is probably not greater than 2–3%, but the relative accuracy of stress readings should be two or three times better than this. Observations with resistance strain-gauges have given confirmatory results.

All the observations to be described in this paper have been made on commercially pure copper. As the work has extended over a number of years, two or three different batches of materials have been involved, some O.F.H.C. quality, and some H.C. No significant difference in behaviour has been apparent between the different batches, although it has been found that the fatigue life for a given stress depends a good deal on the previous thermal history of the material. The normal procedure for the production of a specimen was as follows: The starting material was usually $\frac{5}{8}$ in. diameter rolled bar, as supplied by the makers. The specimens were machined to size, the finishing cuts along the gauge length being not more than 0·001 in. They were then polished mechanically down to 000 emery followed by 'Brasso' and 'Silvo'. With each new grade, the polishing was done first circumferentially and then longitudinally. Specimens were then electropolished in syrupy phosphoric acid, using a potential of 2 volts. Polishing for 45 seconds removed about 2 microns from the surface. Finally they were annealed *in vacuo* for 1 hour at 600°C and furnace cooled: a second light electro-polish produced a surface suitable for microphotography. The resulting grain diameter was of the order of 0·1 mm, with the usual numerous annealing twins.

§ 3. Experimental Observations

(*a*) *General*

In the course of the work some data have been accumulated on the endurance of the material under the conditions of test. Some of this is shown in fig. 2. Curve A shows the relation between fatigue life and stress, obtained when the specimens were annealed at 400°C instead of the usual 600°C. This was done in an attempt to compare our results, obtained at 1000 cycles per second, with data obtained at the N.P.L. using a frequency of 33 cycles per second. It was later discovered that the fatigue properties of this material depend critically on the annealing temperature, when this is in the neighbourhood of 400°C. Thus if any speed effect were present, it would readily be masked by changes due to small variations in heat treatment.

Subsequent specimens were annealed at 600°C at which temperature the conditions are not so critical. Curves B and C both refer to material which had had this treatment, but in different furnaces. One was continuously evacuated, and in the other, the specimens were treated in sealed tubes containing argon. In the former, the work was cooled in the furnace: in the latter the tubes were removed and cooled in air.

It is thought that the difference between curves B and C is most probably due to these differences in heat treatment, although this cannot be considered as established with certainty.

In later paragraphs, whenever comparisons of fatigue life are made, they always refer to specimens which were prepared under identical conditions, so that this uncertainty is not present. It will be noticed from fig. 2 that when conditions are carefully controlled, the amount of scatter on the endurance curve is quite small. A number of factors probably contribute to this result. The material itself is reasonably pure and homogeneous : the surface was carefully prepared in a reproducible manner, and in the gauge length there is a homogeneous, uniaxial tensile stress which will nowhere exceed its nominal value by any significant amount. The consequence is that a ratio of 1·5 : 1 between the fatigue lives of two *individual* specimens tested at the same stress can probably be considered to be significant.

Fig. 2

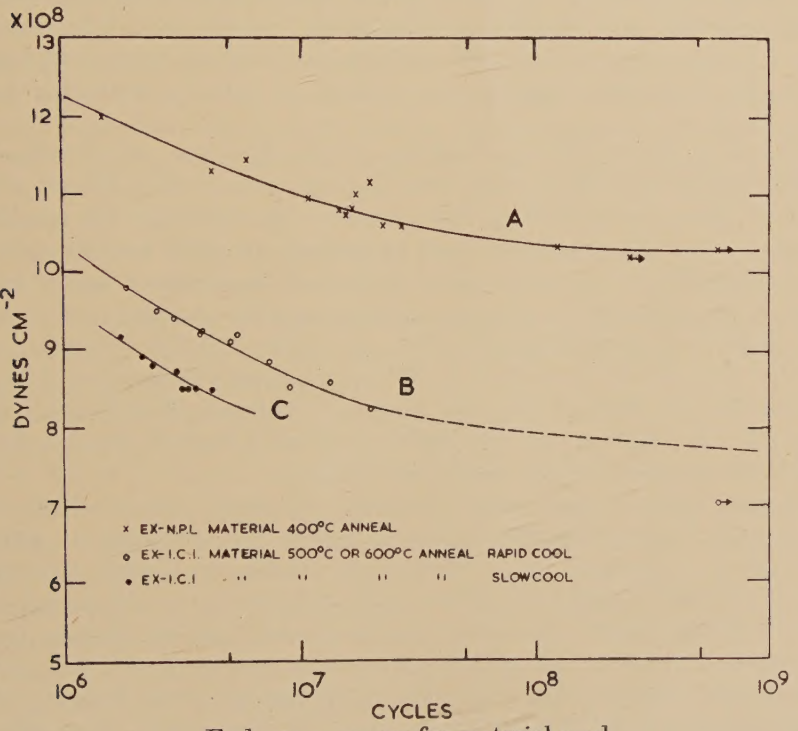

Endurance curves for material used.

(b) Microscopic Observations

When tested at stresses giving a fatigue life of 10^6–10^7 cycles, the specimens showed slip markings on the surface at a very early stage. These became more numerous and some of them became more intense as the test proceeded. It was found that the energy dissipated per cycle in the fatigue specimen increased gradually during most of the test

after an initial rapid decrease, and that this increase was correlated with the increase in the number of slip bands. Microscopic examination of the eventual fatigue crack showed that for most of its length it was surrounded by a zone of dense slip bands. The general direction of the crack was always normal to the tensile stress. Near its centre there was always at least one straight section, about one grain diameter long, free from the dense slip. The regions above and below this central line often had a density of slip markings somewhat less than the average for the specimen as a whole. The centre portion of the crack was parallel to any slip lines appearing in the same grain as itself. Figure 3 (Plate 3) shows the centre portion of a typical crack, and illustrates these features.

These observations suggest that the crack originated in a slip-band at a fairly early stage of the test. Its presence would give rise to a stress concentration at its tip, so causing abnormally dense slip there : the crack would advance through this region. In addition, the presence of the crack would reduce the stress on either side of itself and so produce the observed patches with less than the normal density of slip markings. The suggestion that the fatigue crack starts in a slip band is by no means new ; but the present evidence suggests that it must have been present, with the mechanical properties of a crack, at a fairly early stage of the test.

The high density of slip markings made detection of a crack in its early stages very difficult ; in order to restrict the field of search, a small shallow groove was filed in the side of a specimen to act as a stress concentrator. The surface of this groove was polished mechanically and electrolytically in the same way as the rest of the specimen before testing. The centre portion of the groove was photographed at intervals throughout a fatigue test, which lasted for $3{\cdot}2\times10^5$ cycles. A line following much of the path of the eventual crack was clearly visible after $2{\cdot}15\times10^5$ cycles (67% of the life) and some part of it showed after $6{\cdot}5\times10^4$ cycles (20%). The place where the crack eventually formed was marked by slip-bands as early as $1{\cdot}5\times10^4$ cycles (5%).

In an attempt to distinguish between a slip-band and the early stages of a crack, it was decided to electro-polish the specimen at intervals throughout a fatigue test. Preliminary trials established a standard ' dose ' of electro-polish which was sufficient to remove almost all of the slip markings ; about 2 microns was removed from the surface by this treatment. Another grooved specimen was prepared and the previous experiment repeated, the sequence of operations being fatigue, photograph, electro-polish, photograph, etc. It was found that although almost all the slip-bands were removed by the standard electro-polishing treatment, some remained, and even appeared to be brought into greater prominence by the process. A second dose of electro-polish immediately following the first usually left these persistent bands still present, indicating that they were not just abnormally large steps on the surface, but were in some way qualitatively different from the remainder. On repeating the sequence of operations, it was found that some of these

persistent bands increased in intensity, and after continued application of the fatigue stress, a few of them eventually developed into cracks which spread into neighbouring grains.

Following this preliminary trial, all subsequent observations were made on specimens without any groove, so as to avoid the complication of the uncertain stress concentration factor. The use of the electro-polishing technique meant that places likely to be of interest were not obscured by a welter of normal slip bands, and were less likely to be overlooked.

After fatiguing for a known time, chosen to be a small fraction of the estimated fatigue life, a specimen was electro-polished. Examination of the whole surface revealed a number of typical 'persistent slip bands' and the more prominent of these were photographed before the specimen was replaced in the fatigue machine. This cycle of processes was repeated at intervals until the specimen finally broke after $3{\cdot}65\times10^6$ cycles.

The characteristic persistent slip bands were observed the first time the test was interrupted, which was after about 4% of the fatigue life; these became more marked as the test progressed, but most of those which had been kept under observation from the early stages did not spread beyond the grain in which they started. However, figs. 4–7 (Plate 3) show one such field of view in which progressive changes were observed. Figures 4 and 5 show it, respectively, before and after electro-polishing, when $7\frac{1}{2}$% of the fatigue life had elapsed. A few persistent slip bands are visible in fig. 5, but unfortunately the point which subsequently proved most interesting is just off the edge of the negative. Figures 6 and 7 show the same field after electro-polishing when 42% and 77% respectively of the life had elapsed. The marks are more numerous in fig. 6, and by fig. 7 one of them has developed into a crack, extending into neighbouring grains.

The crack which eventually led to the fatigue failure in this specimen was first photographed after 42% of the life (fig. 8, Plate 4). At that stage it was the only one of the many similar markings observed which had already shown signs of spreading into neighbouring grains—a behaviour similar to that shown at a later stage by the other crack already illustrated. Figures 9 and 10 (Plate 4) show this same crack at 77%, and almost 100% of the life.* Taken together, the two series of photographs present a fairly complete picture of the stages in the development of a fatigue crack under the conditions of these observations. Persistent slip bands were visible after $7\frac{1}{2}$% of the life; one had developed into a crack involving neighbouring grains after 42% of the life, and the most serious crack was already many grains long after 77% of the life. Similar slow rates of growth were shown for other cracks both on this specimen and on other specimens. It has also been verified that the general course of events is not affected by the number of times that the

* It should be noted that figs. 9 and 10 are both mosaics, and that the specimen was *not* electro-polished at the conclusion of the test, before fig. 10 was taken.

specimen is polished during a test; nor is the fatigue life significantly altered by these interruptions. The fatigue process, in short, is not being modified by the steps taken to observe it.

(*c*) *Tensile Tests*

It is still far from obvious at what stage a ' persistent slip band ' may properly be called a ' crack '. In an attempt to throw more light on this problem, a partially fatigued specimen was chosen which showed a number of ' cracks ' ranging from 3 to 12 grains long, and many ' persistent slip bands ' extending across a single grain. The specimen was then given a 5% slow tensile extension, and re-examined. The cracks more than one grain long had all opened into large cavities, but none had shown any tendency to extend lengthways. Persistent slip bands confined to one grain had not opened up by any detectable amount, but there is a suggestion of some broadening of those that were just beginning to invade the neighbouring grains. Figures 11 and 12 (Plate 4) show one such borderline case before and after the 5% strain. This experiment would suggest that the grain boundaries play an important role in the early history of a fatigue crack. Such a view also receives some support from the results already quoted, that while persistent slip bands were visible after 4% of the life of one specimen, they were only beginning to invade neighbour grains at about 40% -and, in this one case at least— it was the crack which first spread in this way which led to the final failure.

(*d*) *Experiments on Single Crystals*

In view of these results, some interest attaches to observations made on single crystals. Four such specimens have been examined so far. The crystals were grown from the melt by the usual techniques, carefully machined to size and then treated in the same way as the polycrystals in the matter of surface preparation. The phenomena observed were qualitatively exactly parallel to those shown by polycrystals, and the observations are not sufficiently numerous to justify any close comparison of details. Figures 13 to 18 (Plates 5 and 6) show some photographs of one of these specimens at various stages of its life.* Apart from figs. 14 and 18, the specimen had been electro-polished just prior to the photographs being taken. This crystal was orientated so that slip took place preferentially on one system, although the stress on a second system was only slightly less. (A number of curious patches of slip on this second system were observed: fig. 14 shows one such.) For the most part, however, slip was confined to the single system. Some of these slip markings persisted after an electro-polish at 18% of the eventual fatigue life (fig. 13). The persistent marks were rather short, typically about 50 microns long and arranged in rows along the slip bands. Further stressing showed a tendency to increase the intensity and length

* In these and all other cases the tensile axis of the specimen is parallel to the long edge of the individual frames of the mosaic.

of some of these markings—or it may be that the shorter ones in or near the same slip band joined together (figs. 15 and 16, 36% and 54% respectively). After 90% of the life, it was seen that some of the persistent slip marks had developed into cracks which in places did not exactly follow the slip bands (fig. 17). This was much more obvious when the test was finally stopped after a further 10% when numerous large cracks were present (fig. 18). For appreciable parts of their length the cracks followed the direction of the first or—more rarely -the second slip system, but the *general* direction of the main failure, and of other, shorter cracks in the same specimen was the usual one, i.e. normal to the direction of the tensile stress. Another single crystal specimen, which was run to failure without any intermediate polishing, showed the same general form of crack—initially following the active slip plane but later deviating from it, to run approximately normal to the tensile stress.

An interesting feature on fig. 14 is the traces of slip on the second system which have appeared at the ends of the persistent slip bands left by the previous polish. (Figure 19 (Plate 7) shows an example, at greater magnification, from the fourth single crystal specimen which was also run to failure without interruption.) Their presence clearly indicates that in these regions the local stress is abnormal. Such a stress concentration might quite well be produced at the tip of a crack ; but similar effects would also be expected from, for example, a closely packed group of dislocations.

(*e*) *Depth of Persistent Slip Bands*

Two further experiments should be mentioned concerning these persistent slip markings and their relation to fatigue fracture. The first concerns their surface origin. Although they are revealed in the first place by a light electro-polish which removes about 2 microns from the surface, continued electro-polishing will eventually remove them completely. Figures 20 to 22 (Plate 7) show a series of photographs of a partially fatigued specimen which illustrate this point. The same field of view is shown after electro-polishing to remove about 2, 10 and 18 microns. A further photograph, taken after 34 microns had been removed, showed no trace of the marks. Experience suggests that, in the first half of fatigue test on a polycrystalline specimen, most of the persistent marks are fairly shallow, and that the deepest of them does not penetrate more than about 100 microns. This is the same order of magnitude as the grain diameter on the material used. It is noteworthy, that in all the observations of this kind which have been made, the removal of metal from the surface has never revealed any new markings of the same kind ; all of them have their origin on the free surface.

Nevertheless, even at an early stage of the test the persistent slip bands represent a source of weakness, and contain within them the seeds of fatigue failure. A striking illustration of this point was provided by the following experiment : A fatigue test was stopped after 25% of the estimated endurance, and the specimen was heavily electro-polished

until all the persistent markings had been removed. This necessitated the removal of a layer of metal about 30 microns thick. The test was then continued at the same stress as before, for a further, equal time, and the polishing repeated. This was done nine times in all, so that the specimen had survived 225% of its normal life. In view of the small amount of scatter obtained in our observations, this is quite a significant increase. Moreover, even after this treatment, microscopic observation showed no difference between this specimen and a piece of virgin material, and there appeared to be no reason why the process could not be continued indefinitely, as long as any metal remained.

(*f*) *Experiments on Annealing*

Finally, we might mention some experiments on the effect of periodic annealing during the course of a fatigue test. Sinclair and Dolan (1951) have carried out an extensive investigation of this kind on polycrystalline α-brass. They annealed their specimens for 30 minutes, at 400°C, every 20% of the expected fatigue life. They found that the endurance of such specimens was statistically indistinguishable from that of untreated specimens.

We have made similar observations on three polycrystalline copper specimens. The annealing conditions were 1 hour at 600°C—a treatment which completely re-softens the material without producing any noticeable grain growth or recrystallization. One specimen was given this treatment after 50% of its expected, unannealed life, and one was given it every 20%. Both of them broke after a life not significantly different from that of normal specimens.

The third specimen was annealed every 10% of its expected life. After the first run, it was electro-polished and showed the usual persistent slip bands. After annealing, followed by a second electro-polish, the same markings still persisted. The sequence of fatigue, polish, anneal, polish, was repeated five more times. A photograph taken at this stage showed persistent markings already spreading into neighbouring grains, the general appearance at this stage being intermediate between that shown by another, unannealed, specimen photographed at 42% and 77% of its actual life (figs. 8 and 9). There is little doubt, in fact, that the events were following their normal course, unaffected by the annealing. Unfortunately the specimen had been slightly dented while being removed from the fatigue machine for the first anneal; a crack formed at the bottom of this dent, and the specimen broke there, mid-way through the seventh fatigue period.

§ 4. Discussion

To summarize, it appears that after only a few per cent of the fatigue life has elapsed, some of the numerous slip bands undergo some modification of their structure which causes them to react differently to the electro-polishing conditions. The change, whatever its nature, originates on the free surface of the specimen. At some stage, the modification confers upon the slip band the essential property of a crack—a surface

across which it is not possible to transmit a tensile stress. A few of the slip bands go through this sequence more rapidly than the majority, and have developed into obvious fatigue cracks, several grain diameters long, before the longest of them is so large that the specimen can be said to be broken. The modification to the slip band structure cannot be reversed by annealing.*

It has been noticed that, of these persistent slip bands which develop into cracks, an abnormally high proportion lie very close to twin boundaries. The explanation of this is not clear: but the proximity of the twin boundary cannot be an essential feature in the formation of the crack since the events follow the same general pattern in single crystals.

(*a*) *Effect of Oxygen Atmosphere*

The observations are consistent with the hypothesis that the slip band changes directly to a series of micro-cracks, but it is not easy to conceive of a detailed mechanism for this which requires, as an essential feature, that the change must originate on a free surface. As an alternative, therefore, we have explored the possibility that the diffusion of oxygen from the atmosphere into the slip band forms an intermediate step in the process. The persistent slip bands in their earliest stages might then well be regions of abnormally high oxygen concentration. This explanation, too, is consistent with all the observations so far recorded. If it is correct, one would expect that the endurance of a specimen might be increased if access of oxygen to the surface were prevented. It was found that just such an effect had been reported a number of years ago by Gough and Sopwith (1932, 1935, 1946). They showed that the life of a copper specimen was prolonged if, during the fatigue test, it was placed in a partial vacuum (10^{-3} mm Hg), or in an atmosphere of dry, oxygen-free nitrogen.

It was thought desirable to repeat the experiments of Gough and Sopwith to verify that the effect was obtained with our material, and under our conditions of test. The construction of the apparatus did not readily lend itself to experiments *in vacuo*, but an atmosphere of nitrogen could readily be provided by surrounding the specimen with a light polythene bag, more or less air-tight, and maintaining in it a pressure of gas slightly greater than atmospheric. The nitrogen was obtained from a cylinder, and was claimed by the suppliers to contain not more than 1 part in 10^5 of oxygen or water vapour. Six specimens from the same batch were tested, all at the same stress, either in nitrogen

* Some reference should be made at this point to an early paper by Ewing and Humfrey (1903) which is in danger of being forgotten. In this they describe microscopic observations on flat specimens of Swedish iron, fatigued in rotating bending. The sequence of events described is closely similart to that found by us for copper: slip lines growing broader, more diffuse and more numerous, with cracks eventually appearing in such broadened slip bands. The differences in material, in stress system, and in technique help to establish the facts more clearly in the case of copper but it would appear that, at least in broad outline, the story is the same for iron.

or in air. The values obtained for the fatigue life are shown in the table :

Specimen No.	Atmosphere	Life
58	Air	$3{\cdot}3\times10^6$
66	Nitrogen	20·3
67	Air	3·4
68	Nitrogen	10·4*
69	Air	3·2
70	Nitrogen	17·5

* The fatigue crack started at one of a number of very small depressions on the surface. These had presumably been overlooked when the specimen was originally polished. This was the only occasion on which they were seen, and their presence could well account for the short life of No. 68, compared to Nos. 66 and 70.

There is little doubt that the life in nitrogen is considerably greater than that in air, particularly in view of the good reproducibility normally obtained. The average increase in life—of the order of 5–6 times—is also in rough quantitative agreement with Gough and Sopwith, who found an increase in fatigue 'limit' of 13% (calculated on the basis of an endurance of 3×10^7 cycles) : the two figures are consistent with the slope of the stress-log (cycles) curve.

With specimen No. 70 the test was interrupted at intervals for the usual electro-polishing and surface examination. Figures 24 to 27 (Plate 8) are a selection of the photographs taken. At about 5% of the expected life *in air*, the surface appearance was not very different from that which would have been found if the test had been running in air (fig. 24). By 42% of the expected life, there was little change (fig. 25). At 164% the persistent marks had developed further (fig. 26) ; this point proved to represent 30% of the actual life in nitrogen. By 400% there was little further change in the length of most of the persistent slip bands that had been kept under observation although they were more numerous (fig. 27). However, at one place a crack in a more advanced stage was discovered, and this eventually proved fatal. It is not easy to speak with confidence about qualitative observations of this kind, but the general impression gained from a study of the numerous photographs taken was that the absence of oxygen had little effect on the first appearance of the persistent slip bands, and that the major effect was to slow down the transition from this stage to the point at which there could be no doubt that the bands had turned into cracks. Further propagation of the crack was slowed down also.

(*b*) *Role of the Oxygen*

In the light of these results, there is little room for doubt that the pressure of oxygen in the atmosphere around a copper specimen has an effect on the fatigue life. Further, the effect of the atmospheric oxygen seems to be intimately concerned with the transition from slip band to crack, and with the early stages of crack development.

It is well known that an adsorbed mono-layer of oxygen forms very rapidly on a fresh copper surface and that, once formed, it is very difficult to remove (see, for example, Schlier and Farnsworth 1954). A rough calculation suggests that there would be ample opportunity for such a layer to form on the freshly exposed surface in the slip band during one half cycle of a fatigue test. On the following half cycle, one can envisage three possibilities: (i) The oxygen will be 'scraped off' and slip will take place in the reverse sense on the same plane; this would appear to be somewhat improbable. (ii) The slip in the reverse sense will take place on some neighbouring plane: this could well be the beginning of a process leading to extrusion of metal from the slip bands, as reported already by Forsyth (1955). Such an effect has, in fact, been observed by us on a single crystal of copper (figs. 23 (*a*) and (*b*), Plate 7). The loss of this material from the interior of the crystal just below the surface would give rise to an effective cavity, the stress field of which would represent a potential source of a crack. (iii) Slip in the reverse sense will take place to some extent on the same plane, and some of the freshly adsorbed oxygen will be drawn in to the body of the crystal in the form of dissolved atoms. This oxygen, replenished by fresh supplies drawn into the crystal in the same manner each cycle, could then diffuse down the slip band, building up an abnormally high concentration of oxygen in and near the band and weakening the crystal so much that a crack eventually forms there.

On this latter view the persistent slip bands would be regions of high oxygen concentration. It is at once clear that no ordinary diffusion process could account for the penetration of the persistent bands to an appreciable fraction of a grain diameter ($\approx 10^{-2}$ cm) in times of the order of 10^3 sec. This would require a diffusion coefficient of order 10^{-7} cm^2/sec—which is only reached for copper at about 800°c (Ransley 1939). However, examples are multiplying of metallurgical changes occurring under fatigue conditions which are explicable if one postulates abnormally fast diffusion (see, for example, Holden 1954, Hanstock 1954). Several possible mechanisms suggest themselves, such as an increased vacancy concentration, and high local temperatures due to 'thermal spikes' (Seitz 1952); such efforts will be most pronounced near an active slip band.

An objection to any mechanism in which diffusion is the rate-determining process is that it would tend to make fatigue a very temperature sensitive phenomenon, and would predict a considerable frequency effect, since the production of a given state of the crystal would depend on the duration of the test in seconds rather than in cycles. Neither of these effects is well marked in fatigue phenomena in general. If, however, diffusion were merely capable of equalizing the oxygen concentration across a slip plane at the end of each half-cycle the relative movement of the two parts of the crystal during slip would result in oxygen being drawn down the slip band. In this case the number and extent of the cycles of slip would be the rate-determining process, and the above objection would be removed.

However, any hypothesis in which the oxygen plays an essential role will have difficulty in accounting for the fact that fatigue fracture takes place in copper at 4°K (Rosenberg, private communication). An alternative interpretation of our results which avoids this trouble would be that the persistent slip bands already have the character of minute cracks at a very early stage (say 5% of the total life, or less). This evades the question of how the crack forms in the first place and why it forms only on the surface, and assigns to the oxygen the part of expediting the growth of the crack in its earliest stages. Certainly the formation of an adsorbed layer of oxygen on the faces of a freshly opened crack would tend to prevent it closing again on the next half-cycle. If, following this line of thought, a persistent slip band in its earliest stages consists of many small cracks, each too small to be seen individually, then its appearance would not be expected to change appreciably due to any opening of the cracks under the influence of a steady tensile stress.

On either of the two views one can see that a moderate annealing treatment would not suffice to undo the damage already done to the crystal early in the fatigue test. Thus both hypotheses are in accord with the observations which we have made to date, and more experimental work is needed before the mechanism can be clearly established.

Acknowledgments

The authors wish to express their indebtedness to Professor N. F. Mott, and numerous colleagues, for many helpful discussions, and to the workshop staff of the H. H. Wills Physical Laboratory, whose skill in producing the apparatus and the specimens has made the investigation possible.

One of us (N. L.) acknowledges financial assistance from the Department of Supply, Australia, and another (N. W.) was in receipt of a D.S.I.R. Maintenance Grant duing the period of the work. The work described has received financial support from the Mechanical Engineering Research Board of the Department of Scientific and Industrial Research, as part of their research programme. The paper is published after consultation with the Director of the Mechanical Engineering Research Laboratories.

The assistance received from all the above bodies is acknowledged with gratitude.

References

Ewing, J. A., and Humfrey, J. C. W., 1903, *Phil. Trans. R. S.*, **200**, 241.
Forsyth, P. J. E., 1955, *J. Inst. Met.*, **83**, 395.
Gough, H. J., and Sopwith, D. G., 1932, *J. Inst. Met.*, **49**, 93 ; 1935, *Ibid.*, **56**, 55 ; 1946, *Ibid.*, **72**, 415.
Hanstock, R. F., 1954, *J. Inst. Met.*, **83**, 11.
Head, A. K., 1953, *Phil. Mag.*, **44**, 925.
Holden, J., 1954, *N.P.L. Report* No. HT. 75/54.
Ransley, C. E., 1939, *J. Inst. Met.*, **65**, 147.
Schlier, R. E., and Farnsworth, H. E., 1954, *J. Appl. Phys.*, **25**, 1333.
Seitz, F., 1952, *Advances in Physics*, **1**, 43.
Sinclair, G. M., and Dolan, T. J., 1951, *Proc. 1st U.S. Nat. Congress of Appl. Mech.*, 647.

XII. *Radiative Transitions in Light Elements: II*

By D. H. Wilkinson*
Nuclear Physics Branch, Atomic Energy of Canada Limited,
Chalk River, Ontario, Canada†

[Received September 14, 1955]

Abstract

A survey is presented of our present knowledge concerning radiative transitions in nuclei of $A \leqslant 20$. Over a hundred transitions, chiefly dipole, are analysed in terms of the Weisskopf units, and the following chief conclusions are drawn:

(i) E1 transitions have a most probable speed of about 0·032 Weisskopf units with a spread in speed of about a factor of seven either way;

(ii) The corresponding quantities for M1 transitions are a speed of 0·15 Weisskopf units and a spread of a factor of 20 either way;

(iii) These distributions are consistent with shell model expectations;

(iv) If a transition shows $\Gamma_\gamma(\text{ev})/E_\gamma{}^3\,(\text{Mev}) > 0{\cdot}02$, then it is very probably E1;

(v) There is no clear dependence of transition speed on level spacing or other feature;

(vi) Some of the higher multipole transitions are inconsistent with shell model expectation and give evidence of collective motion.

§ 1. Introduction

Two years ago a survey of radiative transitions in light nuclei (Wilkinson 1953 a—referred to as I) revealed some 22 dipole transitions, equally divided numerically between electric and magnetic in character, which had been established with fair to good probability, and whose widths were known with accuracies varying from a few per cent to a factor of two or three.

From this scanty material it emerged that E1 transitions were by no means weak as a rule, and indeed possessed strengths of about one-hundredth to one-tenth of the rough single-particle shell model estimate that has come to be called the Weisskopf unit (Weisskopf 1951—for a detailed treatment see Moszkowski 1955):

$$\Gamma_{\gamma w}(\text{E1}) = 0{\cdot}11 A^{2/3} E_\gamma{}^3 \text{ ev}.$$

E_γ is the energy of the transition measured in Mev, and we have used a

* Permanent address: Cavendish Laboratory, Cambridge.
† Communicated by the Author.

nuclear radius of $1{\cdot}5\times A^{1/3}\times 10^{-13}$ cm.* The radiative width of a transition in these Weisskopf units is then a measure of the associated matrix element, and is written as $|M|^2$. It also appeared from I that the spread in the values of $|M|^2$ was not very great for E1 transitions that did not suffer the inhibition of the isotopic spin selection rule, but so few transitions were involved that little confidence could be felt on this point. It was pointed out by Lane and Radicati (1954) and emphasized by Lane and Wilkinson (1955) that, even within the pure shell model, we must expect transition strengths relative to the single-particle strength to vary widely, ranging from very small values (including zero) to values of greater than unity. This wide departure to be expected from the single-particle width or the Weisskopf unit is due to five causes :

(i) In a real transition we are not concerned as a rule with the behaviour of one isolated particle, but rather with the behaviour of the often many (n) particles needed for a full specification of the states between which the transition takes place. Since we do not know which particle actually makes the transition, we must multiply the one-particle matrix element by n. This leads to a speeding up of the transition, and accounts for the fact that some theoretical shell-model transitions have $|M|^2$ values of greater than unity. We may think of this enhancement effect as due to the correlations imposed on the motions of equivalent nucleons by the Pauli principle.

(ii) The requirement that radiative transitions proceed only through common parents gives a diminution of the matrix element except in rare cases, and can lead to the transitions being completely forbidden.

(iii) In general the (Racah) coefficients that describe the various vector couplings taking place in the transition lead to a diminution, often substantial, of the matrix element.

(iv) The ' potential well ' within which the transition takes place is not infinitely massive and uncharged as is assumed to calculate the single-particle estimate or Weisskopf unit, but rather has a charge and is of finite mass. This means that the ' well ' recoils from the motion of the radiating

* There is some evidence from the treatment of the Coulomb energy of light nuclei, taking into account exchange contributions (see e.g. Cooper and Henley 1953, Carlson and Talmi 1954), that a better value for the constant in this expression for the radius would be about 1·3. This is in line with other familiar evidence in heavy nuclei that the radius constant is about 1·2. However, the evidence from the dynamical properties of light nuclei seems to favour the larger radius for computations of the present sort. Use of the larger radius in computing the Weisskopf units also makes some allowance for the fact that, in most of the transitions with which we concern ourselves, the radiating nucleon is unbound in its initial state, and so gives a contribution to the matrix element from outside the nucleus which does not occur in the computation of the Weisskopf unit. The extra contribution for the cases of interest here usually speeds the transition so the smaller radius with the proper wave functions gives about the same result as the Weisskopf unit computed for the big radius.

particle and, since the well is charged, this constitutes a current opposing that of the radiating particle if it is a proton. In a classical calculation this results, for E1 radiation, in replacing the charge e of the radiating proton by the familiar ' effective charge ' $(1-Z/A)e$, or, if the ' radiating particle ' is a neutron, by $(Z/A)e$. In a proper shell model treatment the situation is more complicated, but a similar effect obtains, and so we see that, even neglecting the many-particle complications (i), (ii), and (iii) above, E1 transitions of a single particle should not be expected to display strengths of one Weisskopf unit, but of only about $(N/A)^2$ or $(Z/A)^2$—one-quarter of a Weisskopf unit. This point is much less important for magnetic transitions, while for electric transitions of higher order, for a radiating proton, the expected strength is about $(1-Z/A^k)^2$ Weisskopf units (for a 2^k-pole transition), which is very close to unity, and for a ' radiating neutron ' the expected strength is about $(Z/A^k)^2$, which is very close to zero.

(v) The Weisskopf unit is correct only for transitions ending in a state of zero orbital angular momentum and where the initial state has $J=k+\frac{1}{2}$. If this is not so the expected width even in the idealized one-particle case is different from the Weisskopf estimate. The difference may be easily a factor of three or more in a practical case. This is discussed in more detail later. Another difference is that between the radial overlap integral evaluated with ' realistic ' shell model wave-functions and with the rectangular wave-funtcion of the Weisskopf unit. This latter difference is not great in the cases of present interest.

To avoid confusion we should state that throughout this survey $|M|^2$ in connection with an experimental transition means always the actual radiative width Γ_γ divided by the Weisskopf estimate $\Gamma_{\gamma w}$ appropriate to that type (multipole and parity change) of transition as written out above for E1 transitions and later for others. We do not, in quoting $|M|^2$, apply any ' correction factors ' for any of these five points just enumerated.

Such considerations show that the observed dispersion of $|M|^2$ values is qualitatively quite consistent with transitions taking place within the pure shell model; this point we return to later.

The M1 transitions analysed in I were also of very roughly the strength expected from shell model type calculations. Here the appropriate Weisskopf unit has the value :

$$\Gamma_{\gamma w}(\mathrm{M1})=0{\cdot}021\ E_\gamma{}^3\ \mathrm{ev}.$$

It appeared both that the spread in $|M|^2$ values was somewhat greater for M1 than for E1 transitions and that these $|M|^2$ values were somewhat higher for the magnetic than for the electric transitions. We might note that if considerations (i), (ii), and (iii) above are similar for M1 and for E1 transitions then, *ceteris paribus*, we should expect point (iv) to result in values of $|M|^2$ for E1 transitions running, in the mean, about a factor four less than those for M1 transitions.

The spreads in $|M|^2$ values recorded in I were so great that it was felt that no safe distinction could in general be made between E1 and M1 transitions on the basis of radiative width alone.

The intervening years since the publication of I have seen a great increase in the volume of material pertaining to the radiative properties of light nuclei, and it is now possible to analyse some 105 transitions instead of the 22 of 1953. This is a sufficient bulk of material to begin to treat statistically, and from this present survey it emerges that the main tentative conclusions of I concerning dipole transitions are substantiated ; they may now be stated more quantitatively. A new feature is the beginnings of information on transitions of higher multipole order, but as yet data are extremely sparse. For those transitions of interest in the present survey we have the Weisskopf units (for a radiating proton) :

$$\Gamma_{\gamma w}(\mathrm{E2}) = 1{\cdot}2 \times 10^{-7}\, A^{4/3}\, E^5 \text{ ev},$$
$$\Gamma_{\gamma w}(\mathrm{E3}) = 8{\cdot}7 \times 10^{-14}\, A^2\, E^7 \text{ ev}.$$

Also since the publication of I there has appeared a number of detailed attempts to apply the shell model to calculate in detail various *dynamical* properties of light nuclei including radiative widths of certain special transitions (Lane 1953, 1955). These attempts, on nuclei in the 1p-shell, have met with an encouraging success and suggest that the shell model may indeed be the basis for a first-order description of certain states of light nuclei. Again the attempt by Inglis (1953) to account for the level positions of 1p-shell nuclei in terms of the shell model shows a sufficient relationship to experiment to give the impression that any prediction of the shell model in this region of the periodic table must be taken seriously. The work of Redlich (1955) and of Elliott and Flowers (1955) on the nuclei just beyond ^{16}O shows how agreement in respect both of level positions and dynamical properties may also be achieved between experiment and shell model theory at the beginning of the 1d–2s shell. These results provide encouragement for a continued examination of the predictions of the shell model about radiative transitions in light nuclei. This examination may take the form of a search for detailed shell model descriptions of specific transitions as, in particular, Lane has done, or we may make an omnibus comparison of the predictions of the shell model as to strengths and dispersion of strengths of radiative transitions with the whole ensemble of experimental fact. This latter approach is pursued in this survey.

Other more recent publications have confirmed the feeling that much qualitative if not quantitative truth resides in the shell model's view of radiative transitions as summarized in the Weisskopf units. Thus the initial survey of isomeric transitions by Goldhaber and Sunyar (1951), which was in large measure responsible for triggering off the present considerable interest in the dynamical predictions of the shell model, has been extended (Goldhaber and Sunyar 1955) and confirms the earlier impression that the gross structure of isomeric transitions conforms to the general pattern of shell model expectation. Detailed comparisons are,

however, difficult to make in this field of the heavier nuclei, and in particular it can be seen from the work of Goldhaber and Sunyar that in certain respects the simple shell model breaks down—for example, there is little sign that selection rules specific to the shell model are well obeyed. and again there is little difference evident between the strengths of odd-proton and odd-neutron electric transitions of high order. To some degree such behaviour may be understood in terms of configuration interaction, but it seems likely that some more far-reaching revision will be needed. At one point the shell model seems to fail rather completely, and that is for E2 transitions in heavy nuclei which frequently have values of $|M|^2$ so much greater than unity (up to 100 or more) that it appears rather artificial to attempt a shell model interpretation, and the collective model (Bohr and Mottelson 1953) must be accepted as the more realistic approximation. Much interest will centre on the systematics of E2 and E3 transitions in light nuclei when more data become available. The present survey can only make a small beginning in this direction but, as will be seen, there is some suggestion that, for transitions of this type, we may be already confronted by evidences of collective motion even in the 1p shell. Collective motion of the type envisaged by Bohr and Mottelson does not produce enhancement of E1 transitions and, since considerable equilibrium distortions are not to be expected in the lightest nuclei. we should not expect shell model predictions to be very greatly modified by collective properties of the ' rotational ' type ; ' vibrational ' oscillations are to be expected. On the other hand we must remember the possibility of collective oscillations of the ' polarization ' type (Goldhaber and Teller 1948), which may result in enhanced E1 transitions. As yet there is little direct evidence for such polarization oscillations : the ' giant resonances ' of nuclear photodisintegration for which they were postulated have been shown to be susceptible of an alternative interpretation within the frame-work of the shell model (Wilkinson 1955).

A further recent important contribution to our knowledge of E1 transitions comes from work on the gamma-ray spectra following capture of slow neutrons (Kinsey and Bartholomew 1954, Kinsey 1955), where it is found that, where they are possible, E1 transitions predominate and have a radiative width that, on the basis of about a dozen transitions, may be written :

$$\Gamma_\gamma \sim 0{\cdot}06 D \Gamma_{\gamma w}$$

where D is the spacing (in Mev) of levels, at the excitation from which the gamma-ray is emitted, of spin and parity such that they may combine by radiation of the given type with the final state. Such a factor (Blatt and Weisskopf 1952) is needed to take into account the configuration interaction, many-particle excitation and similar effects that play so important a rôle in the close crowding of levels at high excitation. The very rough expectation of the shell model is that, on account of these effects, the numerical factor in the above equation should be as an upper limit somewhere between 0·05 and 0·5 (taking into account the effective

charge factor in (iv) above). We see therefore that the results of Survey I for the light elements and the work of Kinsey chiefly for heavier elements agree that the expectations of the shell model so far as E1 transitions go are fairly well realized. Indeed if we insert for D in Kinsey's expression a value of about unity appropriate for the light nuclei of Survey I, we find that the properties of transitions in heavy nuclei extrapolated in this way into the region of the light nuclei agree very well with what we find in practice for light nuclei—transitions whose strength is of the order of a tenth of the Weisskopf unit. It is not yet clear how important configuration interaction and allied effects will be for the light nuleci with which we are here concerned, and what place the spacing of levels will have in determining radiative properties ; this point will be returned to later.

Other interesting recent work concerns the total radiative widths of individual slow neutron resonances (Hughes and Harvey 1954). It seems likely that such results will be more informative about statistical aspects of the nucleus such as the dependence of level density upon various parameters than they will about the nature of the radiative process itself.

We now present the experimental material which, as before, has been arbitrarily restricted to $A \leqslant 20$.

§ 2. Experimental Material

The experimental material that is the source of this survey is necessarily of very variable quality and reliability. In some cases the type of the transition (multipolarity and whether electric or magnetic) is established with good probability ; such transitions are granted Status A in the following tables. In other cases the evidence for one assignment rather than another is direct but only fairly good, or good but only circumstantial ; here Status B is given. Where the evidence is not strong enough to give a clear preference for one assignment over others the transition is ignored even though it may be well-established and of accurately-measured strength. Where the strength of a transition is known to a few tens of per cent or better a star is attached under Status ; strengths of transitions not so marked may be in error by as much as a factor of two or three or even more.

In determining the type of a transition ' bootstrap ' arguments have been avoided as much as possible. We have very occasionally, however, in special cases allowed ourselves to be guided by the strength of a transition in determining whether it is M1 or E1. As will be seen later, it appears that if a transition shows a value of the quantity Γ_γ(ev) divided by $E_\gamma{}^3$ (Mev) of greater than 0·02, then there is about a 10 : 1 chance that it is E1 rather than M1. This criterion has been admitted to assign E1 character to the transitions in ^{14}N between the following pairs of states—8·62–6·23 Mev ; 8·70–5·69 Mev ; 9·18–6·44 Mev ; 9·49–5·10 Mev—which show values of the above quantity of 0·10, 0·18, 0·06, and 0·10 respectively. These assignments receive Status B (in any case the existence of the

second of these is not established with certainty). A case such as the transition between the 8·90 and 5·83 MeV states of ^{14}N, which has a value of the above quantity of 0·014, cannot be classed by the use of this criterion and so is ignored.

It sometimes arises that while the product of the radiative width and the statistical weight factor of a disintegration cross section is well known, the spin J of the radiating state has only been determined within limits. This means that only $(2J+1)\,|M|^2$ can be quoted with accuracy rather than the more interesting $|M|^2$. However, spins are known in a sufficient majority of cases now for us to tabulate $|M|^2$ rather than $(2J+1)\,|M|^2$ as we had to do in I.* In cases of unknown J we have quoted a value of Γ_γ and so of $|M|^2$ which is the mean of the values derived from the various alternative spin possibilities. This has been done in three cases in ^{15}O and one in ^{7}Be where the radiating state is in each case $J=1/2$ or $3/2$. The error introduced by our procedure is 50% or less, which is not worrying in view of the large dispersion in the distribution of $|M|^2$ values to which these transitions are contributing. In order to enable corrections to be made in the event of re-assignments we list in the following tables the value or values of the spin J of the initial (emitting) state that we have assumed in computing Γ_γ from the experimental results.

In one case, the probable M1 transition from the 18·14 MeV state of ^{8}Be, it is not known to which of two states the transition goes, the ground

---

* We shall for the greater part of this survey eschew any explicit consideration of statistical weight factors as such. The subject is rather a vexed one and it is the responsibility of each author to justify his own use of any particular statistical weight factor or set of symbols likely to be mistaken for a statistical weight factor (or equally to justify his neglect of such factors). In I we stated with care that we were quoting $(2J+1)\,|M|^2$ because that was what we knew about from experiment, but now the experimental situation is much better and we can quote $|M|^2$. We believe that this is the most sensible quantity to tabulate in our case and that, in a general tabulation such as this, application of any statistical weight factor at any stage *after* extraction of Γ_γ from experiment is meaningless. The Weisskopf unit in terms of which we tabulate $|M|^2$ is computed for the transition of one particle in a featureless, spinless well from a state of $J=k+\frac{1}{2}$ to one of $J'=\frac{1}{2}$; k is the multipole order of the transition and the final state is an s-state. The radiating particle is responsible for the entire spin of the 'nucleus'. Consider now another such one-particle transition of the same type, again in a spinless well, but between states whose spins are not given by the above relationships (say, for example, the final state is not an s-state). Then the statistical weight factor giving the speed of this second transition in terms of that of the first (that is to say in Weisskopf units) is perfectly definite. For electric transitions for example it is (Kennedy and Sharp 1954—whom see for the most complete statement of statistical weight factors in both electric and magnetic transitions):

$$(2J'+1)(2l+1)(2l_1+1)W^2(l_0Jl_1J';\ \tfrac{1}{2}k)\left[C\begin{smallmatrix} l_0 & l_1 & k \\ 0 & 0 & 0 \end{smallmatrix}\right]^2.$$

l_0 and l_1 are the initial and final orbital angular momentum quantum numbers.

state or that at 2·9 MeV, or whether it goes to both. It has here been assumed that the transition is to the ground state only. Any other possibility will introduce a change of less than a factor of two in the value of $|M|^2$ deduced from this datum.

In computing the M1 radiative width of the 8·89 MeV level in ^{10}B an ambiguity arises because of the two alternative values for the competing alpha-particle width ; however these values differ only by a factor two ; we have used the mean of the two values thereby introducing an error of about 40%.

In certain transitions from states in ^{15}O formed in ^{14}N (p,γ)^{15}O we have assumed that the greater part of the radiative width represents transitions to the ground state. This is based on the report that at these resonances the ground state transition is ' relatively intense ', although detailed decay schemes have not been published.

A word is necessary about the choice $J=1-$ for the 9·49 MeV level of ^{14}N since this is not one of the possibilities appearing in the references from which other properties of the transition (to the 5·10 MeV level) are drawn. As mentioned above we believe this to be an E1 transition. The level at 5·10 MeV decays in fairly equal strength to the ground state (1+) and first excited state (0+, $T=1$) of ^{14}N. This seems to fix it as 1+ since 1− would mean that one or other of these two equal-strength branches would be forbidden by the isotopic spin rule. This in turn implies 0, 1, or 2 for the 9·49 MeV state. Zero is eliminated because of the

---

This is the factor that was given explicitly by Moszkowski (1953) for dipole and quadrupole transitions ; Hughes (1954) has given it for $k=1$. It in fact depends only on J and J' and perhaps for this reason the impression has sometimes been given that it is a meaningful factor to apply to a real nuclear transition between states of spin J and J' irrespective of how these spins are made up. However this factor is significant only if we believe there is some sense in supposing that the nuclear spin in both initial and final states is due to one particle only—to the one that is making the radiating jump. This may sometimes be true in low-lying isomeric transitions, but it obviously cannot be true for example in any nucleus of even A or for a transition following the addition of a slow neutron to a nucleus of non-zero spin. And it obviously cannot be true either for the great majority of the light nucleus transitions with which we deal in this survey since so many of the states are produced by rearrangement within a configuration. As soon as we begin to deal with transitions between states whose spins are made by coupling the spins of two or more nucleons together, as is the case for nearly all our light nucleus transitions and indeed for nearly all nuclear transitions except very special cases, the situation is much more complicated and no simple statistical weight factor depending only on J and J' can be specified. Nor does the above expression factor out of the complete statistical weight expression except in rare and particular cases. We therefore see that it would be in general erroneous and confusing to apply to the experimental $\Gamma\gamma$ any statistical weight factor depending only on the spins of the initial and final states and on the multipolarity of the transition.

The application of a statistical factor depending on l_0 and l_1, the orbits between which the radiating particle jumps (which in general have no direct relationship with J and J'), is a different matter. It is certainly meaningful to express the experimental radiative width in terms of that expected for a

observed anisotropy of the gamma-radiation in the reaction ^{13}C (p, γ) ^{14}N; 2 gives a correlation in the wrong sense; 1 gives a correlation in accord with experiment for pure d-waves but with the possibility of a large s-wave admixture.

A further approximate procedure has been resorted to in computing radiative widths from radiative capture cross sections for thermal neutrons. Such cross sections are known for several light elements and in many cases the spectrum of the ensuring gamma-radiation has been measured. Since we are here certain of the parity of the radiating state we may usually be sure of the type of the transition if the spin and parity of the final state are known. It is then possible to compute the associated radiative widths using methods outlined earlier (Wilkinson 1953 b). These estimates may well be in error by a factor of three or so. Where the target nucleus has non-zero spin and where both states corresponding to the two initial spin possibilities may radiate to the final state, it has been assumed that they both do so in computing the radiative width (which has been taken to be the same for both possible transitions, but has been listed only once). The maximum error introduced here is a factor of three. One case has been omitted from these analyses of thermal neutron cross sections, namely ^{7}Li (n, γ) ^{8}Li, which is known (Thomas 1951) to proceed chiefly through *extra*-nuclear contributions to the El matrix element.

The only material admitted to this survey concerns direct measurements of radiative widths or lifetimes of transitions supposed to be largely pure

---

particle making the same basic orbital jump but in a featureless well. To do this we should have to modify the Weisskopf unit (which has $l_1=0$) by what could be called a statistical weight factor, but which would depend only on l_0 and l_1, and not at all on J and J'. It is in terms of such a modified unit that Lane and Radicati (1954), for example, express their theoretical radiative widths, and it is, of course, essential that in attempted one-to-one correspondences this modification be made. But as a rule we do not know l_0 and l_1 and in any case to apply such a factor would to some degree implicitly prejudge the issue of whether the shell model had any relevance for the transition. Even in cases such as transitions in our 1p-shell nuclei where we may be fairly sure in some cases that $l_1=1$, it is still not an easy matter to settle l_0. Take as an example a compound nucleus state formed by adding rather slow protons to a target nucleus. By angular distribution measurements we may find that these added protons are almost entirely s-wave. We are therefore tempted to say $l_0=0$. But it may be that the actual compound nuclear wave-function thereby set up consists predominantly of the target nucleus plus d-wave protons with very little s-wave; the small s-wave admixture however predominates in setting up the state by addition of protons from outside because the centrifugal barrier cuts down the d-wave so strongly. In this case we should really use $l_0=2$, not $l_0=0$. Such considerations make it very difficult to know what basic orbital jump is taking place even if we wish at the outset to commit ourselves to a shell model viewpoint. This makes the application of a statistical weight factor of the orbital type too hazardous a procedure except in especially clear cases.

These considerations lead to the view that in all but very special cases, and certainly in the present case, we should use simply $|M|^2$ in terms of unmodified Weisskopf units and not apply any statistical weight factor.

in multipole character. For a few transitions angular correlation measurements have suggested small admixtures of higher multipoles and so from them an estimate may be made of the partial gamma-ray width appropriate to the higher multipole. However such interpretations are usually ambiguous and in any case the operation of extracting the mixing coefficient is one of notorious delicacy, so this small body of data has been systematically ignored.

As well as actual widths, the following tabulations include limits to widths where these are of interest. It is felt that much valuable information could be obtained from records of *limits* to widths and branching ratios even though no actual determination may have been made.

In the following tables the transitions have been arranged under the various types, within which the sequence is that of increasing mass of the radiating nucleus. E_i is the excitation energy in Mev of the level from which radiation is emitted, and J is its assumed spin ; E_f is the excitation in Mev of the level to which the transition takes place, and E_γ is the energy of the gamma-ray. Γ_γ is the radiative width in ev and $|M|^2$ is this width divided by the Weisskopf unit $\Gamma_{\gamma w}$ appropriate to the type of transition. The meaning of Status has already been explained. The references have been kept as few as possible and the guiding principle has been to quote only the best determination or determinations of the radiative width and to trust that those interested in the history of a particular gamma-ray will be able to work backwards from the quoted reference. An exception is made where the best value is believed to come from unpublished work ; here a reference to earlier published work is also given. Where the quoted width depends on more than one measurement, for example a measurement of total gamma-ray width by one source and of branching ratios by another or a determination of thermal neutron capture cross section by one group and of emitted gamma-ray spectrum by another, both measurements are given as reference. In general no reference is given for the spins and parities of the states concerned or for the type of transition. This information can in most cases be easily found in the review article of Ajzenberg and Lauritsen (1955), whose assessment of the reliability of particular assignments has by-and-large been followed, although it has sometimes been found possible to award Status A even though spins have not been determined with certainty. As explained earlier, in those few cases where assignment as to type has been made on the basis of internal evidence, Status B only has been awarded. The only exceptions made to the rule of not giving references for spins and parities are when the references are not self-evident from Ajzenberg and Lauritsen. A few difficult cases have already been discussed.

In the cases of the reactions ^{12}C (e, e′) ^{12}C, ^{16}O (γ, n) ^{15}O and ^{16}O (γ, p)^{15}N the experimentally-observed transition is 'upwards' from the lower to the upper state; the quoted Γ_γ is that inferred for the 'downward' transition.

§ 3. Discussion of Dipole Transitions

We will discuss first of all the E1 and M1 transitions and then the higher multipoles. A glance at the tables shows that $|M|^2$ displays wide dispersion. This is seen graphically in the following figures.

Figure 1 shows the $|M|^2$ values for E1 transitions plotted against the atomic weight of the radiating nucleus. The closed circles indicate transitions forbidden by the isotopic spin selection rule for E1 transitions ($\Delta T = \pm 1$ when $T_z = 0$) : Radicati (1952), Gell-Mann and Telegdi (1953) ; the open circles represent transitions that do not suffer this inhibition.

Fig. 1

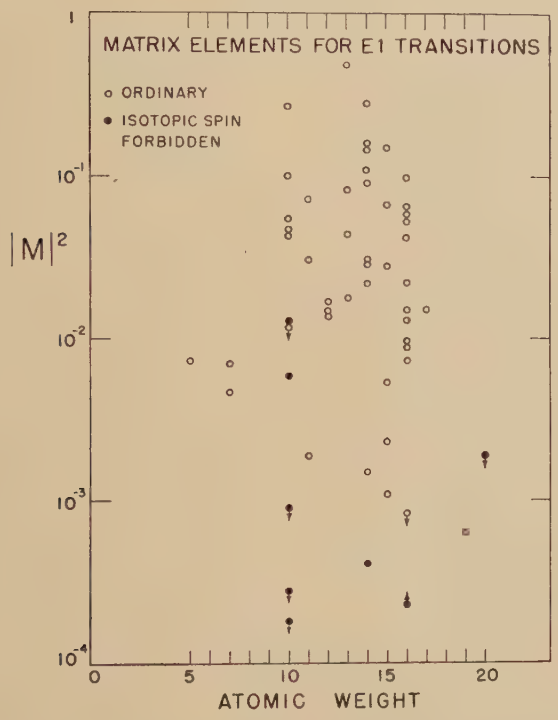

Matrix elements for E1 transitions. Transitions forbidden by the isotopic spin selection rule in self-conjugate nuclei are distinguished. In this figure and in figs. 3 and 6 points have been prevented from overlapping by small upward or downward displacements by their diameter or less. The exact $|M|^2$ values may be taken from the tables.

The effectiveness of this isotopic spin rule has been established in a number of cases additional to those displayed in fig. 1 in experiments where only comparisons are made between transitions of different type and so which are not considered in this survey which concerns itself only with absolute measurements (see Wilkinson 1953 c and MacDonald 1955 for comment) ; but it is also clear from the limited data of fig. 1 that such a discouragement is very marked. The forbidden transitions of high $|M|^2$ value in ^{10}B

Electric Dipole

Reaction	E_i	E_f	E_γ	J	Γ_γ	$\lvert M \rvert^2$	Status	Refs.
^{3}He(d, γ)^{5}Li	16·80	0	16·80	$\frac{3}{2}$	11	$7{\cdot}3\times10^{-3}$	A*	(a)
^{6}Li(p, γ)^{7}Be	6·35	0	6·35	$\frac{1}{2}, \frac{3}{2}$	0·7	$7{\cdot}0\times10^{-3}$	B	(b) (c)
^{6}Li(p, γ)^{7}Be	6·35	0·43	5·92	$\frac{1}{2}, \frac{3}{2}$	0·4	$4{\cdot}7\times10^{-3}$	B	(b) (c)
^{9}Be(n, γ)^{10}Be	6·81	0	6·81	1	7·0	0·043	A	(d) (e)
^{9}Be(n, γ)^{10}Be	6·81	3·37	3·44	1, 2	0·9	0·043	A	(d) (e)
^{6}Li(α, γ)^{10}B	5·11	0	5·11	2	$<0{\cdot}012$	$<1{\cdot}8\times10^{-4}$	B*	(f)
^{6}Li(α, γ)^{10}B	5·11	0·72	4·39	2	$<0{\cdot}012$	$<2{\cdot}8\times10^{-4}$	B*	(f)
^{6}Li(α, γ)^{10}B	5·11	2·15	2·96	2	$<0{\cdot}012$	$<9{\cdot}1\times10^{-4}$	B*	(f)
^{9}Be(p, γ)^{10}B	6·89	0·72	6·17	1	0·7	$5{\cdot}9\times10^{-3}$	B	(g) (h)
^{9}Be(p, γ)^{10}B	6·89	1·74	5·15	1	3·8	0·055	B	(g) (h)
^{9}Be(p, γ)^{10}B	6·89	2·15	4·74	1	0·7	0·013	B	(g) (h)
^{9}Be(p, γ)^{10}B	6·89	5·16	1·73	1	0·7	0·27	B	(g) (h)
^{9}Be(p, γ)^{10}B	7·48	0	7·48	2	21	0·10	A*	(i)
^{9}Be(p, γ)^{10}B	7·48	0·72	6·76	2	<2	$<0{\cdot}013$	A	(i)
^{7}Li(α, γ)^{11}B	9·28	0	9·28	$\frac{5}{2}$	0·8	$1{\cdot}9\times10^{-3}$	B	(j) (k)
^{7}Li(α, γ)^{11}B	9·28	4·46	4·82	$\frac{5}{2}$	1·9	0·031	B	(j) (k)
^{7}Li(α, γ)^{11}B	9·28	6·81	2·47	$\frac{5}{2}$	0·6	0·073	B	(j) (k)
^{11}B(p, γ)^{12}C	16·57	4·44	12·13	2	15	0·015	A*	(l)
^{11}B(p, γ)^{12}C	17·22	0	17·22	1	40	0·014	B*	(l)
^{11}B(p, γ)^{12}C	17·22	4·44	12·78	1	20	0·017	B*	(l)
^{12}C(n, γ)^{13}C	4·95	0	4·95	$\frac{1}{2}$	1·3	0·018	A	(e) (m)
^{12}C(n, γ)^{13}C	4·95	3·68	1·27	$\frac{1}{2}$	0·6	0·48	B	(e) (m)
^{12}C(p, γ)^{13}N	2·37	0	2·37	$\frac{1}{2}$	0·67	0·083	A*	(n)
^{12}C(p, γ)^{13}N	3·51	2·37	1·14	$\frac{3}{2}$	0·04	0·044	A	(o)
^{13}C(n, γ)^{14}C	8·17	0	8·17	1	0·5	$1{\cdot}5\times10^{-3}$	A	(p)
^{13}C(p, γ)^{14}N	8·06	0	8·06	1	10·2	0·031	A*	(q) (r)
^{13}C(p, γ)^{14}N	8·06	2·31	5·75	1	5×10^{-2}	$4{\cdot}1\times10^{-4}$	A	(s) (t)
^{13}C(p, γ)^{14}N	8·06	3·95	4·11	1	1·3	0·029	A*	(q) (r)
^{13}C(p, γ)^{14}N	8·62	6·23	2·39	0	1·4	0·16	B*	(q) (r)
^{13}C(p, γ)^{14}N	8·70	0	8·70	0	46	0·11	A*	(q) (r)
^{13}C(p, γ)^{14}N	8·70	5·69	3·01	0	5	0·28	B	(q) (r)
^{13}C(p, γ)^{14}N	9·18	0	9·18	2	10·6	0·022	A*	(q) (r)
^{13}C(p, γ)^{14}N	9·18	6·44	2·74	2	1·18	0·091	B*	(q) (r)
^{13}C(p, γ)^{14}N	9·49	5·10	4·39	1	8·2	0·15	B	(q) (r)
^{14}N(n, γ)^{15}N	10·83	0	10·83	$\frac{1}{2}, \frac{3}{2}$	4·6	$5{\cdot}4\times10^{-3}$	A	(d) (u)
^{14}N(n, γ)^{15}N	10·83	6·33	4·50	$\frac{1}{2}, \frac{3}{2}$	4·0	0·067	B	(d) (u)
^{14}C(p, γ)^{15}N	11·43	0	11·43	$\frac{1}{2}$	2·3	$2{\cdot}3\times10^{-3}$	A*	(v)
^{14}C(p, γ)^{15}N	11·57	0	11·57	$\frac{1}{2}$	28	0·028	A*	(v)
^{14}N(p, γ)^{15}O	8·79	0	8·79	$\frac{1}{2}$	0·48	$1{\cdot}1\times10^{-3}$	A	(w)
^{14}N(p, γ)^{15}O	9·77	0	9·77	$\frac{1}{2}, \frac{3}{2}$	92	0·15	A	(w)
^{16}O* lifetime	7·12	0	7·12	1	$>0{\cdot}058$	$>2{\cdot}3\times10^{-4}$	A	(x)
^{15}N(p, γ)^{16}O	13·05	0	13·05	1	150	0·098	A	(y)
^{15}N(p, γ)^{16}O	13·05	6·05	7·00	1	$<0{\cdot}2$	$<8{\cdot}4\times10^{-4}$	A	(z)
^{16}O(γ, n)^{15}O	20·33	0	20·33	1	43	$7{\cdot}4\times10^{-3}$	B*	(a^1)
^{16}O(γ, n)^{15}O	20·58	0	20·58	1	54	$8{\cdot}9\times10^{-3}$	B*	(a^1)
^{16}O(γ, n)^{15}O	20·79	0	20·79	1	58	$9{\cdot}3\times10^{-3}$	B*	(a^1)
^{16}O(γ, n)^{15}O	20·93	0	20·93	1	83	0·013	B*	(a^1)
^{16}O(γ, n)^{15}O	21·21	0	21·21	1	143	0·022	B*	(a^1)
^{16}O(γ, n)^{15}O	21·52	0	21·52	1	98	0·015	B*	(a^1)
^{16}O(γ, n)^{15}O	22·37	0	22·37	1	322	0·042	A*	(a^1)
^{16}O(γ, n)^{15}O	22·54	0	22·54	1	480	0·059	A*	(a^1)
^{16}O(γ, n)^{15}O	22·76	0	22·76	1	549	0·066	A*	(a^1)
^{16}O(γ, n)^{15}O	23·02	0	23·02	1	501	0·059	A*	(a^1)
^{16}O(p, γ)^{17}F	3·86	0	3·86	$\frac{7}{2}$	0·6	0·015	A	(b^1) (c^1)
^{19}F* lifetime	0·11	0	0·11	$\frac{1}{2}$	$6{\cdot}7\times10^{-7}$	$6{\cdot}4\times10^{-4}$	A*	(d^1)
^{19}F(p, γ)^{20}Ne	13·70	1·63	12·07	2	2·8	$\sim1{\cdot}9\times10^{-3}$	A*	(e^1)

Magnetic Dipole

Reaction	E_i	E_f	E_γ	J	Γ_γ	$\lvert M \rvert^2$	Status	Refs.
^{7}Li* lifetime	0·48	0	0·48	$\frac{1}{2}$	$4{\cdot}6\times10^{-3}$	2·0	A*	(f^1)
^{7}Be* lifetime	0·43	0	0·43	$\frac{1}{2}$	$3{\cdot}3\times10^{-3}$	2·0	A*	(f^1)
^{7}Li(p, γ)^{8}Be	17·63	0	17·63	1	16·7	0·14	A*	(g^1) (h^1)
^{7}Li(p, γ)^{8}Be	17·63	2·90	14·73	1	8·3	0·13	A*	(g^1) (h^1)
^{7}Li(p, γ)^{8}Be	17·63	4·2	13·4	1	0·45	$9{\cdot}0\times10^{-3}$	B	(i^1)
^{7}Li(p, γ)^{8}Be	17·63	5·4	12·2	1	0·43	0·011	B	(i^1)
^{7}Li(p, γ)^{8}Be	17·63	7·55	10·08	1	0·25	0·012	B	(i^1)
^{7}Li(p, γ)^{8}Be	18·14	0	18·14	1	5·3	0·042	B	(j^1) (k^1)
^{6}Li(α, γ)^{10}B	4·77	0·72	4·05	1	0·15	0·11	B	(f)
^{6}Li(α, γ)^{10}B	5·16	0	5·16	2	0·03	0·010	B	(f)
^{6}Li(α, γ)^{10}B	5·16	0·72	4·44	2	0·15	0·082	B	(f)
^{6}Li(α, γ)^{10}B	5·16	2·15	3·01	2	0·42	0·74	B	(f)
^{9}Be(p, γ)^{10}B	7·56	0·72	6·84	0	4·8	0·72	A*	(i)
^{9}Be(p, γ)^{10}B	7·56	2·15	5·41	0	1·2	0·36	A*	(i)
^{9}Be(p, γ)^{10}B	8·89	0·72	8·17	2	8	0·75	A*	(l^1)
^{7}Li(α, γ)^{11}B	9·19	0	9·19	$\frac{5}{2}$	$<0{\cdot}010$	$<6{\cdot}2\times10^{-4}$	B	(j) (k)
^{7}Li(α, γ)^{11}B	9·19	4·46	4·73	$\frac{3}{2}$	0·4	0·18	B	(j) (k)
^{7}Li(α, γ)^{11}B	9·19	6·81	2·38	$\frac{3}{2}$	0·07	0·25	B	(j) (k)
^{10}B(p, γ)^{11}C	9·70	0	9·70	$\frac{3}{2}$	2·3	0·12	B	(m^1) (n^1)
^{11}B(p, γ)^{12}C	16·10	4·44	11·66	2	70	2·1	A	(l)
^{12}C(p, γ)^{13}N	3·51	0	3·51	$\frac{3}{2}$	0·67	0·74	A*	(n)
^{13}C(p, γ)^{14}N	8·62	0	8·62	0	0·73	0·055	A*	(q) (r)
^{13}C(p, γ)^{14}N	8·62	3·95	4·67	0	3·1	1·48	A*	(q) (r)
^{13}C(p, γ)^{14}N	8·98	0	8·98	1	0·17	0·011	A*	(q) (r)
^{14}C(p, γ)^{15}N	10·70	0	10·70	$\frac{3}{2}$	0·12	$4{\cdot}7\times10^{-3}$	A*	(v)
^{14}C(p, γ)^{15}N	10·81	0	10·81	$\frac{3}{2}$	0·01	$3{\cdot}8\times10^{-4}$	A	(v)
^{14}N(n, γ)^{15}N	10·83	7·36	3·47	$\frac{1}{2}$, $\frac{3}{2}$	2·5	2·8	B	(d) (u)
^{14}N(n, γ)^{15}N	10·83	8·28	2·55	$\frac{1}{2}$, $\frac{3}{2}$	0·9	2·6	B	(d) (u)
^{14}N(n, γ)^{15}N	10·83	9·16	1·67	$\frac{1}{2}$, $\frac{3}{2}$	0·4	4·0	B	(d) (u)
^{14}C(p, γ)^{15}N	11·30	0	11·30	$\frac{1}{2}$	0·25	$8{\cdot}4\times10^{-3}$	A*	(v)
^{14}N(p, γ)^{15}O	8·34	0	8·34	$\frac{1}{2}$, $\frac{3}{2}$	1·3	0·11	A	(w)
^{14}N(p, γ)^{15}O	8·98	0	8·98	$\frac{3}{2}$	0·30	0·020	B	(w)
^{14}N(p, γ)^{15}O	9·04	0	9·04	$\frac{1}{2}$, $\frac{3}{2}$	1·04	0·067	B	(w)
^{19}F(n, γ)^{20}F	6·60	0	6·60	0, 1	0·2	0·033	A	(o^1) (p^1)
^{19}F(p, γ)^{20}Ne	13·19	0	13·19	1	$<0{\cdot}7$	$<0{\cdot}015$	A	(q^1)
^{19}F(p, γ)^{20}Ne	13·19	1·63	11·56	1	$<0{\cdot}9$	$<0{\cdot}028$	A	(q^1)
^{19}F(p, γ)^{20}Ne	13·51	0	13·51	1	$<0{\cdot}02$	$<3{\cdot}9\times10^{-4}$	A	(q^1)
^{19}F(p, γ)^{20}Ne	13·51	1·63	11·88	1	2·3	0·065	A*	(r^1) (s^1)
^{19}F(p, γ)^{20}Ne	13·76	0	13·76	1	$<2{\cdot}1$	$<0{\cdot}039$	A	(q^1) (t^1)
^{19}F(p, γ)^{20}Ne	13·76	1·63	12·13	1	$<3{\cdot}5$	$<0{\cdot}094$	A	(q^1) (t^1)

Electric Quadrupole and Octupole

Reaction	E_i	E_f	E_γ	J	Γ_γ	Type	$\lvert M \rvert^2$	Status	Refs.
^{10}B* lifetime	0·72	0	0·72	1	$1{\cdot}0\times10^{-6}$	E2	2·0	A*	(u^1)
^{12}C(e, e′)^{12}C	4·44	0	4·44	2	$1{\cdot}0\times10^{-2}$	E2	1·7	A*	(v^1)
^{12}C(e, e′)^{12}C	9·61	0	9·61	2	$2{\cdot}0\times10^{-3}$	E2	7×10^{-3}	B	(v^1)
^{11}B(p, γ)^{12}C	16·10	0	16·10	2	3	E2	0·84	A	(l)
^{16}O* lifetime	6·14	0	6·14	3	$6{\cdot}0\times10^{-5}$	E3	7·3	A	(x)
^{16}O* lifetime	6·91	0	6·91	2	$>0{\cdot}038$	E2	$>0{\cdot}50$	A	(x)
^{16}O(γ, p)^{15}N	14·7	0	14·7	2	46	E2	14	B	(w^1) (x^1)
^{17}O* lifetime	0·87	0	0·87	$\frac{1}{2}$	$2{\cdot}7\times10^{-6}$	E2	1·0	A*	(u^1)
^{19}F* lifetime	0·20	0	0·20	$\frac{5}{2}$	$4{\cdot}6\times10^{-9}$	E2	2·4	A*	(y^1)

Table References

(a) Blair, J. M., Hintz, N. M., and van Patter, D. M., 1954, *Phys. Rev.*, **96**, 1023.
(b) Erdman, K. L., Warren, J. B., James, D. B., and Alexander, T., 1954, *Phys. Rev.*, **96**, 858.
(c) Bashkin, S., and Carlson, R. R., 1955, *Phys. Rev.*, **97**, 1245.
(d) Hughes, D. J., *et al.*, 1952, *AEC Unclassified Report* No. 2040.
(e) Bartholomew, G. A., and Kinsey, B. B., 1953, *Canad. J. Phys.*, **31**, 49.
(f) Jones, G. A., and Wilkinson, D. H., 1954, *Phil. Mag.*, **45**, 703.
(g) Carlson, R. R., and Nelson, E. B., 1955, *Phys. Rev.*, **98**, 1310.
(h) Clegg, A. B., and Wilkinson, D. H., unpublished work.
(i) Hornyak, W. F., and Coor, T., 1953, *Phys. Rev.*, **92**, 675.
(j) Bennett, W. E., Roys, P. A., and Toppel, B. J., 1951, *Phys. Rev.*, **82**, 20.
(k) Jones, G. A., and Wilkinson, D. H., 1952, *Phys. Rev.*, **88**, 423.
(l) Beckman, O., Huus, T., and Zupančič, C., 1953, *Phys. Rev.*, **91**, 606.
(m) Way, K., Fano, L., Scott, M. R., and Thew, K., 1950, *National Bureau of Standards Circular* 499.
(n) Seagrave, J. D., 1951, *Phys. Rev.*, **84**, 1219.
(o) Woodbury, H. H., Tollestrup, A. V., and Day, R. B., 1954, *Phys. Rev.*, **93**, 1311.
(p) Hennig, G. R., 1954, *Phys. Rev.*, **95**, 92.
(q) Seagrave, J. D., 1952, *Phys. Rev.*, **85**, 197.
(r) Woodbury, H. H., Day, R. B., and Tollestrup, A. V., 1953, *Phys. Rev.*, **92**, 1199.
(s) Clegg, A. B., and Wilkinson, D. H., 1953, *Phil. Mag.*, **44**, 1269.
(t) Hird, B., Whitehead, C., Butler, J., and Collie, C. H., 1954, *Phys. Rev.*, **96**, 702.
(u) Kinsey, B. B., Bartholomew, G. A., and Walker, W. H., 1951, *Canad. J. Phys.*, **29**, 1.
(v) Bartholomew, G. A., Brown, F., Gove, H. E., Litherland, A. E., and Paul, E. B., 1954, *Phys. Rev.*, **96**, 1154.
(w) Duncan, D. B., and Perry, J. E., 1951, *Phys. Rev.*, **82**, 809; see also Li, C. W., 1953, *Phys. Rev.*, **92**, 1084.
(x) Devons, S., Manning, G., and Bunbury, D. St. P., 1955, *Proc. Phys. Soc.* A, **68**, 18.
(y) Schardt, A., Fowler, W. A., and Lauritsen, C. C., 1952, *Phys. Rev.*, **86**, 527.
(z) Goldring, G., 1954, *Proc. Phys. Soc.* A, **67**, 930.
(a^1) Penfold, A. S., and Spicer, B. M., 1955 (in course of publication).
(b^1) Laubenstein, R. A., Laubenstein, M. J. W., Koester, L. J., and Mobley, R. C., 1951, *Phys. Rev.*, **84**, 12.
(c^1) DuBridge, L. A., Barnes, S. W., Buck, J. H., and Strain, C. V., 1938, *Phys. Rev.*, **53**, 447.
(d^1) Thirion, J., Barnes, C. A., and Lauritsen, C. C., 1954, *Phys. Rev.*, **94**, 1076 (uncorrected for internal conversion).
(e^1) Wilkinson, D. H., and Clegg, A. B., 1953, *Phil. Mag.*, **44**, 1322.
(f^1) Devons, S. (unpublished)—see Ajzenberg, F., and Lauritsen, T., 1955; also Elliott, L. G., and Bell, R. E., 1949, *Phys. Rev.*, **76**, 168 for Li^{7*}.
(g^1) Fowler, W. A., and Lauritsen, C. C., 1949, *Phys. Rev.*, **76**, 314.
(h^1) Walker, R. L., and McDaniel, B. D., 1948, *Phys. Rev.*, **74**, 315.
(i^1) Inall, E. K., and Boyle, A. J. F., 1953, *Phil. Mag.*, **44**, 1081.
(j^1) Kraus, A. A., 1954, *Phys. Rev.*, **93**, 1308.
(k^1) Liberman, D. A., 1955—see § XIV of Ajzenberg, F., and Lauritsen, T. (1955).
(l^1) Mackin, R. J., 1954, *Phys. Rev.*, **94**, 648, and unpublished work.
(m^1) Walker, R. L., 1950, *Phys. Rev.*, **79**, 172.
(n^1) Brown, A. B., Snyder, C. W., Fowler, W. A., and Lauritsen, C. C., 1951, *Phys. Rev.*, **82**, 159.
(o^1) Seren, L., Friedlander, H. N., and Turkel, S. H., 1947, *Phys. Rev.*, **72**, 888.
(p^1) Kinsey, B. B., Bartholomew, G. A., and Walker, W. H., 1951, *Phys. Rev.*, **83**, 519.
(q^1) Clegg, A. B., and Wilkinson, D. H. (unpublished)—see also (e^1).
(r^1) Carver, J. H., and Wilkinson, D. H., 1951, *Proc. Phys. Soc.* A, **64**, 199.
(s^1) Clegg, A. B., Jones, G. A., and Wilkinson, D. H., 1955, *Proc. Phys. Soc.* A, **68**, 538.
(t^1) Farney, G. K., Givin, H. H., Kern, B. D., and Hahn, T. M., 1955, *Phys. Rev.*, **97**, 720.
(u^1) Thirion, J., and Telegdi, V. L., 1953, *Phys. Rev.*, **92**, 1253.
(v^1) Hofstadter, R., and Ravenhall, D. G. (private communication).
(w^1) Spicer, B. M., 1955, *Phys. Rev.*, **99**, 33.
(x^1) Wilkinson, D. H., 1955, *Phys. Rev.*, **99**, 1347.
(y^1) Jones, G. A., Phillips, W. R., Johnson, C. M. P., and Wilkinson, D. H., 1954, *Phys. Rev.*, **96**, 547 (uncorrected for internal conversion).

are anomalously strong and probably represent a very high admixture of $T=1$ in the predominantly $T=0$ state at 6·89 MeV, although they only have Status B and we cannot yet be sure of them. In the coming discussion we set aside such isotopic spin forbidden transitions and consider only the 'ordinary' ones. Figure 2 shows the 'ordinary' E1 transitions grouped according to their $|M|^2$ value. The ordinate is the actual number of transitions in the given range of $|M|^2$; 46 transitions are represented;

Fig. 2

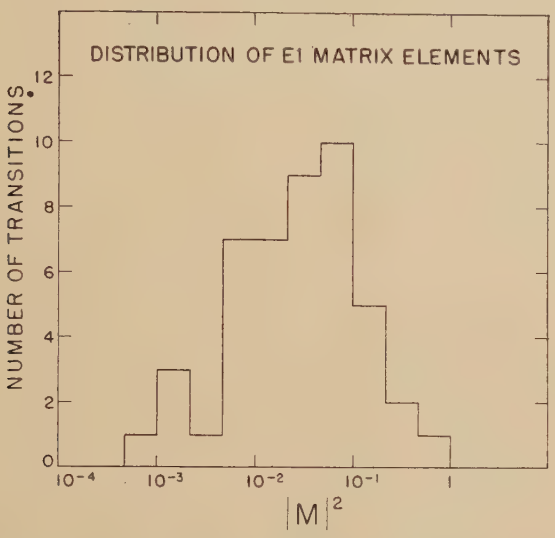

Distribution of E1 matrix elements. Transitions forbidden by the isotopic spin rule are omitted and transitions for whose strength we have only limits are not shown.

those for which only limits are available are not shown. This distribution is a rather tidy one; it centres on $|M|^2=0{\cdot}032$, and a variation by a factor of seven in speed on either side of this value covers 85% of the transitions.* This indicates the degree of reliability of an offhand estimate of the width of an E1 transition in a light nucleus and suggests that the best guess will be $\Gamma_\gamma \sim 0{\cdot}032\Gamma_{\gamma w}$. At the same time we must bear in mind that rather weak transitions do occur, sometimes from the same level as a strong one of the same type: a good example is given by the transitions from the

* We must ask whether the rapid fall of the distribution on the side of low $|M|^2$ is perhaps artificial and really due to the missing of weak transitions, not to their absence. While it is felt that this is largely a genuine fall we must certainly be ready to find many more weak transitions, and again it should be stressed that there is a lot of interest in looking for and comparing all transitions of a given type that can occur from a given radiating level, and at any rate placing and publishing limits on their strengths when the actual transition cannot be detected. This is particularly important for the omnibus comparison of the experimental distributions with the expectations of shell theory—see later.

1— state of ^{16}O at 13·05 Mev to the 0+ ground state and to the 0+ state at 6·05 Mev; the former has a $|M|^2$ value of 0·098, while the latter has $|M|^2 < 8{\cdot}4 \times 10^{-4}$. There seems to be a tendency for the very weak E1 transitions to involve states that are rather unusual in other respects such as the low-lying odd parity state in ^{19}F ($\frac{1}{2}$— at 110 kev) and the pair state of ^{16}O (0+ at 6·05 Mev). It may be that these weak transitions merely emphasize that these states are indeed 'curious' and not very closely related to their neighbours so that they sometimes do not combine very well with them. A similar impression is gained from the few low-lying E1

Fig. 3

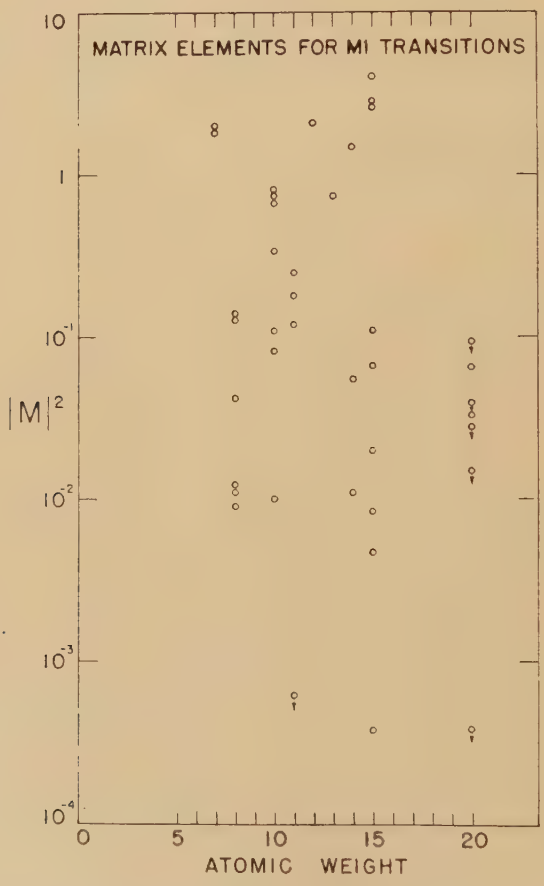

Matrix elements for M1 transitions (see also caption of fig. 1).

transitions established and measured in heavy nuclei (Goldhaber and Sunyar 1955) which all have very low $|M|^2$ values. In all these cases in heavy nuclei the low-lying state with the change of parity is a 'curious' state that has interloped into the expected level structure.

Figure 3 shows the $|M|^2$ values for M1 transitions in the same way as does fig. 1 for E1 transitions. Again we see a considerable spread in

$|M|^2$ values, and this is displayed in the histogram of fig. 4. This distribution is to be compared with that of fig. 2 for E1 transitions; it contains 34 transitions. The M1 distribution differs in two ways from the E1: it is a wider, more rambling distribution—a factor 20 in speed is now needed on either side of the mean before we include 85% of the transitions:

Fig. 4

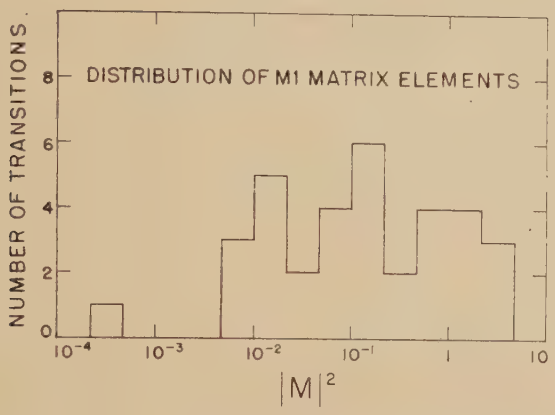

Distribution of M1 matrix elements. Limits are not shown.

secondly it centres on $|M|^2=0{\cdot}15$, which is a factor of 4·7 greater than the corresponding centring point for the E1 distribution. We may now recall the remark of § 1 that, for shell model transitions, we might expect $|M|^2$ values about a factor of four greater for M1 than for E1 transitions because of the diminution in the E1 Weisskopf unit due to the effective charge. This expectation seems to be realized.

The greater spread in the M1 distribution can also perhaps be understood qualitatively in shell model terms. In the first place M1 transitions are somewhat more complicated than E1 since they contain both space and spin contributions and this gives the possibility of greater fluctuations. Secondly M1 transitions take place largely by rearrangements within a given configuration—the 1p shell in the majority of our examples—and this means both that much larger values of the quantity n^2 times the parentage overlap (Lane and Wilkinson 1955) are on occasion possible for them than for E1 transitions, and also that, because of the multiplicity of common parents often associated with transitions within a configuration, small values of the parentage overlap due to cancellation of contributions from the various parents will also tend to occur rather frequently. We contrast this situation with that obtaining for E1 transitions where, because of the change of configuration necessarily involved for the radiating particle, the largest value that can be taken by the square of the product of the fractional parentage coefficients of the initial and final states for any common parent is n^{-1}. This fact must be taken together with the observation that 2s and 1d nucleon interactions with 1p-shell nuclei tend

to display reduced widths of the order of the single-particle value (Lane 1954) which shows that there will often be a unique or almost unique parentage for the initial state. These two remarks imply that we cannot get such big enhancements for E1 as for M1 transitions and also, since the parentage is often almost unique, that we do not have so much possibility of weak transitions due to cancellation of contributions from several parents. All these effects then suggest that the larger spread found for the M1 strengths than for the E1 strengths is in qualitative accord with shell model expectations.

We may now ask whether in fact the shell model can give an account of the actual numerical strengths and spread in strengths that we have displayed in figs. 2 and 4. We have discussed in § 1 how we should in fact expect, within the pure shell model, a rather considerable straggle in the theoretical $|M|^2$ distribution. The situation in respect of M1 transitions is really too complicated to do anything about statistically because of the great multiplicity of parents but, as we have just noted, for the E1 transitions we can assume as a very crude approximation, and neglecting all configuration interaction, that the parentage is unique. This effects an enormous simplification. Consider now an E1 transition from an initial state of quantum numbers L, S, J, T consisting of a 2s or 1d nucleon (the l_0 orbit) plus $n-1$ 1p nucleons into a final state of quantum numbers L', S', J', T' with all n nucleons in the 1p shell. (All but two of our experimental E1 transitions are in 1p-shell nuclei.) We now make our assumption that the initial state has some unique parent in $1p^{n-1}$; the final state has fractional parentage coefficient $\langle|\rangle$ for this parent state whose quantum numbers are L_p, etc. Then (Lane and Radicati 1954):

$$|M|^2=\frac{3n}{4}\left\{U(11LL_p;l_0L')U(1L'JS;LJ')\langle|\rangle U(1\tfrac{1}{2}TT_p;\tfrac{1}{2}T')\times C\begin{matrix}1T'T\\OM_TM_T\end{matrix}\right\}^2$$

where

$$U(abcd\ ;\ ef)=\sqrt{(2e+1)(2f+1)}W(abcd\ ;\ ef).$$

Note that $|M|^2$ in this theoretical formula is not defined in quite the same way as we use throughout this survey in connection with *experimental* transitions. For the experimental transitions $|M|^2$ always means the width in the appropriate Weisskopf units; in the above formula it means the width in terms of that of the appropriate single-particle transition (2s→1p or 1d→1p). There is little difference between the two definitions of $|M|^2$ for these 1p-shell transitions, and it is not here worthwhile to apply a correction factor before comparing the experimental results with the theoretical. In an attempted one-to-one correspondence between a *particular* transition and theory the correction factor to allow for the actual orbits involved is of course essential as is the use of more realistic wave functions than the uniform wave functions of the Weisskopf unit.

As mentioned earlier we do not now attempt the dangerous task of specifying the quantum numbers and parentage relationships of individual

experimental transitions, but rather simply ask how the gross assembly of experimental E1 transitions summarized in fig. 2 compares with the gross assembly of theoretical E1 shell-model transitions computed for the same region of the periodic table and between states whose excitations it is reasonable to suppose might correspond roughly with those of the states actually concerned in the experimental transitions (the review of Inglis (1953) is taken as a guide here). In other words we ask in general terms if the shell model predicts the same sort of $|M|^2$ values and spread in those values that obtain in practice. In this spirit of general enquiry we have therefore used the above expression to compute the theoretical $|M|^2$ values of a great number of E1 transitions (about 250 of them) between states satisfying the above criteria.* These $|M|^2$ were reduced to a histogram as were the experimental values; the smoothed theoretical distribution is shown in fig. 5. It bears a most remarkable resemblance

Fig. 5

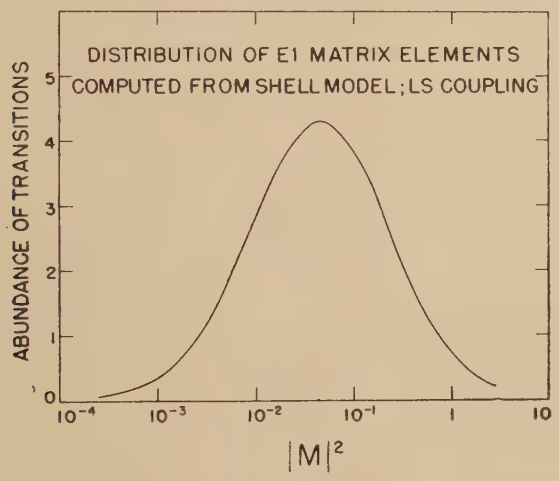

The expected distribution of E1 matrix elements computed in *LS* coupling for 1p-shell nuclei and states of 'reasonable' excitation under the assumption of unique parentage.

in absolute $|M|^2$ values and in spread to fig. 2. While we are very willing to admit that this detailed resemblance is due largely to chance, we feel that we should insist that this computation, or *jeu d'esprit*, does show that the pure shell model predicts that the run-of-the-mill E1 transition in the 1p shell should have a strength much less than a single-particle unit, and that a large straggle in strengths should obtain, just as is found in practice.

* The largest $|M|^2$ value found was 5/3— for the transition $1p^{-1}\,1d$ ($L=1$, $S=0$, $J=1-$, $T=1$) → $1p^{12}$ ($L'=0$, $S'=0$, $J'=0+$, $T'=0$).

We have used *LS* coupling in drawing up fig. 5 because it seems from other data (e.g. Christy 1953) to be the better approximation of the extreme schemes in the 1p-shell ; jj coupling gives a very closely similar distribution —and so, we may feel sure, would any intermediate coupling.

We may notice in this omnibus comparison that the rapid fall of the theoretical shell-model distribution on the side of low $|M|^2$ is reproduced by experiment. However, as we have stressed earlier, the possible importance for the experimental distribution of weak missed E1 transitions, although probably not great, is not really known at the moment, and will not be known until a conscious effort is made to look for and set limits on all transitions of given type that can occur from given levels. If transitions of low $|M|^2$ do not appear in relatively greater abundance than at the moment we may probably construe the agreement between figs. 2 and 5 on the side of low $|M|^2$ as some evidence for the absence of much remote configuration interaction and similar effects in light nuclei at these excitations.

It is of considerable practical interest to see how far we may base determinations of parity change in light nuclei on the strength of gamma-ray transitions. That is, we ask whether we can tell apart E1 from M1 transitions on the basis of their radiative widths. Now although the E1 Weisskopf unit is some 20 to 30 times greater than the M1 unit in our light nuclei, we have seen that $|M^2|$ values are in the mean some four or five times lower for E1 than for M1 transitions and also that each distribution shows a considerable spread. We therefore expect a great deal of overlapping of strengths for transitions of the two types. This is shown in fig. 6 where we display E1 and M1 transitions together, merely taking out the E_γ^3 factor to compare 'reduced' strengths. The open circles are the E1 transitions and the closed circles are the M1 transitions. It is seen that there is indeed a great deal of overlap between the two distributions and that in general we cannot base a distinction on the strength of the transition. It is seen, however, that the very strong transitions tend to be E1 and the very weak ones M1. This former, E1, tendency is made clearer by a few remarks about the strong M1 transitions. The two strong M1 transitions at $A=7$ are the low-lying mirror transitions in ^{7}Li and ^{7}Be. These transitions take place between closely related simple states in an especially favourable manner, and this situation is unlikely to occur again ; and we may therefore regard them as a special case. The fast transitions at $A=15$ are derived from ^{14}N(n, γ)^{15}N ; this derivation of widths from thermal neutron capture cross sections is the least satisfactory of the methods we have employed and, as we have remarked, the error in the deduced widths may be considerable ; in addition, these transitions have only Status B. The fast point at $A=12$ is from the low-lying resonance in ^{11}B plus proton, some of whose cross sections, as Ajzenberg and Lauritsen remark, derive from work of considerable antiquity and uncertainty. So, excluding the special points at $A=7$, there remains only one reliable fast M1 transition above

Γ_γ (ev)/E_γ^3 (Mev)=0·02 as against twenty-odd E1 transitions above the same value. It is felt that if any new transition shows a value of Γ_γ (ev)/E_γ^3 (Mev) greater than 0·02 then there is something like a 10 : 1 chance that it will be E1. As mentioned above we have already used this criterion for classing as E1 transitions four gamma-rays in ^{14}N whose strengths exceeded this limit by factors of three and more.

Fig. 6

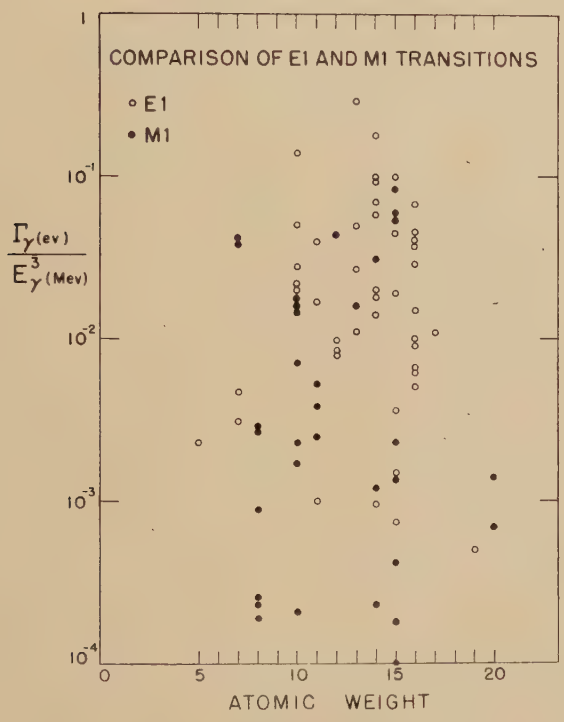

The comparison between E1 and M1 radiative widths after removal of the E_γ^3 factor. Isotopic spin forbidden E1 transitions are omitted as also are all limits and an M1 point at $A=15$ with Γ_γ (ev)/E_γ^3 (Mev)$=8\times10^{-6}$ (see also caption to fig. 1).

Because of the possibility of yet-to-be-discovered long, low-strength tails to both E1 and M1 distributions, we feel that it would be unsafe to base any present recommendation on the apparent predominance of M1 transitions among the weakest gamma-rays.

It was mentioned in § 1 that, when configuration interaction and more complicated effects set in strongly, we must expect a dependence of transition strength on level density to appear, and that such an effect is

manifest among the heavy nuclei. It is therefore of interest to look for this effect in the light nuclei of the present survey. It does not seem to be strongly evident. D, the level spacing in Mev, varies from perhaps three to six for low-lying levels of the lightest nuclei down to about 0·2 for the sequence of 1— levels found in $^{16}O(\gamma, n)^{15}O$, and yet no parallel diminution in $|M|^2$ occurs. Even if exception is taken to this illustration on the ground that these ^{16}O states are in the region of the 'giant resonance' and so perhaps not very typical, yet there remain examples such as $^{13}C(p, \gamma)^{14}N$ where levels are several times as dense as in the lightest elements but radiate just as strongly. It may be that this observation of the relative insensitivity of $|M|^2$ to D means that in these light nuclei for dipole transitions at the excitations with which we concern ourselves, effects such as configuration interaction and multiple-particle excitation have not yet become very important, and that we are indeed dealing chiefly with states whose shell-model description may still be made largely in terms of the change of orbit of one nucleon or rearrangement within a pure configuration. We note that this is also the conclusion at which we have tentatively arrived above if we are to regard the sharp falling-off of the $|M|^2$ distribution at low $|M|^2$ values as genuine. Perhaps with ^{20}Ne we see the beginnings of a dependence of $|M|^2$ on D. It will be of interest for this reason to extend this survey to the region above $A=20$ but at the moment this is not considered very profitable because there is there a definite experimental tendency to establish information about the strongest transitions, and so a distorted picture would be obtained.

There is also no clear dependence of $|M|^2$ on the evenness or oddness of N, Z and A for either the E1 or the M1 transitions. Such a dependence is not especially to be expected from the shell-model computation for E1 transitions or from more general considerations.

§ 4. Discussion of Higher Multipole Transitions

As we may see from the table of E2 and E3 transitions, our knowledge of the higher multipole transitions is very restricted. But already it can be seen that they tend to be fast, some of them very fast. It might be argued that those higher multipole transitions which have inherently low width will be essentially chosen by the experimenter for their large $|M|^2$ value because he will be able to see only the strongest ones. This is a valid criticism at this stage, and would preclude any reliable attempt to systematize, say, E2 transitions in the way we have done for E1 and M1 transitions. It applies to the $^{11}B(p, \gamma)^{12}C$ and $^{16}O(\gamma, p)^{15}N$ entries (and in any case we should strongly discount the strength of this transition in ^{12}C as based on the old and unreliable work referred to in § 3; the true width may well be an order of magnitude less). But it does not apply to the other transitions which we shall now discuss, all of which are based on lifetimes measurement which would have been made more easily had the widths been less rather than more. So although we may not treat

the present sample as representative, we may examine the transitions as individuals, many of which are very instructive.*

The transitions in ^{10}B, from the 4·4 Mev state of ^{12}C, and from the 6·91 Mev state of ^{16}O are fast but not very remarkably so and need not detain us.† The rest, however, contain noteworthy examples which seem to indicate quite clearly that the shell model is not adequate to explain all aspects of radiative transitions in light nuclei; it must be admitted that cooperative model shave a place even below $A=20$.

Consider first the 14·7 Mev transition in ^{16}O. If it turns out that this is indeed an E2 transition as we suppose it to be, we have a very clear contradiction with the shell model which is not capable of finding a $|M|^2$ value greater than 7/5 for this transition—which it gives for LS coupling when we take the upper state as $1p^{-1}1f$ ($L=2, S=0, J=2+, T=0$): it has been suggested (reference (x^1) above) that this may be a one-phonon transition in the Bohr–Mottelson sense, the state at 14·7 Mev being the first state of surface oscillation of ^{16}O. The hydrodynamical parameters needed to describe this experimental transition agree to within a factor of about two with the 'classical' parameters of the Bohr–Mottelson scheme, the senses of departure being those naively expected for a double-closed-shell nucleus such as ^{16}O. Because of the high excitation involved and the attendant breakdown of the adiabatic approximation it may be that this state of surface oscillation is in fact shared among several 'ordinary' states, but most densely around 14·7 Mev. The existence of such a powerful cooperative E2 state as this, although we cannot yet regard it as definitely established, is of great use in discussing the next of these interesting fast E2 transitions, namely that in ^{17}O. This appears to have about the right strength of one Weisskopf unit until one notices that the 'radiating particle' is a neutron and not a proton and so should, on the shell model, give a strength of $|M|^2 \sim (Z/A^2)^2 = 10^{-3}$ rather than unity.‡

* We might at this point mention a curious phenomenon in connection with the transition from the 7·48 Mev 2− state in ^{10}B to the ground state for which Devons and Goldring (1954) have measured the angular correlation of internally-converted pairs. These workers find a pair distribution that is inconsistent with a simple E1 transition but which could be explained if roughly half the radiative width were made up of M2 or E3 radiation. If this half were M2 it would have $|M|^2 \sim 3\times10^3$, while if it were E3 it would have $|M|^2 \sim 10^6$. These figures are so huge and so much in excess even of Z^2 that we cannot accept them at their face value and must suppose that the apparent anomaly of the distribution is due to some unsuspected mechanism or to approximations in the as yet incompletely established theory.

† The parentage situation in ^{10}B is complex and so shell-model calculations are not especially trustworthy. It is, however, difficult to achieve $|M|^2=2$ in any E2 shell-model calculation. The situation in ^{12}C for the 4·44 Mev transition on the other hand is rather simple in both extreme coupling schemes, and we may have more trust in the computation; we find $|M|_{LS}{}^2=14/25$ and $|M|_{jj}{}^2=1/5$.

‡ Actually for a pure one-particle $2s\rightarrow1d_{(5/2)}$ transition such as this the shell model leads us to expect, for a radiating proton, $|M|^2=3$ (see the footnote on statistical weights in § 2). But this factor is of little use against the discrepancy of $\times10^3$.

This transition is therefore an *anathema maranatha* for the shell model. As Thirion and Telegdi (reference (u[1]) above) have remarked, the way out of this dilemma that does least violence to our hope that ^{17}O should a rather good shell-model nucleus (cf. its small ground-state quadrupole moment) is to suppose that there exists somewhere in ^{16}O a 2+ state possessed of a very fast E2 transition to ground which can act as an auxiliary parent for the ^{17}O states and which is responsible for the ^{17}O transition. (In this inverted sense we should rather regard the odd neutron as the parent of both the ^{17}O states, the E2 emission being effected by the one-phonon transitions of the attached ^{16}O.) We now see that the above-discussed fast E2 transition from the 14·7 Mev state of ^{16}O is ideal for this rôle of ' radiating core ' in ^{17}O ; an admixture of about 7% in intensity of this ^{16}O state in the 0·87 Mev state of ^{17}O suffices to explain the observed transition. This does not seem quite unreasonable. The same *deus ex machina* may suffice to explain the too-fast E2 transition in ^{19}F where some such help is certainly needed since addition of neutrons to a proton can never speed an E2 shell-model transition (contrast the situation for E1 transitions).*

The last of these fast transitions is the E3 in ^{16}O. Again the shell model cannot account for so great an enhancement ; the largest shell-model for $|M|^2$ is found in LS coupling and is 5/7 when the upper state is $1p^{-1}1d$ ($L=3$, $S=0$, $J=3-$, $T=0$) (unless we are prepared to go into the g-shell where an enhancement of 9/7 can be found). The increase in nuclear radius of 30% to 40% needed to reconcile this transition with shell-model expectation seems rather implausible and it seems likely that we are again witnessing some sort of cooperative phenomenon. This time it does not seem probable that this is itself a state of surface oscillation since the E3 one-phonon mode is expected at a considerably higher energy

---

* An equivalent way of speaking of these too-fast transitions in ^{17}O and ^{19}F is to say that the motion of the external particles induces a quadrupole distortion of the ^{16}O core, and, since this distortion in the Bohr–Mottelson weak coupling approximation is determined by the number of the external particles and not by their charge, the result is to add a constant effective additional charge to each external particle irrespective of its own proper charge. In this way we can include these anomalous transitions in ^{17}O and ^{19}F within a single scheme (Elliott and Flowers 1955). An even more picturesque alternative view is to think of a neutron's motion as that of a neutral volume in a nucleon fluid of mean charge density e 2 per nucleon volume, which it displaces as it moves so that its motion is equivalent to that of a body of charge $-e$ 2 moving in a vacuum. Some such picture is held by many people who contemplate, say, the independence of E3 transition speed in heavy nuclei on whether the jump is that of a neutron or a proton. The present writer first heard of such a picture from O. R. Frisch. It is a very attractive picture but one which seems difficult to fit in with the idea of shell model orbits since it seems to depend on one nucleon rather actively pushing others out of its way. Perhaps the attempts of Brueckner and his co-workers to reconcile the shell model with strong nucleon–nucleon interactions should permit a quantitative formulation of this notion.

than the E2 which, as we have seen, is quite probably at 14·7 MEV. It is still possible that the transition from this 3— state at 6·14 MEV is speeded by some admixture of the remote one-phonon state (just as that from the 2+ state at 6·91 MEV may benefit by admixture of the one-phonon state at 14·7 MEV). However another possibility resides in the possible applicability of the alpha-particle model for ^{16}O (Dennison 1954). According to this model the 3— state is one of simple rotation of the basic tetrahedron, and although the dynamical properties of the model have not yet been fully worked out, it seems rather likely that it will predict a rather fast E3 decay for this state. This transition will in fact provide a good test for a model that in other respects is not without its difficulties.

§ 5. CONCLUSIONS

We may summarize the findings of this survey of the radiative properties of nuclei of $A \leqslant 20$:

(i) The $|M|^2$ values of E1 transitions show a (logarithmic) distribution which is rather symmetrical about the value 0·032 and of a width such that 85% of observed transitions have a strength within a factor of seven of this value. Isotopic spin forbidden transitions are excepted from this classification and tend to show much smaller widths.

(ii) The $|M|^2$ distribution for M1 transitions centres on $|M|^2 \sim 0{\cdot}15$ from which an excursion by a factor of 20 in strength in either direction is needed to cover 85% of the observed transitions.

(iii) These E1 and M1 distributions are consistent with expectation based on crude shell-model computations.

(iv) It is in general impossible to distinguish between E1 and M1 transitions on the basis of radiative width though if a transition shows a value of Γ_γ (ev)/$E_\gamma{}^3$ (MEV) of greater than 0·02 then it is very probably an E1 transition.

(v) There is no clear dependence, in the 1p shell, of dipole radiative width on level density. There is some suggestion from this and from the shape of the $|M|^2$ distribution for E1 transitions that most states so far met with in light nuclei are rather simple ones. In this connection it is urged that weak transitions are of considerable interest and merit study.

(vi) From the few E2 and E3 transitions so far measured there seem to be clear signs that collective mechanisms such as surface oscillations may have a place in the structure of these light nuclei; the E2 or E3 transition rates predicted by the shell model fall well short of experiment in several cases.

ACKNOWLEDGMENTS

I should like once more very sincerely to acknowledge my debt to F. Ajzenberg and T. Lauritsen for their invaluable compilation.

References

Ajzenberg, F., and Lauritsen, T., 1955, *Rev. Mod. Phys.*, **27**, 77.

Blatt, J. M., and Weisskopf, V. K., 1952, *Theoretical Nuclear Physics* (New York: John Wiley), p. 644.

Bohr, A., and Mottelson, B. R., 1953, *Kgl. Danske Videnskab. Selskab. Mat.-fys. Medd.*, **27**, No. 16.

Carlson, B. C., and Talmi, I., 1954, *Phys. Rev.*, **96**, 436.

Christy, R. F., 1953, *Phys. Rev.*, **89**, 839.

Cooper, L. N., and Henley, E. M., 1953, *Phys. Rev.*, **92**, 801.

Dennison, D. M., 1954, *Phys. Rev.*, **96**, 378.

Devons, S., and Goldring, G., 1954, *Proc. Phys. Soc.* A, **67**, 413.

Elliott, J. P., and Flowers, B. H., 1955, *Proc. Roy. Soc.* A, **229**, 536.

Gell-Mann, M., and Telegdi, V. L., 1953, *Phys. Rev.*, **91**, 169.

Goldhaber, M., and Sunyar, A. W., 1951, *Phys. Rev.*, **83**, 906; 1955, *Beta- and Gamma-Ray Spectroscopy*, Ed. K. Siegbahn (Amsterdam: North Holland Publishing Co.), chap. XVI (II).

Goldhaber, M., and Teller, E., 1948, *Phys. Rev.*, **74**, 1046.

Hughes, D. J., 1954, *Phys. Rev.*, **94**, 740.

Hughes, D. J., and Harvey, J. A., 1954, *Nature, Lond.*, **173**, 942.

Inglis, D. R., 1953, *Rev. Mod. Phys.*, **25**, 390.

Kennedy, J. M., and Sharp, W. T., 1954, *A.E.C.L. Chalk River Report* CRT-580.

Kinsey, B. B., 1955, *Beta- and Gamma-Ray Spectroscopy*, Ed. K. Siegbahn (Amsterdam: North Holland Publishing Co.), chap. XXV.

Kinsey, B. B., and Bartholomew, G. A., 1954, *Phys. Rev.*, **93**, 1260.

Lane, A. M., 1953, *Proc. Phys. Soc.* A, **66**, 977; 1954, *A.E.R.E. Harwell Document* T/R 1289; 1955, *Proc. Phys. Soc.* A, **68**, 189, 197.

Lane, A. M., and Radicati, L. A., 1954, *Proc. Phys. Soc.* A, **67**, 167.

Lane, A. M., and Wilkinson, D. H., 1955, *Phys. Rev.*, **97**, 1199.

MacDonald, W. M., 1955, *Phys. Rev.*, **98**, 60.

Moszkowski, S. A., 1953, *Phys. Rev.*, **89**, 474; 1955, *Beta- and Gamma-Ray Spectroscopy*, Ed. K. Siegbahn (Amsterdam: North Holland Publishing Co.), chap. XIII.

Radicati, L. A., 1952, *Phys. Rev.*, **87**, 521.

Redlich, M. G., 1955, *Phys. Rev.*, **98**, 199.

Thomas, R. G., 1951, *Phys. Rev.*, **84**, 1061.

Weisskopf, V. K., 1951, *Phys. Rev.*, **83**, 1073.

Wilkinson, D. H., 1953 a, *Phil. Mag.*, **44**, 450; 1953 b, *Ibid.*, **44**, 1019; 1953 c, *Nature, Lond.*, **172**, 576; 1955, *Proceedings of the* 1954 *Glasgow Conference on Nuclear and Meson Physics* (London and New York: Pergamon Press), p. 161.

XIII. *The Tensile Strengths of Liquids under Dynamic Loading*

By T. H. Bull
Imperial Chemical Industries Limited, Akers Research Laboratories, Welwyn, Herts.*

[Received October 14, 1955]

Abstract

A method of measuring the dynamic tensile strengths of liquids, involving the use of an electrical pressure bar, is described. Cavitation phenomena in water subjected to large transient tensile stresses have been observed using a spark shadowgraph technique. Under similar conditions of transient loading the cavitation thresholds of water and of glycerol are approximately 17×10^6 dynes/cm^2 and 63×10^6 dynes/cm^2 respectively.

§ 1. Introduction

Experimental determinations of the tensile strengths of liquids have been made by a large number of workers, using a wide variety of techniques, during the last hundred years. Critical discussions of some of the methods have been given by Temperley and Chambers (1946) and by Blake (1949). These surveys reveal that the tensile strength of a liquid may vary by a factor of 100 or more, depending both on the observer and the method; for example, the maximum value claimed for the tensile strength of water is 200 atmospheres (Briggs 1950) while the lowest is 1 atmosphere. It seems reasonable to conclude that the experimental knowledge of the tensile strenths of liquids is meagre and uncertain.

Even the highest experimental value claimed for water falls far short of the theoretical predictions of Temperley (1947), Fisher (1948) and Fuerth (1941). Although these theoretical estimates are deduced using very different approaches to the problem, all three yield values of the tensile strength of water at 17°c of approximately 1000 atmospheres.

The principal difficulty in realizing high tensions in liquids arises from the presence of gaseous or solid nuclei in the liquid. Just as the tensile strength of brittle solids is determined by the size and distribution of Griffith flaws in the material, so the maximum tension a liquid can withstand is limited by the size of gaseous bubbles or unwetted nuclei of solid matter present in that liquid. In practice, the tensile strength of a liquid under static loading is governed by the size of the largest bubble or nucleus present.

The majority of methods for the determination of the tensile strength, or cavitation threshold, of a liquid employ static or quasi-static loading,

* Communicated by the Author.

and bubbles or voids within the sample have time to grow as the tension increases. If, however, a transient tensile stress of short duration is applied to a liquid, any bubbles which tend to become unstable may not have time to enlarge sufficiently, either to be observed photographically or to affect the further transmission of tension. A liquid may therefore remain non-cavitated for quite large stress amplitudes. This effect has been described by Kolsky, Lewis, Sampson, Shearman and Snow (1949) in work on the surface phenomena attending underwater explosions. The present paper describes two types of experiment which are part of a programme of research to investigate cavitation effects in liquids caused by large transient tensile stresses. The experiments reported were made to determine the cavitation thresholds of water and of glycerol under dynamic loading conditions.

§ 2. Experimental Methods

The technique for producing a large transient tensile stress in a liquid is based on the fact that a compression wave incident normally at a free surface is reflected as a wave of tension, which travels through the tail of the compression pulse. The resultant stress at a point within the liquid, at any instant during reflection, may be found by adding the amplitudes of the incident and reflected waves at that point. Figure 1 illustrates this type of reflection for a steep-fronted wave, represented at any point by a discontinuous rise in pressure followed by an exponential decay in

Fig. 1

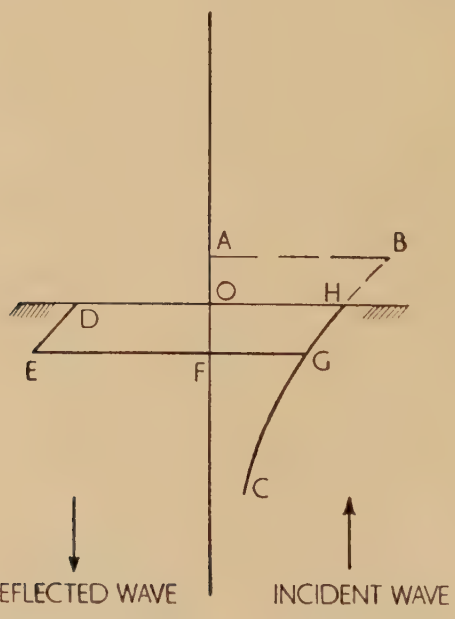

Reflection of a shock wave at free boundary.

time. *ABC* represents the pressure characteristics of such a wave, which has been partially reflected at the free liquid surface *DOH*, the characteristic being shown as a function of distance. The leading portion *ABH* of the shock wave is reflected into the liquid as a tension wave *DEF*, and in this particular case the stress in the liquid at any depth between *O* and *F* is tensile, and equal in magnitude to (*DE–HG*) at the depth concerned. When the value of (*DE–HG*) exceeds the cavitation threshold of the liquid it ruptures and ideally, if the amplitude of the incident wave is sufficiently great, a layer of liquid is thrown up with part of the momentum of the incident wave trapped in it. Reflection of the remainder of the wave then occurs at the new surface created by the detached layer.

By observing the depth at which cavitation occurs, using high-speed photographic methods, during the reflection of a wave of known pressure-time characteristics or by measuring the pressure changes during reflection, it is possible to deduce the cavitation threshold or dynamic tensile strength of the liquid. These two methods are described in this paper. In both cases the test liquid was contained in a vessel through the bottom of which protruded a steel or Perspex rod, supported vertically. The firing of an electric detonator in close contact with the lower end of the rod resulted in a large amplitude compression pulse travelling up the rod and into the liquid.

The electrical pressure bar technique for measuring transient pressure waves in liquids, described in section § 3, was developed by Professor R. M. Davies and his colleagues at University College of Wales, Aberystwyth. The method has been used both for measuring transient pressures in detonating gases (Davies, Edwards and Thomas 1950) and for the measurement of the tensile strengths of liquids under dynamic stressing (Davies, Lewis, Rees and Trevena 1955).

§ 3. The Measurement of Pressure Changes below a Free liquid Surface During the Reflection of a Compression Pulse

3.1. *Apparatus*

(a) General

The arrangement of the apparatus is shown diagrammatically in figure 2. The test liquid was contained in a steel cylinder, length 18 in. with a nominal bore of 1 in. and outer diameter $1\frac{1}{2}$ in. A silver-steel rod (hereafter called the firing rod), 1 in. diameter and length 4 ft. was sealed into the bottom of the cylinder. Both ends of the rod were carefully ground. The bore of the cylinder was such that the rod made a good sliding fit into it. A stress wave was produced in the firing rod by exploding a Nobel's No. 6 electric detonator in close contact with a cylindrical hardened steel anvil wrung on to its lower face.

Transient pressures at a point in the liquid were measured using an electrical pressure bar with a parallel-plate condenser microphone (Davies 1948). The pressure bar, of silver steel, diameter $\frac{1}{2}$ in. and 3 ft. long,

was sealed into the side of the cylinder at its mid-point. The face of the measuring bar in contact with the liquid was machined flush with the inner wall of the cylinder. It was essential that neither the initial compression pulse set up in the firing rod nor the pulses produced in the measuring bar should be distorted during passage through the container seals. Following numerous tests, the most suitable seals for this purpose were found to be Weston Oil seals, which are manufactured complete with metal housing. The characteristics of the stress wave in the firing rod could be measured using a cylindrical condenser microphone placed at any desired position on the bar.

Fig. 2

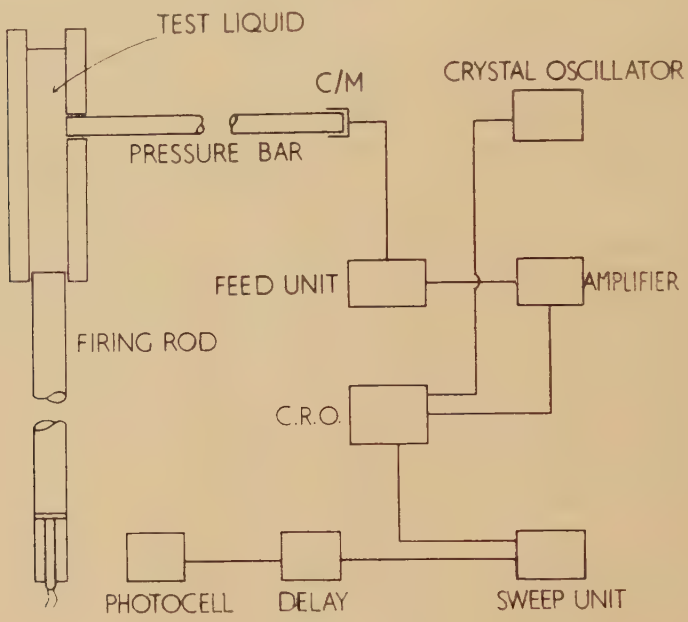

General arrangement of apparatus.

The output of the electrical pressure bar feed unit was amplified and displayed upon one set of Y-plates of an independent-gun, high-speed cathode-ray oscillograph. A 100 kc/s crystal oscillator, connected to the second pair of Y-deflector plates, provided a time calibration for the traces. Both pairs of X-plates of the cathode-ray oscillograph were connected across a balanced, single-sweep time base unit (Kolsky 1949). A brightening pulse for the oscillograph was derived from the sweep unit. The oscillograph traces were recorded with an $f/1{\cdot}0$ lens camera upon Ilford H.P.3 plates.

Light from the detonator explosion was picked up by a photocell and the resulting pulse amplified before being delayed by a variable thyratron-controlled RC delay circuit. A sharp-fronted pulse from the cathode

circuit of the final thyratron triggered the sweep unit a few microseconds before the stress pulse in the measuring bar arrived at the condenser microphone.

(*b*) *The electrical pressure bar*

Descriptions of the use of an electrical pressure bar for the measurement of transient pressures have been given in papers by Davies (1948) and Kolsky (1949). It is shown that if a plane compression pulse is propagated in a cylindrical bar under the conditions that (*a*) the pressure does not exceed the elastic limit of the material, and (*b*) the pulse is long in duration compared with the time taken to travel a distance equal to the diameter of the bar, then the following relations hold

$$c=(E/\rho)^{1/2} \quad \text{and} \quad p=\rho cv$$

where c=velocity of propagation of the pulse, E=Young's modulus for the bar material, v=particle velocity at any point, p=pressure amplitude at that point, ρ=density of the material.

At the free or measuring end of the bar a compression pulse is reflected as one of tension and vice versa. The velocity of the end of the bar is therefore twice the corresponding particle velocity associated with a pulse travelling in the bar remote from either extremity. Thus if the displacement of the end of the bar is x at time t after the arrival of the pulse we have

$$p=\tfrac{1}{2}\,\rho c(dx/dt).$$

A parallel-plate condenser microphone records the variation of x. If the time interval during which the variation takes place is known, together with ρc for the bar material, then the pressure–time relation of the pulse may be found.

In the experiments described here the pulse duration was about 35 microseconds, and the maximum pressure recorded with the bar approximately $7{\cdot}7\times10^7$ dyn/cm^2 or 0·5 tons/in.^{2}. The time taken for a compression pulse to travel $\frac{1}{2}$ in., the diameter of the pressure bar, is about 2 microseconds, and the elastic limit of silver steel is of the order of 30 tons/in.^{2}; thus the pulses were propagated through the pressure bar with very little distortion.

Ideally, the sensitive element of a mechanical device for measuring transient pressures should be dimensionless, in order that the pressure over the element should be uniform at all times during the passage of the transient across it. A 35 microsecond pulse in water has a length of approximately 5 cm, whilst the diameter of the bar used in the experiments was 1·27 cm, hence the ideal conditions were not realized here. This factor was, to a certain extent, offset by the use of a cylindrical condenser microphone on the firing rod, which provided a check of the characteristics of the pulse entering the liquid.

3.2. *Results*

Two series of experiments were performed using first untreated tap water and then glycerol as the test liquids. The procedure was first to line up the sensitive face of the measuring bar flush with the inner face of the cylinder. The cylinder was then filled with the test liquid to a known height above the end of the measuring bar and allowed to reach temperature equilibrium with the surroundings. The separation between the insulated plate of the condenser microphone was adjusted with slip gauges. The detonator was then fired and the output of the condenser microphone feed unit, suitably amplified, recorded with the high-speed cathode-ray oscillogrpah. This was repeated for various distances of the measuring bar below the free surface. In order to determine the initial form of the compression pulse in the liquid, the cylinder was filled until the depth of liquid above the measuring bar was 20 cm, and the procedure repeated. Under these conditions there was no interference, at the pressure device, between the initial wave and any reflected wave.

Figure 3(*a*) (Plate 9) is an enlargement of a plate taken with 20 cm of water above the end of the measuring bar. The upper trace is a timing wave with a frequency of 100 kc/s, increasing time being measured from left to right. The lower curve is due to the amplified transient voltage from the condenser microphone. It will be seen that after the initial rise in voltage due to the compression pulse, the voltage remains constant and is followed by a number of oscillations due to dispersion in the bar. In fig. 3(*b*), which is an enlargement of the record obtained with 1·0 cm of water above the measuring bar, the initial rise in voltage, due to the initial compression pulse, is followed by a sharp decrease, lasting for about 10 microseconds, and then a more gradual and sustained decrease with small oscillations superimposed on it. The sharper decrease is due to the effect of reflection of the compression pulse at the free surface. To determine the variation of pressure below the surface with time at a given point, the displacement time curves were differentiated numerically.

Figure 4 gives curves showing the variation of maximum observed tension in the two test liquids with distance of the measuring bar below the free surface. No existence of tension was observed at distances greater than about 4·3 cm below the free surface. The maximum tensions observed were $18\times10^6(\pm5\%)$ dyn/cm^2 for water and $63\times10^6(\pm5\%)$ dyn/cm^2 for glycerol. It was considered that possibly these figures gave only an indication of the tension at which these liquids cavitated at the face of the measuring bar. Therefore, the high-speed photographic method of determining cavitation thresholds, described in § 4, was used to investigate cavitation in water.

§ 4. Photography of Cavitation in Water

The spark shadowgraph method was used to record the type of transient cavitation with which this paper is concerned. This method is useful because not only may very short exposure times (<1 microsecond) be

obtained using spark gaps in air but the auxiliary equipment is exceedingly simple. Further, the density changes in a fluid caused by a pressure wave give rise to corresponding changes in refractive index and, owing to the deviation of light caused by these changes, the pressure distribution in the fluid may be ascertained at any instant.

Fig. 4

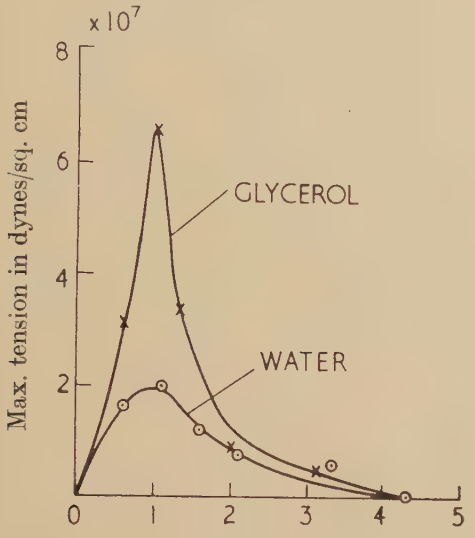

4.1. *Apparatus*

The liquid was contained in a large, rectangular metal tank with two parallel plate-glass sides. A Perspex rod, diameter 1 in. and 4 ft. long, supported vertically, passed through a Weston Oil seal into the centre of the base of the tank. An electric detonator, fired against a $\frac{1}{8}$ in. hardened steel anvil wrung to the lower face of the Perspex rod (firing rod), resulted in a compression wave travelling up the rod and into the liquid. Perspex was chosen as the material for the firing rod since its acoustic impedance is only about twice that of water, giving a pressure amplitude transmission of approximately 70%.

Supported parallel to and 8 cm away from one of the glass windows of the tank was a photographic half-plate behind a mechanically operated shutter. The spark shadowgraph was recorded on this plate by light from an enclosed point-source spark gap, positioned 98 cm from the other glass window and level with the surface of the liquid. The spark gap electrodes, with an emission area of 4×10^{-2} cm^2, were constructed of aluminium and supported in a cylinder of similar material. The spark was produced by the discharge of a 0·1 microfarad condenser, charged to 10 kv, across the electrodes. The condenser was specially selected for its low resistance supports and plates. The mechanical arrangement of the

spark gap and condenser was such that the inductance of the discharge loop was a minimum.

Light from the detonator explosion was picked up by a photocell and the ensuing electrical impulse used to trigger both a microsecond counter and a preset *RC* delay circuit. The delayed pulse triggered the spark gap. A second photocell unit was triggered by part of the light emitted from the spark gap and provided a pulse which stopped the microsecond counter. A record was therefore obtained of events occurring in the tank and of the time between the firing of the detonator and the peak output of the spark gap.

The characteristics of the initial pulse of compression in the firing rod were measured with a cylindrical condenser microphone. The surface of the Perspex rod was used as the earthed conductor of the condenser system and for this purpose was coated with a smooth, even layer of graphite over required regions. The determination of the shape and amplitude of the compression pulse in the liquid, as a function of distance from the upper face of the firing rod, was made in auxiliary experiments. An electrical pressure bar was sealed horizontally into one side of the tank in such a way that only its sensitive face, machined plane, was in contact with the liquid. The face of the bar was positioned perpendicular to, and directly above the upper face of the firing rod. The distance between the measuring bar and firing rod was varied by moving the latter vertically.

4.2. *Results*

With a depth of 8 cm of water above the end of the firing rod a series of shadowgraphs was obtained of cavitation effects at increasing times after the firing of the detonator. The first five photographs of fig. 5 (Plate 10) are of such shadowgraphs, with times after detonation given below each.

The plate at 537 microseconds was taken before the compression wave had been transmitted to the water. The upper end of the firing rod is shown at the bottom of the picture, and the free water surface is indicated by the horizontal black line near the top. At 575 microseconds the compression wave has been transmitted to the water. In this photograph appear two sets of bands, each set consisting of a dark band followed by a lighter one. The upper set of bands, which are rather faint, but which can be clearly seen on the original plate, is very narrow and represents the position of the head of the compression wave. The origin of the broader bands will be discussed later. This identification of the upper bands is supported by the evidence in the sixth photograph. Here a large depth of water was used and a steel plate arranged obliquely in the tank. The photograph shows the narrow set of bands, representing the head of the wave, near the upper edge of the photograph and also the reflection of the wave at the steel plate, giving rise to a wavefront moving from left to right in the picture. Referring again to the photograph taken at 575 microseconds, a disc of cavitated water appears on the face of the firing rod with a few cavitation bubbles above it.

At 592 microseconds the head of the compression wave has advanced further into the water, and a multitude of secondary wavelets appear to originate from a point a few centimetres below the end of the rod. The photograph at 611 microseconds shows the cavitation about to develop below the free surface, since part of the initial wave has already been reflected. At 625 microseconds the cavitation has developed quite considerably. The bubbles at the lower edge of the cavitated region are smaller than those in the centre, the latter region having been under hydrostatic tension for a greater period. A region of non-cavitated liquid exists immediately below the free surface, indicating that here the liquid was able to withstand the transient tensile stress applied to it.

The broad set of bands appearing in some of the photographs are assumed to indicate the tail of the compression pulse, although the reason that they are so well defined is uncertain. The large bubble or group of bubbles which always forms on the face of the firing rod grows with time and then collapses, the whole process lasting about 1·5 milliseconds. There are two possible explanations of this effect. First, it is known (Davies 1948) that the very sharp compression pulse produced by an explosive in contact with the end of a cylindrical bar is lengthened as it travels along the bar. For steel the pulse reaches an approximately stable form after it has travelled a distance equal to about twelve times the diameter of the bar; for Perspex this distance is much greater owing to the added effects of the absorption. The stable form of the pulse consists of a main compression pulse followed immediately by a train of high frequency oscillations which extend into the tensile region. The reflection of the tensile portion of the pulse at the Perspex-water interface results in the end of the rod moving momentarily away from the liquid, this movement being sufficient to cause cavitation at the end of the rod. The second possibility arises from the fact that here we are dealing with hydrostatic pressures, which act equally in all directions. The liquid, while under compression, tends to flow radially outward from the face of the rod, leaving a vapour-filled cavity at the interface.

The spark shadowgraphs show only the central section of the cavitated zone, since the width of the photographic plates was only one-third that of the tank. The full extent of the cavitated zone is shown in fig. 6, Plate 11. The photograph shows the transient cavitation in water a few microseconds after the initial compression wave has been completely reflected at the free surface immediately above the rod. The event was recorded with a quarter-plate camera, the illumination being provided by a Mullard L.S.D.2 flash tube. These flash tubes give an effective exposure of about 1 microsecond, if adequate care is taken in the selection of discharge condenser, and the inductance and resistance of the discharge loop kept to the minimum. The main cavitated zone is lenticular in form. A region of non-cavitated water remains between this zone and the water surface, indicating that here the water has been able to withstand the applied tension. The height of the upper limit of the cavitated

zone decreases with distance out from the axis of the firing rod. This effect might be expected from the geometry of the system. The greater the distance from the axis of the bar the weaker the reflected wave becomes, and has therefore to travel a greater distance through the tail of the compression pulse before the necessary negative pressure to cause visible cavitation is reached. The lower limit of the cavitated zone indicates that the front of the compression wave is approximately spherical in form.

In order to estimate the cavitation threshold of water from the spark shadowgraphs, it was required to know the shape and amplitude of the wave impinging on the free surface. Using the arrangement described earlier, the transient pressure was measured as a function of the vertical distance R above the firing rod. The depth of water above the measuring bar and the dimensions of the tank were such that the initial wave was measured before any reflected waves arrived at the detector. The pressure amplitude at zero distance was computed from a knowledge of the stress amplitude in the Perspex rod, given by measurements with the cylindrical condenser microphone, and the relative acoustic impedance of Perspex and water. The pressure amplitude varies as $R^{-0\cdot9}$ for values of R between 0 and 2·5 cm and as $R^{-1\cdot2}$ for R between 2·5 and 8 cm. Theoretically the propagation of a small-amplitude spherical wave from a point source in an ideal infinite fluid results in the pressure amplitude decreasing as R^{-1} where R is the radial distance from the source. In the apparatus described here, the arrangement was equivalent to a piston-like source in an infinite medium for small values of R. For distances from the piston comparable with the piston diameter, the propagated wave is intermediate between a plane and a spherical form, hence the pressure amplitude does not decay as rapidly as R^{-1}. At larger values of R, departure from the acoustic case becomes more pronounced for a different reason; the pressure amplitude falls off more rapidly than R^{-1}, owing to absorption brought about by inhomogeneities in the water.

The simplest and most direct way of estimating the cavitation threshold P_c from the shadowgraphs is to base the measurements on the upper limits of the cavitated region. Figure 8 shows diagrammatically the stress distribution in a liquid with an infinite value of P_c when a compression wave has been completely reflected normally at a free surface. The stress distribution is indicated by the solid lines and is shown for two waves of differing amplitude. If now the liquid cavitates under a tension P_c, the upper limit for cavitation is the line AB in the case of wave (a) and CD for wave (b). These limits are indicated in the shadowgraphs. To convert measurements on the shadowgraphs to corresponding distances in the central vertical plane of the tank a spark shadowgraph was taken of a wire grid placed in this plane. The shadowgraph had a magnification of 1·2 diameters.

Measurements made with water depths of 8 and 10 cm indicated that the minimum tensile stress required to cavitate water was about 15×10^6dyn/cm^2.

Fig. 7

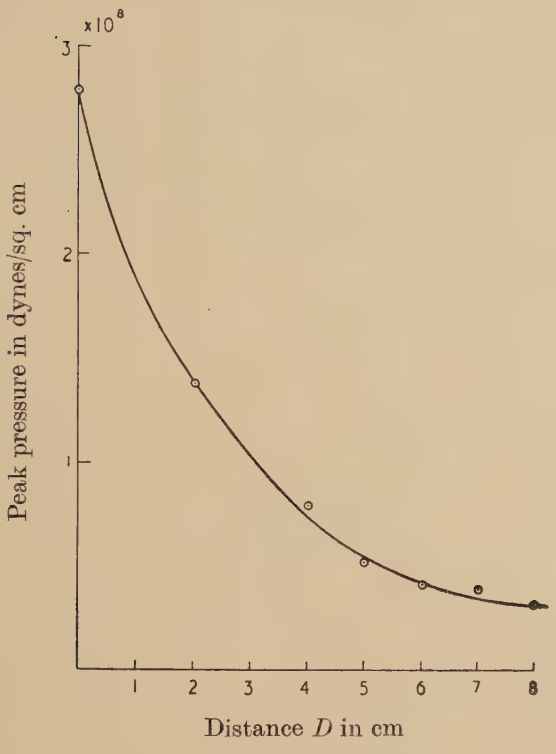
x10⁸
3
2
1
Peak pressure in dynes/sq. cm
1
2
3
4
5
6
7
8
Distance D in cm

Fig. 8

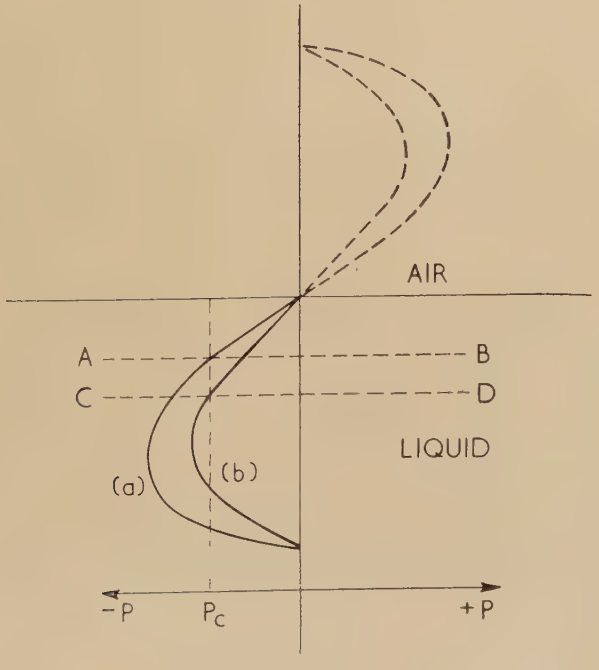
AIR
A
B
C
D
LIQUID
(a)
(b)
-P
Pc
+P

§ 5. Discussion

It is of interest to compare the cavitation threshold of water, found from photographic measurements, with the maximum tensile stress of 18×10^6 dyn/cm^2 recorded using the pressure bar technique. The photographic technique gives a measure of the minimum tension necessary, at the particular loading employed, for nuclei in the water to become unstable and grow to a visible size. The electrical pressure bar measurements indicate the extent to which a cavitated liquid may continue to transmit tension. From these considerations it is to be expected, as found in the experiments described here, that the electrical pressure bar would yield slightly higher results.

The equation of static equilibrium for a spherical bubble in the body of a liquid is

$$p_0=p_i-2\sigma/R$$

where p_0 and p_i are the external and internal pressures respectively, and σ is the macroscopic value of the surface tension. The condition that the bubble should grow is that p_0 be reduced below the value $p_i-2\sigma/R$. Taking the mean value of 16×10^6 dyn/cm^2 as the cavitation threshold of water, the minimum radii of the bubbles which become unstable under tensions greater than this were of the order of 10^{-5} cm. This is many times the molecular dimensions, hence the cavities which became unstable were almost certainly gas or vapour filled bubbles.

The lowest resonant frequency f of a bubble in a liquid is given by Smith (1935) as

$$f=\frac{1}{2\pi r}\left\{\frac{3\gamma[p_0+(2\sigma/r)]-2\sigma/r}{\rho}\right\}^{1/2}$$

where ρ is the density of the liquid, p_0 the hydrostatic pressure, γ the ratio of specific heats of the gas, and σ the surface tension. The lowest natural pulsation period of an air or vapour filled bubble in water with a radius of 10^{-5} cm is thus about 10^{-8} seconds. The duration of the transient tensile stress was about 30 microseconds, i.e. much greater than the pulsation period of the bubbles or nuclei, which therefore had time to enlarge. Strasberg (1955) has shown that for water the maximum radius $R_{\max}$ to which a bubble grows is given by the approximate relation

$$R_{\max}=T\{\Delta p/\rho\}^{1/2}$$

where Δp is approximately numerically equal to the peak amplitude of the transient pressure and T its duration. In the experiments described in § 4 the peak amplitude of the negative pressure transient was about $3{\cdot}3\times10^7$ dyn/cm^2. Substitution in the equation above yields $R_{\max}=0{\cdot}17$ cm. This value is in good agreement with the maximum radius of 0·1 cm for bubbles observed in these experiments.

The maximum tensile stress recorded in glycerol was approximately $6{\cdot}3\times10^7$ dyn/cm^2, i.e. roughly four times that recorded in water. At 17°C the surface tensions of glycerol and water are about the same, whilst the viscosity of glycerol is nearly fifteen hundred times that of water.

As no attempt was made to degas or purify these liquids it would seem reasonable to assume that viscous forces markedly affect the growth of cavities or bubbles in liquids under transient tensile loading.

Acknowledgments

The author wishes to thank Dr. H. Kolsky for valuable discussions and advice during the course of this work.

References

Blake, F. G., 1949, *Harvard Univ. Acoustics Research Laboratory, Technical Memo.* 9.

Briggs, L. J., 1950, *J. Appl. Phys.*, **21,** 721.

Davies, R. M., 1948, *Phil. Trans. Roy. Soc.* A, **240,** 375.

Davies, R. M., Edwards, D. H., and Thomas, D. E., 1950, *Proc. Roy. Soc.* A, **204,** 17.

Davies, R. M., Lewis, G. M., Rees, N. J. M., and Trevena, D. H., 1955, *Symposium on Cavitation in Hydrodynamics*, N. P. L., Paper No. 5.

Fisher, J. C., 1948, *J. Appl. Phys.*, **19,** 1062.

Fuerth, R., 1941, *Proc. Camb. Phil. Soc.*, **37,** 276.

Kolsky, H., 1949, *Proc. Phys. Soc.* B, **62,** 676.

Kolsky, H., Lewis, J. P., Sampson, M.T., Shearman, A. C., and Snow, C. I., 1949, *Proc. Roy. Soc.* A, **196,** 379.

Smith, F. D., 1935, *Phil. Mag.*, **19,** 1061.

Strasberg, M., 1955, *Symposium on Cavitation in Hydrodynamics.* N.P.L., Paper No. 6.

Temperley, H.N.V., 1947, *Proc. Phys. Soc.*, **59,** 199.

Temperley, H. N. V., and Chambers, Ll. G., 1946, *Proc. Phys. Soc.*, **58, 420.**

XIV. *Angular Correlation Measurements on* ^{88}Sr

By C. F. Coleman
Atomic Energy Research Establishment, Harwell*

[Received October 21, 1955]

Abstract

Three semi-circular focusing spectrometers, making use of a common magnetic field, have been used to measure the angular correlation of the internal conversion electron pairs produced in the decay of the 1·85 Mev state of ^{88}Sr. The results support the assignment 2+ for this state. Similar equipment has been used to measure the angular correlation of certain conversion electron cascades. With a polarimeter having good energy resolution, direction–polarization measurements have been carried out on the 0·90, 1·85 Mev gamma-ray cascade in ^{88}Sr. These show that the 1·85 and 2·75 Mev levels in this nucleus have even and odd parity respectively.

§ 1. Introduction

The measurement of gamma-ray angular correlations has proved a powerful technique for determining nuclear spins and multipole mixture ratios (Kraushaar and Goldhaber 1953, Steffen 1954), particularly in even–even nuclei, for which the ground state spins are known to be zero, and transitions to the ground state must be pure multipoles. Occasionally, however, cascade transitions occur in which the conversion coefficients are so great that only conversion–gamma or conversion–conversion correlation measurements will give adequate coincidence rates. Such measurements encounter several difficulties. If the conversion coefficient of the final transition is appreciable ($\gtrsim 5\%$) the lifetime of the intermediate state is likely to be long enough ($\gtrsim 10^{-9}$ seconds) for perturbation effects to be serious. To minimize scattering the sources must be very thin, so that material of high specific activity is required, and the techniques successfully employed to minimize perturbations in gamma–gamma correlations are difficult to apply. Finally, conversion electron spectra are usually rather complex, so that apparatus with good energy resolution is required to isolate and observe particular transitions. Siegbahn (1952) has described a system of two thin lens ring-focusing spectrometers which can be used for this purpose. Equipment described later in this paper achieves the same end by much simpler means, though with some loss in resolution and flexibility.

* Communicated by the Author.

The angular correlation between internal conversion electron pairs (Horton 1948) can also be measured with this equipment. Since such a measurement involves only one transition its interpretation is fairly straightforward, and perturbation effects do not arise. On the other hand the energy of the transition must be well in excess of 1 Mev, and the conversion coefficients are very small ($\lesssim 10^{-3}$). To avoid interference from external pair creation very thin sources are again required. The most serious obstacle to such measurements is the fact that the transition in which the pairs are produced is usually preceded by beta radiation with a maximum energy exceeding that of the pair spectrum. Calculations suggest that even under these conditions it should be possible, by using the shortest resolving times at present available, to obtain pair coincidence rates approaching ten counts per hour which account for the greater part of the total coincidence rate. Because of the strong dependence of this correlation on multipole order and parity, such rates will still be large enough to determine these parameters.

For the determination of relative parities the most generally useful correlation is the gamma polarization–direction correlation. The realization that the standard polarimeter can be used as a low resolution Compton spectrometer (Bishop and Perez 1955, Wood and Jastram 1955) has enabled this type of measurement to be carried out on moderately complex decay schemes. In the present paper a technique is described which gives considerably better resolution without any loss in the overall efficiency of the polarimeter.

§ 2. Equipment for Electron Angular Correlation Measurements

The apparatus to be described makes use of conventional semi-circular focusing in a uniform magnetic field. Figure 1 shows electron orbits, projected on a plane perpendicular to the applied field, for two spectrometer systems, with focusing radii r_1 and r_2, receiving electrons from a common source. It is clear that if one of the spectrometer systems is rotated about the field line through the source the angle θ between the average directions of emission of the electrons accepted by the two systems will be changed, but the energy selection conditions will be completely unaffected. The magnetic field can be adjusted to bring electrons of any desired energy into focus in one of the spectrometers, and electrons of some other energy, which can also be given any desired value by suitable choice of the ratio r_1/r_2, will be simultaneously focused in the other. Thus this system provides all the essential facilities of what Siegbahn has called a ' spectro-goniometer '. It does, however, expose the source to a field of up to a few hundred oersteds perpendicular to the plane of observation, which could produce an appreciable perturbation of the angular correlation to be measured if the intermediate state half life were $\gtrsim 10^{-8}$ seconds.

Geometrical conditions in the spectrometers can be made broadly similar to the ' high source ' specification (Geoffrion 1949), with one important exception. To collect electrons with equal efficiency from all points on the surface of the source, each exit slit must be wide enough to accept the whole image of the source, including all its aberrations. To reduce these it is desirable to reduce the height of the source to about half the height of the exit slit for the spectrometer of smaller radius. Failure to satisfy this condition leads to the coincidence line-sharpening effect noted by Fowler and Shreffler (1950), and might easily produce spurious anisotropies. It is experimentally convenient to use a fixed value for the greater of r_1, r_2, so that each measurement requires a new set of baffles to give the appropriate value of r_1/r_2.

Fig. 1

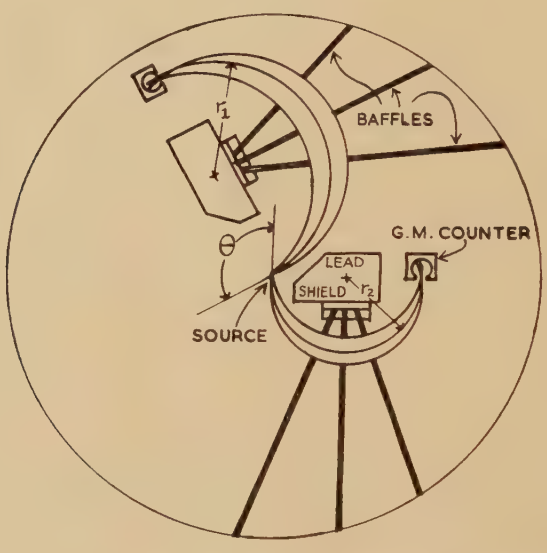

Layout for electron–electron angular correlation measurements.

For the experiments described below the solid angle of collection was fixed at 0·12 steradians, and the greater of the two spectrometer radii at 6 cm. This allowed the whole system to be set up in an evacuated cylindrical chamber 11 in. in diameter and $2\frac{1}{2}$ in. high. Each spectrometer unit was made up of a set of baffles, an exit slit, a geiger counter, and a gamma-ray shield, and could be rotated by making the appropriate changes in the positions of these four components. Since there was very little room in the experimental chamber, small geiger counters were made up with side windows of $2\frac{1}{2}$ mg/cm^2 mica covering bridged slots, 2 in. high and 7 mm side, just large enough to admit the image of the source produced by the 6 cm radius spectrometer. These counters were found to be capable of working into coincidence units of resolving time $2\tau = 4 \times 10^{-7}$ seconds without appreciable loss of coincidences even in fields as great as 1 kilo-oersted.

§ 3. Cascade Conversion Electron Correlation Measurements

The following results are given primarily as examples of the use of the above equipment. All three involve L-shell conversion electrons, for which theoretical calculations are not yet available. The tellurium results were obtained with a source thick enough to produce appreciable distortion of the conversion lines, so that the original anisotropy is appreciably reduced by scattering. The intermediate state lifetime for ^{197}Hg is long enough, as the measurements show, for perturbation effects to be serious.

^{121}Te.—The angular correlation of the 82·1L ; 213K cascade in this nucleus, measured with a tellurium chloride source, was found to be

$$W(180°) : W(150°) : W(120°)=(1·00\pm0·05) : (0·91\pm0·5) : (1·01\pm05).$$

^{123}Te.—The angular correlation of the 88·5L ; 159K cascade in this nucleus, obtained from results similar to those for ^{121}Te, and corrected for finite solid angles but not for scattering, was found to be

$$W(\theta)=1+(0·16\pm0·07)\cos^2\theta.$$

^{197}Hg.—The angular correlation of the 164L ; 133L cascade in this nucleus was found to be given by

$$W(180°) : W(150°) : W(120°)=(1·00\pm0·02) : (1·02\pm0·02) : (0·98\pm0·02).$$

The source was a mixture of $HgCl_2$ and HgS, thin enough to give sharp lines in the spectrometers (fig. 2). The small observed anisotropy contrasts sharply with the 20% effect found by Frauenfelder *et al.* (1950), who used absorption techniques for energy selection, and prepared their sources by simultaneous condensation of gold and mercury vapour. Though the intermediate state is metastable ($t_{1/2}=7\times10^{-9}$ sec) the direct coupling between the spectrometer field (~200 oersteds) and the nuclear moment is much too small to account for the discrepancy. Indirect coupling by way of a non-zero electronic moment may however cooperate with the effects of atomic and crystalline fields in destroying the correlation.

§ 4. Conversion Electron Pair Correlation in ^{88}Sr

For this measurement three spectrometer systems, all of the same radius, were arranged, one to select positrons, the second to select negatrons emitted in the same average direction as the selected positrons, and the third to select negatrons emitted at an average angle of 110° to the selected positrons. The spectrometer field was then scanned through the neighbourhood of the pair line. With this equipment the ratio $W(0°)/W(110°)$ (see fig. 3) was measured for the 1·85 Mev transition in ^{88}Sr. To correct for the effects of external pair creation two sources were used, of which one had an average surface density twice that of the other. The experimental value for $W(0°)/W(110°)$, corrected for external pair creation, was found to be $4·5\pm1·0$. Theoretical values for this ratio,

in the case where the positron and negatron have equal energies, were taken from a paper by Horton (1948) using the Born approximation (Horton and Phibbs 1954). When modified for the experimental angular resolution they become $2{\cdot}2\pm0{\cdot}3$, $7{\cdot}5\pm0{\cdot}9$, and $5{\cdot}5\pm0{\cdot}7$ for E1, M1, and E2 multipoles respectively. Thus the measurement supports the assignment 2+ for the 1·85 Mev level in ^{88}Sr.

Fig. 2

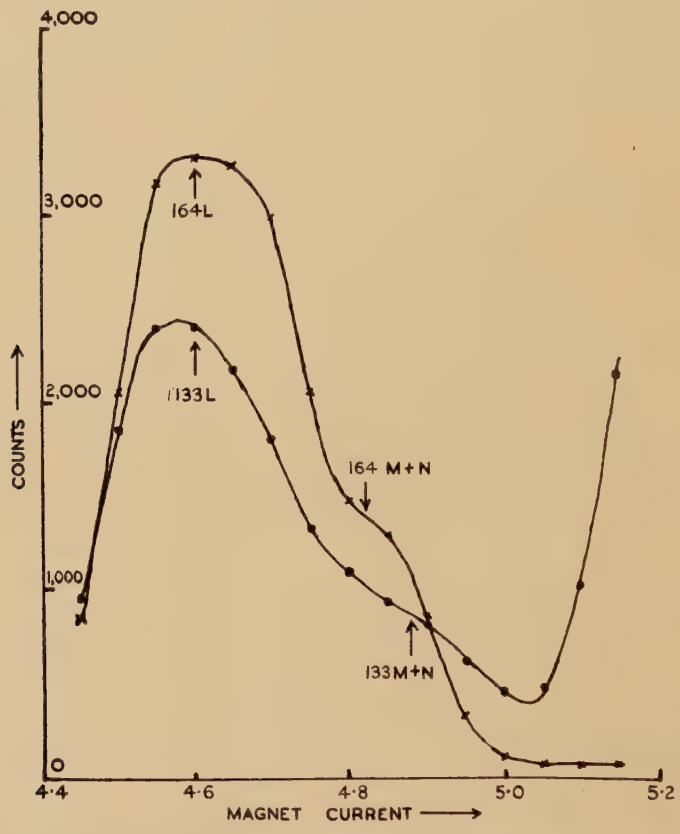

Conversion electron lines of ^{197}Hg observed in electron–electron angular correlation equipment.

§ 5. Equipment for Polarization–Direction Correlation Measurements

The polarimeter is physically similar to the system described by Metzger and Deutsch (1950). The scatterer is a truncated cone of tetraphenylbutadiene in styrene 2 in. long, with a base diameter of $1\frac{3}{4}$ in. and a semi-vertical angle of 10°. The side counter is a 2 in. × 2 in. × $1\frac{1}{4}$ in. block of thallium activated sodium iodide, with its centre $2\frac{1}{4}$ in. from the polarimeter axis. The polarimeter remains fixed, and the polarimeter

angle is changed by rotating the other directional counter about the polarimeter axis, so that the system contains only one moveable counter. Figure 4 shows the experimental arrangement. The polarimeter axis is

Fig. 3

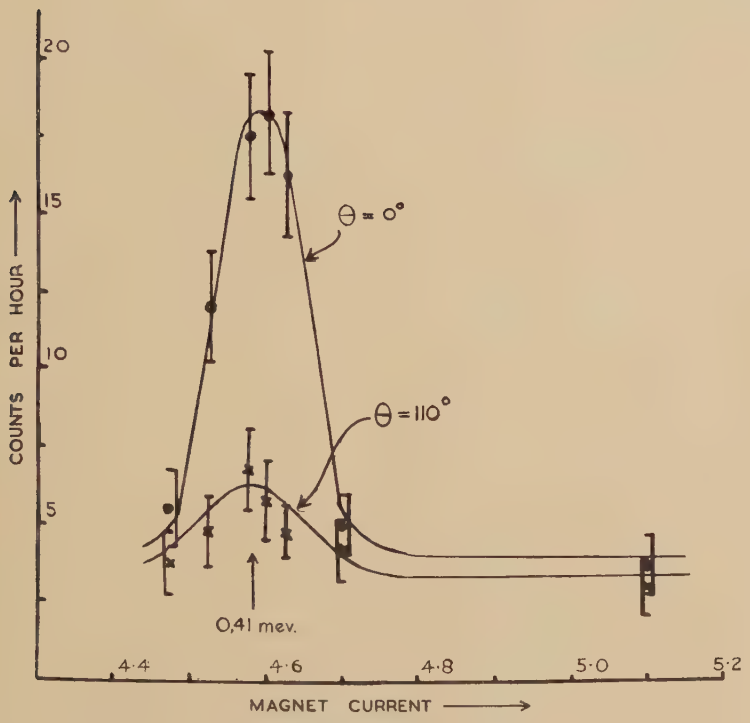

The ^{88}Sr internal conversion pair line observed at $\theta=0°$ and $\theta=110°$.

vertical. The bearings of the swinging arm carrying the unpolarized detector are fastened to a horizontal ring mounting, which rotates to give the polarimeter motion. The directional angle θ can be set at any multiple of 15° from 90° to 180°, and the apparatus then records data automatically at polarimeter angles following the sequence . . . −90°, 0°, 90°, 180°, −90° . . . , and inserts a measurement of the accidental coincidence rate after every third run.

The energy discrimination of the polarimeter is obtained by noticing that, since the energies of the scattered quanta reaching the side counter are rather small, many of them release all their energy in the NaI–Tl phosphor. Thus if pulses from the scattering counter and the side counter are treated so that a given energy release in either phosphor produces a pulse with the same height, shape, and delay, and are then added together, the spectrum of the summed pulses obtained in this way from a source of mono-energetic gamma-rays will show a peak at the high

energy end (see fig. 5). This peak arises from those events in which the energy of the scattered gamma-ray is completely absorbed in the side counter, and shows approximately the same resolution which the scattering phosphor would display in a two crystal spectrometer with a well defined scattering angle. Those scattered quanta which lose only part of their energy in the side counter produce a continuum which extends down from

Fig. 4

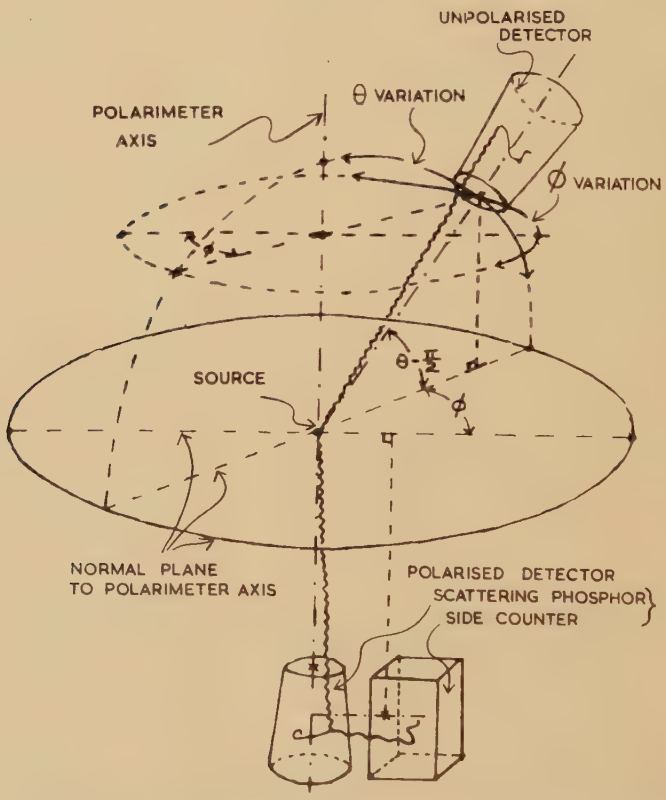

Diagram illustrating the mechanical arrangement of the components for polarization–direction correlation measurements.

the total absorption peak to a cut-off at the low energy end. This cut-off corresponds to the energy of the Compton electrons produced in the scattering phosphor by those quanta which are scattered back only just far enough to reach the side counter. To eliminate the very large background produced in the summing unit by non-coincident pulses from one or other of the polarimeter detectors, only those pulses are selected which are accompanied by coincidences between these detectors. The low-energy cut-off visible in the polarimeter spectrum shown in fig. 5 is partly due to amplitude dependent time shifts in the auxiliary coincidence unit ($2\tau \sim 2 \times 10^{-8}$ sec) used for this selection. This summing technique has

Fig. 5

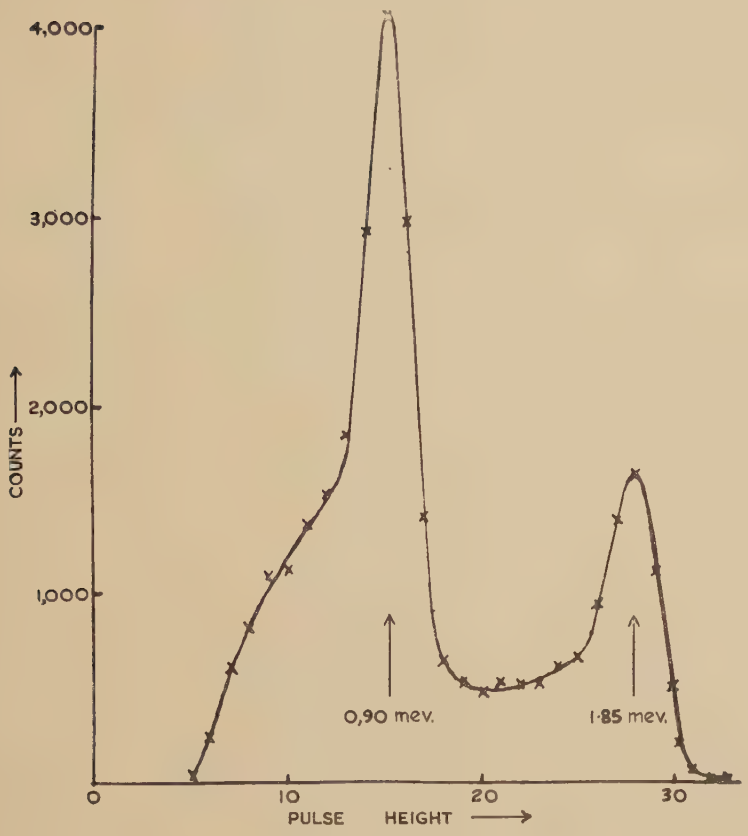

Spectrum of ^{88}Y observed in polarimeter.

Fig. 6

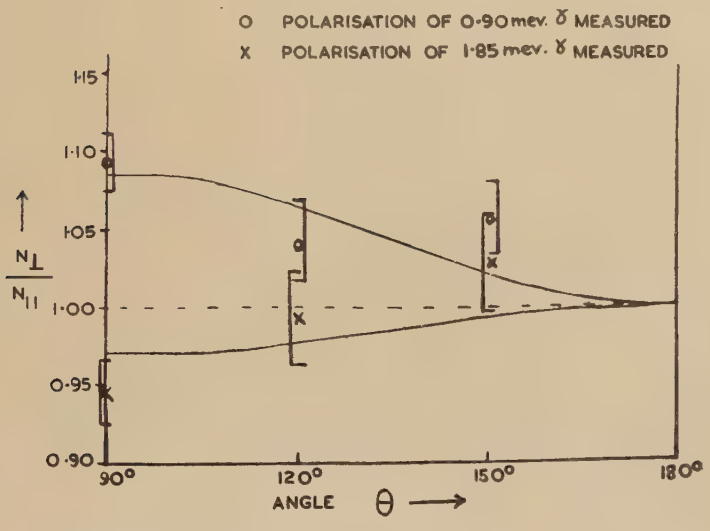

Measured polarization direction correlations in ^{88}Sr.

the advantage over the technique of gating the pulse distribution in the scattering counter (Bishop and Perez 1955, Wood and Jastram 1955) that the side counter can subtend a large solid angle at the scattering phosphor without loss of resolution.

§ 6. Polarization–Direction Correlations in ^{88}Sr

The polarization–direction correlations of the 0·90, 1·85 Mev cascade in ^{88}Sr were measured with the high energy radiation selected first in the polarized and secondly in the unpolarized detectors, corresponding to observation of the polarization of the 1·85 and 0·90 Mev transitions respectively. The experimental results, shown in fig. 6, determine the parities of the 1·85 and 2·75 Mev levels as even and odd respectively, in agreement with the results of Bishop and Perez (1955), and with the internal pair conversion correlation measurement described earlier.

Acknowledgments

The electron–electron angular correlation equipment described above was built, and most of the experimental work with it was carried out, at the University of Birmingham in preparation for a Ph.D. degree. The writer is grateful for the award of an 1851 Exhibition Overseas Science Scholarship, which enabled him to undertake postgraduate study in England, and, at a later period, for a grant from Nuffield Foundation funds. The work of Dr. A. G. Maddock of Cambridge, and particularly Dr. K. F. Chackett of Birmingham, in carrying out radiochemical preparations, and of the workshop staff in constructing the equipment, is gratefully acknowledged. It is a pleasure to thank Professor P. B. Moon for his continued interest and encouragement.

The final measurements on ^{88}Sr and the polarization–direction correlation measurements were carried out at A.E.R.E., Harwell. The mechanical equipment for the latter experiments was built by Mr. F. Razell, and the associated non-standard electronic equipment by Mr. D. A. Boyce. The writer is grateful to Dr. P. E. Cavanagh for his suggestion of the summing technique and for his continued interest in the polarimeter project.

References

Bishop, E. R., and Perez y Jorba, J. P., 1955, *Phys. Rev.*, **98**, 89.
Fowler, C. M., and Shreffler, R. G., 1950, *Rev. Sci. Instr.*, **21**, 740.
Frauenfelder, H., Walter, M., and Zünti, W., 1950, *Phys. Rev.*, **77**, 557.
Geoffrion, C., 1949, *Rev. Sci. Instr.*, **20**, 638.
Horton, G. K., 1948, *Proc. Phys. Soc.*, **60**, 457.
Horton, G. K., and Phibbs, E., 1954, *Phys. Rev.*, **96**, 1066.
Kraushaar, J. J., and Goldhaber, M., 1953, *Phys. Rev.*, **89**, 1081.
Metzger, F., and Deutsch, M., 1950, *Phys. Rev.*, **78**, 551.
Siegbahn, K., 1952, *Archiv f. Physik*, **4**, 223.
Steffen, R. M., 1955, *Proceedings of the* 1954 *Glasgow Conference on Nuclear and Meson Physics* (London and New York: Pergamon Press), p. 206.
Wood, G. T., and Jastram, P. S., 1955, *Bull. Amer. Phys. Soc.*, **30**, 1, 48.

XV. *The Scattering of High Energy Neutrons by a Coulomb Field*

By R. G. P. Voss* and R. Wilson†
The Clarendon Laboratory, Oxford‡

[Received October 28, 1955]

Abstract

A polarized beam of 100 Mev neutrons is obtained from the A.E.R.E. cyclotron; this is scattered from uranium at sufficiently small angles that there is an appreciable scattering from the interaction of the magnetic moment of the neutron with the Coulomb field. The scattering and polarization of the Coulomb field scattering are in agreement with theory, and enable a value for the sign and magnitude of the polarization of the neutron beam to be obtained.

§ 1. Introduction

The scattering of neutrons by a Coulomb field has been investigated theoretically by Schwinger (1948). The calculation shows that neutrons will be appreciably scattered at small angles and that the scattering is spin dependent. Thus a study of the spin dependence enables the process to be used as an analyser for a polarized neutron beam. This experiment was undertaken, partly to study the process itself, and partly to find the magnitude and sign of the polarization of a neutron beam which is used in another experiment (Hillman 1955).

§ 2. Method

A neutron beam which is partially polarized was obtained by allowing protons of 170 Mev energy in the A.E.R.E. cyclotron to strike a beryllium target. Neutrons were observed at an angle of 26° to the incident proton beam. Other targets were also occasionally used.

The neutrons were collimated by a 6·5 mm steel collimator, and then allowed to strike a uranium scatterer. The scattered neutrons were detected by a large liquid scintillator (Thresher 1955 b) used as a threshold detector. The scattered neutrons were detected on both sides of the neutron beam.

The asymmetry is given by $(C_L-C_R)/(C_L+C_R)=P_1P_2$ where P_1 is the (unknown) polarization of the neutron beam and P_2 is the calculated polarization in the magnetic scattering of the neutrons. Hence by measuring C_L and C_R—the counts for the counter scattering to the left

* Now at the University of Liverpool.
† Now at Harvard University.
‡ Communicated by the Authors.

and right—P_1 is determined. In this paper the sign of the asymmetry is taken to be positive if the scattering is greater in the same direction as the initial pn scattering, and negative if in the opposite direction.

§ 3. Apparatus

The counter used was designed to give a good angular resolution. It was 44 cm long $\times$ 2·54 cm wide $\times$ 7·6 cm high. It was viewed from the top by 4 E.M.I. 6260 photomultipliers as before (Thresher 1955 b).

The electronic circuits were the same as used in earlier experiments (Thresher 1955 a), and two biases were used on the counter which gave two energy thresholds for detection of the neutron beam.

The effective energies were measured as before ; for the $\pm 26°$ beryllium targets they were 104 ± 2 Mev for the higher bias, and 97 ± 2 Mev for the lower bias. For the carbon and uranium targets the effective energies were not measured but were almost certainly lower. The energy spread of the neutrons detected was large ; it may be deduced from the data of Snowden (1952), and was about $\pm 20\%$ at half maximum.

§ 4. Targets

The targets were placed in a single sight line through the cyclotron. Two beryllium targets, the $26_+°$ and $26_-°$, were placed where this line intersected a 49 in. radius, so that the neutrons were produced respectively to the left and to the right of the incident protons. The maximum bombarding proton energy is 170 Mev, but the mean is about 150 Mev, due to target thickness and radial oscillations. Another beryllium target is placed so that neutrons from 0° to a 133 Mev proton beam are counted. A carbon target was used at $+10°$ (140 Mev bombarding energy) and a uranium target at $+20°$. The main measurements were made with the $26_+°$ and $26_-°$ targets. One run was also made with a 112 Mev maximum (95 Mev mean) bombarding energy and a 26° Be target. The same sight line and collimation were used in all but the last experiment.

The targets were all designed by Dr. P. Hillman to give the best possible symmetry of the neutron beam.

§ 5. Backgrounds

In spite of great efforts, a large background remained of neutrons scattered from the collimators. This was reduced by the use of two ' clearing ' collimators which prevented many of these neutrons from reaching the counters. The total background was still about $\frac{1}{4}$ of the counting rate from the target and it had to be specially considered. The scatterer considerably attenuated the beam, and also attenuated the background from the collimator scattering. Part of the background, from cosmic rays etc. was not so attenuated. The two could be separated by completely stopping the beam. This procedure has been discussed before (Thresher 1955, van Zyl 1955). The background was measured for every asymmetry cycle.

§ 6. Total Cross Section of Uranium

The attenuation of the neutron beam by the scatterer was experimentally determined, and also yields a value for the total cross section for uranium which was necessary for a computation of the analysing efficiency. The total cross section becomes

$5{\cdot}16 \pm 0{\cdot}06 \times 10^{-24}$ cm^2 at 106 ± 2 Mev effective energy,
$5{\cdot}16 \pm 0{\cdot}06 \times 10^{-24}$ cm^2 at 99 ± 2 Mev effective energy,
$4{\cdot}90 \pm 0{\cdot}15 \times 10^{-24}$ cm^2 at 73 ± 2 Mev effective energy.

The energy scale is directly related to that of Taylor (1953). The results agree well with those of Linlor (1953).

§ 7. Alignment of the Beam

The theoretical cross section varies with angle as $A + B/\theta^2$. It is therefore important at the small angles to align the counters with respect

Fig. 1

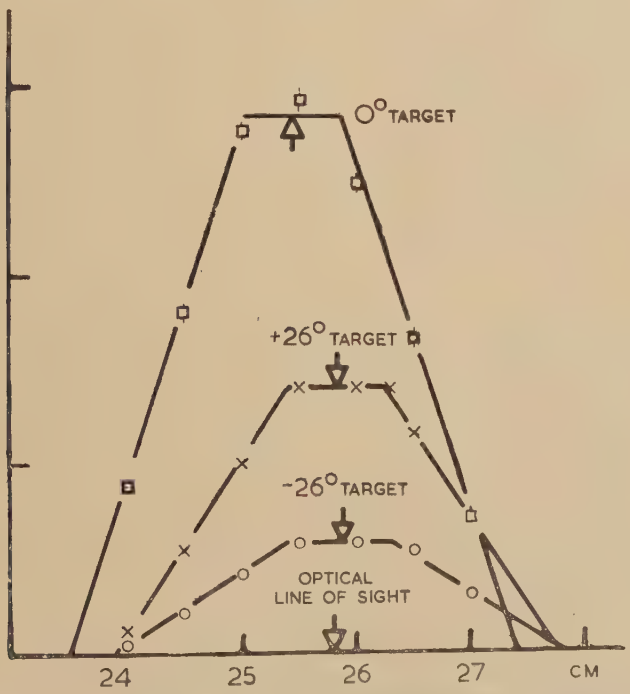

The variation of counting rate as the counter is moved through the beam. The position of the sight line, and the calculated effective centre for each target are shown by arrows.

to the beam accurately. This has been done by moving the counter through the beam (with a reduced beam level) (fig. 1). Although the collimation remained fixed, the optical alignment and determination

of the effective centre of the targets was uncertain and different for each target. The three curves are not, therefore, identical. The curves are a fold of the counter efficiency and the beam intensity. It is seen that the curves are symmetrical and the midpoint may be determined to about $\pm 0{\cdot}2$ mm. This inaccuracy leads to an uncertainty in the asymmetries at $\frac{1}{4}^\circ$ of $1{\cdot}2\%$, at $\frac{1}{3}^\circ$ of $0{\cdot}4\%$ and less at wide angles.

It was necessary for the experiments to be performed at the same time as those of Hillman and Stafford ; as a result the collimator had to be realigned every few days, and the measured asymmetries include several such counter alignments. The error in alignment becomes negligible compared with the other errors.

Checks were also made to show that placing the counter skew to the neutron beam by $\pm 1\frac{1}{2}^\circ$ made less than 2% difference to the counting rate. Since the maximum accidental misplacement could only be $\pm 0{\cdot}1^\circ$, no source of error arises.

§ 8. Angular Resolution

The curve of fig. 1 also defines the major part of the angular resolution of the counter which is about $\frac{1}{4}^\circ$ full width at half maximum. Because of the height of the counter, there is a small further spread at small angles.

The experimental points have all been corrected using the theoretical variation of cross section and polarization with energy. This correction is quite small for the value of the polarization, but is appreciable for the value of the unpolarized cross section. Appropriate errors are assigned to this procedure and included in the final results.

§ 9. Scatterer

The scatterer was chosen to be uranium to give a large amount of scattering, and a nucleus which was as nearly opaque as possible, so that the analysing efficiency should be high. The scatterer was thick to give a high intensity and a high ratio of effect to background.

The thick scatterer involves much multiple scattering. The correction for this follows on the lines of Bratenahl (1950).

Most of the scattering cross section lies within the first diffraction minimum. In this region the cross section may be simply represented by a Gaussian to a high accuracy. With this approximation, the angular distribution of singly scattered neutrons becomes

$$\sigma_1(\theta)=\exp(-\theta^2/a^2).$$

The angular distribution of doubly scattered neutrons is

$$\sigma_2(\theta)=\tfrac{1}{2}\exp(-\theta^2/2a^2)$$

and of neutrons scattered n times is

$$\sigma_n(\theta)=(1/n)\exp(-\theta^2/na^2).$$

The total number of doubly scattered neutrons is x times the number of singly scattered neutrons where x is the ratio of the scatterer thickness

to the mean free path for scattering. The measured cross section is then greater than the singly scattered cross section by the factor $\sum_{n=1}^{\infty}(x^{n-1}/nn!)$. The correction to the asymmetries are less easy ; it is necessary to assume that the neutrons entering the counter after multiple scattering are unpolarized. This is probable, because the multiple scattering for the uranium is principally from addition of two scatters of about 10° where the polarization is very small (Dickson 1955). Thus we must multiply the measured asymmetries by the factor $\sum_{n=1}^{\infty}(x^{n-1}\,nn!)$ which is about 1·13 in our case.

§ 10. Results

The measured asymmetries are summarized in the table.

Table of Results

Target	Angle	Asymmetries (%)		Polarization (%) of beam	
		Low Bias	High Bias	Low Bias	High Bias
26_+°Be	$\frac{1}{4}$	−7·9±1·9	−10·8±1·9	−8·9+2·4	−12·3±2·4
26_+°Be	$\frac{1}{3}$	−5·6±1·5	−7·7±1·2	−7·3±2·0	−10·4±1·8
26_+°Be	$\frac{2}{3}$	−5·9±1·6	−3·2±1·3	−13·2±3·9	−7·4±3·2
26_+°Be	1	−8·6±2·0	−5·0±1·7	−28 ±7·0	−17·2±6·0
26_-°Be	$\frac{1}{3}$	−7·2±1·7	−6·4±2·1	−9·3±2·5	−8·4±3·1
26_-°Be	1	−2·5±1·8	−1·3±2·1	−8·2±6·0	−4·2±7·0
0° Be	$\frac{1}{3}$	+0·7±1·5	−2·6±1·5		
0° Be	1	−0·9±2·0	−3·4±3·0		
10° C	$\frac{1}{3}$	−0·8±0·8	−0·9±0·7	−1·06±1·0	−1·22±0·9
20° U	$\frac{1}{3}$	−3·0±2·2	−6·9±3·3	−3·8±2·6	−8·9±4·0
Weighted average of 26° Be				−9·2±1·3	−10·2±1·3
95 Mev bombardment :—					
26_+°Be	0·4°	−2·3±1·1	−2·3±1·7	−3·2−1·6	−3·2±2·0

Each result is the average of several asymmetries. Standard deviations were calculated in the usual way, and were in agreement with the errors expected from the counting statistics. The errors shown are the larger of the two errors. For the 20° U target, however, only 3 asymmetries were measured, and counting statistics only are quoted.

The unpolarized angular distribution is shown in fig. 2, and the asymmetries at various angles in fig. 3. The theoretical curves are discussed later. The asymmetries from the 0° target are shown in fig. 4 together with the difference in the asymmetries for the 26_+° and the 26_-° targets which, if the experiment is correct, should be zero. Only the figures from the higher bias are plotted in the figures, and discussed in the text.

Fig. 2

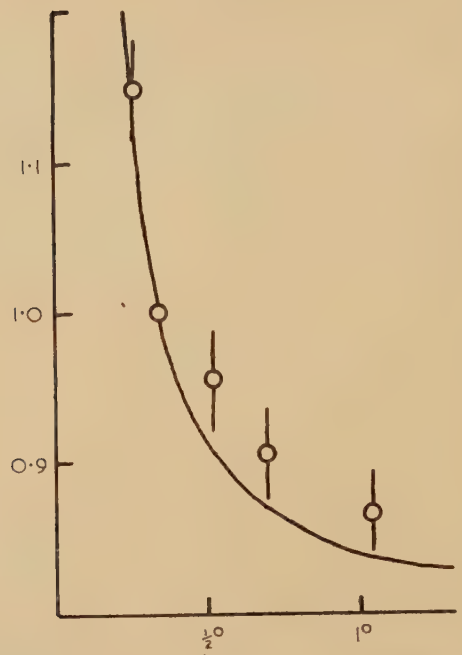

Small angle differential cross sections averaged over polarization. These are compared with the theoretical curve normalized to unity at 1/3°.

Fig. 3

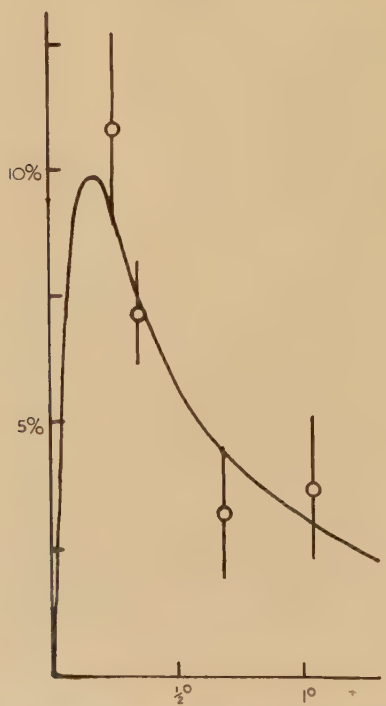

The asymmetry using a beryllium target at 26°, plotted versus angle, and compared with the theoretical curve, normalized to give the best fit to the data.

The tabulated polarizations are also shown in the table, and include the estimated errors of the calculation. The values for the 26° Be targets are averaged on the assumption that there are no systematic errors due to scattering. The beam as used by Hillman has an effective energy of 100 Mev, and a best value for the polarization can therefore be deduced of $9{\cdot}8 \pm 1{\cdot}4\%$.

Fig. 4

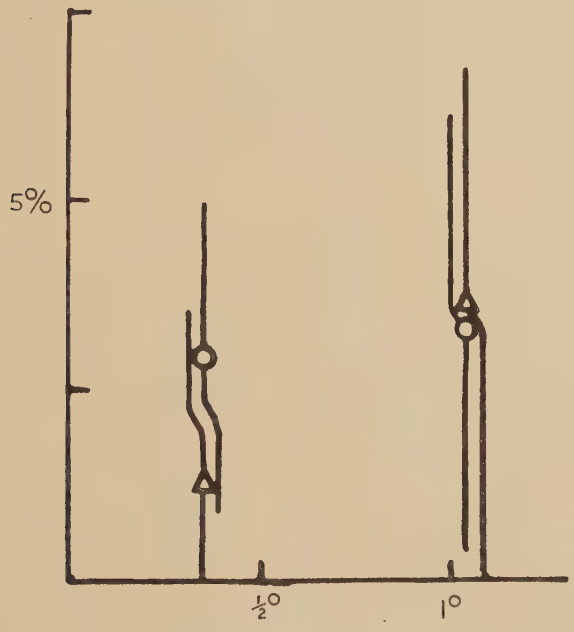

Spurious asymmetries using a beryllium target.

§ 11. Spurious Asymmetries

There are two possible causes of spurious asymmetries apart from the counter misalignment. Firstly, the photomultiplier gain could change as the counter position was varied; secondly, there could be scattering of neutrons off the walls of the counting area increasing the counts in one position. It was unfortunately not possible to arrange for the beam to traverse the counting area symmetrically. Both these effects would be most marked for the 1° asymmetries, where the counter positions were separated by 21 cm.

To check that these spurious asymmetrics were small and to make allowances for them, some runs were performed with a target at 0°; the asymmetry should be zero. Runs were also performed with the $\pm 26°$ targets, so that the neutron beam polarization had the opposite sign from each. The difference between the asymmetries so obtained gives a measure of the spurious effects, and the average gives the correct asymmetry after correction for spurious effect.

Figure 4 shows result of both these checks. It is suggestive that there might be a spurious asymmetry at 1°. If this were due to a gain change, there should be a larger spurious asymmetry for the higher bias than for the lower bias. If due to scattering, the scattered neutrons would enter the counter at an oblique angle, and there should be a larger spurious effect for the lower bias than the higher. No systematic effect is observed and it is possible that the results are a statistical accident. In any case, the averaging procedure tends to correct for any effect which may be present.

The use of a 0° target and the 26_+° and 26_-° targets does *not* correct for spurious asymmetries due to beam misalignment, which are important at small angles and are different for each target.

§ 12. Calculations

Following Schwinger we can define a scattering amplitude

$$(f\theta)+\boldsymbol{\sigma}\,.\,\mathbf{n}\,g(\theta)$$

where $f(\theta)$ has real and imaginary parts ; and $g(\theta)$ is totally imaginary.

Then the scattering cross section for unpolarized neutrons is given by $\sigma(\theta)=f^2(\theta)+g^2(\theta)$ and the polarization in the second scattering by

$$P_2(\theta)=\frac{2\{\mathrm{Re}\,f(\theta)\,\mathrm{Re}\,g(\theta)+\mathrm{Im}\,f(\theta)\,\mathrm{Im}\,g(\theta)\}}{\sigma(\theta)}$$

$g(\theta)$ is determined both as to sign and magnitude by electrodynamics. To determine $P_2(\theta)$, $\mathrm{Re}\,f(\theta)$ and $\mathrm{Im}\,f(\theta)$ must be known.

Over the range of angles used here, we assume that $f(\theta)=f(0)[J_1(kR\theta)/\theta]$. Also we know, from a well known theorem, $\mathrm{Im}\,f(0)=(k/4\pi)\sigma_{\mathrm{tot}}$; σ_{tot} has been measured for this experiment.

If the nucleus were opaque, $\mathrm{Re}\,f(0)$ would be zero. For a transparent nucleus the total cross section varies with energy in such a way that there is a maximum, and near this maximum, $\mathrm{Re}\,f(0)$ is close to zero. The maximum for uranium is near 90 Mev (Linlor 1953), so that $\mathrm{Re}\,f(0)$ is small, and would be zero if the nucleus had sharp edges. Since nuclei have diffuse edges, $\mathrm{Re}\,f(0)$ is not zero. Experimentally Bratenahl (1950) at these energies finds that $\sigma(0)$ for lead may be up to 6% higher than that given by a square well optical model. Here it has been assumed that the nucleus has a constant potential out to a radius R, tapering linearly to zero, either by $1{\cdot}25R$ or $1{\cdot}8R$. Errors are given corresponding to these two extremes.

We then find by calculation : $\sigma(0)=k^2\sigma_{\mathrm{tot}}^2/16\pi^2$ $(1{\cdot}05\pm0{\cdot}03)$.

It is, of course, important to know that the Born approximation calculations of Schwinger are adequate. Calculations using the potential in a small angle approximation (Glauber 1953) show less than 1/10% deviation from the Born approximation value. There is, also, a small correction due to the failure of the assumptions made by Schwinger

of a point nucleus. These have been calculated by assuming a uniform distribution of charge over the nucleus. At 1°, the largest angle studied, the polarization is smaller by 2% and at 1/3° by 0·2%. These are negligible. At these large impact parameters no error arises from the assumption of a point magnetic moment for the neutron.

§ 13. Sign of the Polarization

The interest of the sign of the polarization is to discover whether the sign agrees with the prediction of Fermi (1954) that a nuclear spin–orbit coupling responsible for the shell model is also responsible for high energy polarization.

The overall potential predicted by Fermi is

$$(1+i\epsilon)U(r)+\boldsymbol{\sigma}\cdot\mathbf{r}\times(-i)\,\nabla\left\{\frac{|\mu|Ze}{|r|^3}-\frac{\alpha\lambda^2}{r}\frac{d}{dr}U(r)\right\}.$$

Since $U(r)$ is negative, $(d/dr)U(r)$ is positive, and the spin orbit potential is the opposite sign to the Coulomb potential. Thus the polarization in Coulomb field scattering should be the opposite sign to that in nuclear scattering. The asymmetry in this experiment is negative ; the neutron beam from a charge exchange scattering is polarized in the same direction as the proton beams from nuclear scattering, as shown by Bradner (1954) and Chamberlain (1954). Thus, the sign of the polarization in nucleon–nucleus scattering is indeed in the opposite direction to that of Coulomb field scattering, in agreement with the theory of Fermi, and the other experiments of Marshall (1955) and Brinkworth (1955). The use of this method of obtaining the sign of a polarized neutron beam has been suggested independently by Shapiro (1955).

§ 14. Polarization in Neutron Production

The polarization in the production of neutrons at 26° by 150 Mev protons on Be, is found to be $10{\cdot}2\pm1{\cdot}3\%$. Roberts *et al.* (1954) assumed that a pn reaction in C at 240 Mev was similar to a np reaction in C at 150 Mev to derive a value for the polarization of their neutron beam. By neglecting the energy dependence, they may have obtained too *low* a value of the polarization of their beam by 2% ; their free np scattering polarizations may therefore be too high by 2%. In fig. 5 we have plotted the polarization in the pn reaction on beryllium at 26° as a function of mean bombarding energy from our data and those of Roberts and Bradner (1954). Although these authors did not make measurements at 26°, the values may be obtained by interpolation. Also plotted are the free np scattering polarizations at 150 Mev (Roberts 1954) and 100 Mev (Hillman 1955) similarly obtained. It is seen that there is no discrepancy except at the lowest energy.

The polarization of neutrons at 10° from carbon bombarded by 130 Mev protons is $1{\cdot}2\pm1\%$ which is lower than expected from free np scattering.

On the other hand Roberts and Bradner, both found polarized beams from carbon higher than that from beryllium. This low polarization at 10° could be explained as follows.

Fig. 5

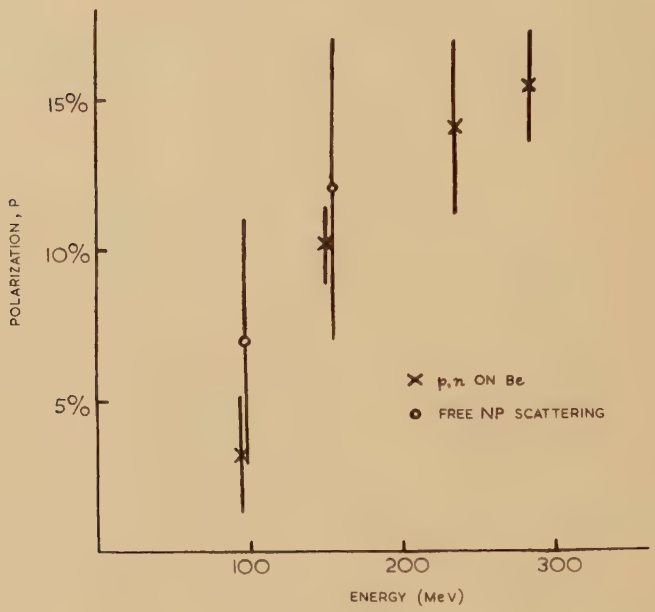

Polarization in the pn reaction in beryllium at 26° as a function of energy. Free np scattering points are included for comparison.

When neutrons are produced in the forward direction, from a ' p, n ' collision inside a nucleus, the proton left behind has little energy. The resultant ^{12}N nucleus must then be in its ground state. There must be a spin change from the 0^+ of the ^{12}C nucleus to the 1^+ of the ^{12}N nucleus. This enhancement of the spin change effect results in a lower polarization than in the free np scattering, following an argument by Tamor (1954). A similar argument applied to the deuteron has been used to explain a low cross section at 0° for the reaction N(+D)→P(+N+N) by Dzelepov (1955). At a lower energy (110 Mev) Hoffman (1953) has shown that the cross section for neutron production by protons on carbon is nearly flat from 0° to 10° whereas those for production by protons on lithium or beryllium rise at 0°, in qualitative agreement with this argument. Quantitative agreement is *not* obtained as discussed by Hoffmann.

ACKNOWLEDGMENTS

We are deeply indebted to the cyclotron group at A.E.R.E. for their assistance. In particular, Dr. Hillman and Dr. Stafford provided the targets and helped us in many ways. Mr. C. P. van Zyl materially assisted in the construction of apparatus.

REFERENCES

BRADNER, H., and DONALDSON, R., 1954, *Phys. Rev.*, **95,** 1701.
BRATENAHL, A., FERNBACH, S., HILDEBRAND, R. H., LEITH, C. E., and MOYER, B. J., 1950, *Phys. Rev.*, **77,** 597.
BRINKWORTH, M., and ROSE, B., 1955, *Phys. Soc. Spring Meeting, Harwell.*
CHAMBERLAIN, O., DONALDSON, R., SEGRÉ, E., TRIPP, R., WIEGAND, C., and YPSILANTIS, T., 1954, *Phys. Rev.*, **95,** 850.
DICKSON, J., ROSE, B., and SALTER, D. C., 1955, *Proc. Phys. Soc.*, **68,** 361.
DZELEPOV, V. P., KAZARINOV, Y. U. M., and FLYAGIN, V. B., 1955, *Doklady Academi Nauk S.S.R.*, **100,** 655.
FERMI, E., 1954, *Nuovo Cimento*, **11,** 407.
GLAUBER, R. J., 1953, *Phys. Rev.*, **91,** 459.
HILLMAN, P., and STAFFORD, G. H., 1955, *Phys. Soc., Summer Meeting, Liverpool,* and private communication.
HOFFMANN, J. A., and STRAUCH, K., 1953, *Phys. Rev.*, **90,** 449.
LINLOR, W. E., and RAGENT, B., 1953, *Phys. Rev.*, **92,** 835.
MARSHALL, L., and MARSHALL, J., 1955, *Phys. Rev.*, **98,** 1398.
ROBERTS, A., TINLOT, J., and HAFNER, E. M., 1954, *Phys. Rev.*, **95,** 1099.
SCHWINGER, J., 1948, *Phys. Rev.*, **73,** 407.
SHAPIRO, I., 1955, *Thesis*, Harvard University (unpublished).
SNOWDEN, M., 1952, *Phil. Mag.*, **43,** 285.
TAMOR, S., 1954, *U.C.R.L. Report*, 2710 (unpublished).
TAYLOR, A. E., and WOOD, E., 1953, *Phil. Mag.*, **44,** 95.
THRESHER, J., VOSS, R. G. P., and WILSON, R., 1955 a, *Proc. Roy. Soc.* A, **229,** 492.
THRESHER, J., VAN ZYL, C. P., VOSS, R. G. P., and WILSON, R., 1955 b, *Rev. Sci. Instr.* (in the press).
VAN ZYL, C. P., VOSS, R. G. P., and WILSON, R., 1955, to be published.

XVI. *The Ductile Fracture of Polycrystalline α-Iron*

By N. J. Petch
Metallurgy Laboratory, University of Leeds *

[Received September 15, 1955 ; revised October 22, 1955]

Summary

Evidence that ductile fracture requires a compressive stress on the dislocation arrays close in value to that required for cleavage is presented. It is shown that the ductile fracture stress σ_f is related to the grain diameter l by the equation $\sigma_f=\sigma_0+kl^{-1/2}$, where σ_0 and k are constants. This is the same form of relationship as already found for cleavage and the slope k is practically the same for both types of fracture.

§ 1. Introduction

It now seems fairly certain that cleavage fracture originates at the head of an array of dislocations pressed against a grain boundary or other obstacle and that the array produces a sufficiently large crack to allow this subsequently to propagate in the Griffith manner by its own concentration of the applied stress (Koehler 1952, Mott 1953, Petch 1953, 1954, Stroh 1954, Greenwood and Quarrell 1954). It also seems probable that ductile fracture at higher temperatures originates in the same way, but that, in this case, the stress concentration produced by the spread of the crack activates neighbouring Frank–Read sources and the energy of the dislocation array is so dissipated that the crack is arrested. Further plastic extension of the specimen is then necessary to complete the fracture.

The mechanism of this completion is of interest. One possibility is that the applied stress has to be increased until the initial crack can propagate in the Griffith manner against the plastic work that its extension entails. But the crack would then propagate as a fast one, since the required energy would come from the stored elastic energy, and a fast-moving crack is contrary to experience for the initial stages of a ductile fracture. It seems more probable that, once a crack has formed ahead of one array, increase in the strain will produce neighbouring arrays and neighbouring cracks, and eventually there will be so many of these cracks that they will link together into the fracture. The subsequent extension of this fracture will then involve further plastic deformation ahead of itself, further crack formation and linkage of the new cracks with the main one.

* Communicated by the Author.

On this view, the maximum stress required in the fracture process (the ductile fracture stress) is determined by the condition for the formation of a crack ahead of a dislocation array, but this will not be the first such crack that forms, but some subsequent one. The stress required on the dislocation array that produces this subsequent crack should not be much different from that required for the initial crack. Thus, although there are clear differences between cleavage and ductile fracture, the stress on the dislocation arrays at the stress for ductile fracture should be much the same as would have produced cleavage, if cleavage had been possible at the temperature in question.

To complete the picture of ductile fracture, it can be said that the maximum stress should occur at an early stage in the fracture process, because of the stress concentration produced by the fracture itself. Subsequent to the maximum stress, further strain by the testing machine will still be necessary for extension of the fracture. Eventually, this will grow to such a size that the work required for its extension can come from the stored elastic energy. The fracture will then become a fast one, independent of the strain by the machine, and the condition for its propagation will resemble that for a Griffith crack, with plastic energy added to the surface energy.

§ 2. Experimental Evidence

Some measurements have been made that bear on this discussion. The figure (*a*) shows the dependence of the cleavage strength σ_c of a polycrystalline mild steel on the grain diameter l at −196°C. This is for zero reduction of area prior to fracture. The relationship is of the form

$$\sigma_c = \sigma_0 + kl^{-1/2},$$

where σ_0 and k are constants. As discussed previously (Petch 1953), this is consistent with the production of cleavage by the stress concentration ahead of an array of dislocations proportional in length to the grain diameter. The term σ_0 represents the stress required simply to move a dislocation, so $(\sigma_c - \sigma_0)$ compresses the array. The slope k includes the proportionality between the length of the array and the grain diameter and is also a measure of the stress required ahead of the array.

The figures (*b*) and (*c*) refer to similar measurements of the relationship between the fracture stress and initial grain size at 18°C and −115°C. These are now ductile fractures and there is considerable plastic deformation prior to the fracture; on average, 67% reduction of area occurs at 18°C and 61% at −115°C, and the variation with grain size is quite small. The ductile fracture stress σ_f is here taken to be the maximum true stress in the tensile test.

It is apparent that the stress at fracture is given by

$$\sigma_f = \sigma_0 + kl^{-1/2},$$

which is the same form of relationship as observed for cleavage. Further, although the actual magnitude of the fracture stress at constant grain size varies considerably between the three cases in the figure, the variation resides in the σ_0 term, while the slope k is nearly constant.

The common form of the relationship between fracture and stress suggests that ductile fracture and cleavage are closely similar and that the ductile fracture stress is concerned with the production of cracks ahead of dislocation arrays that are proportional in length to the grain diameter. It is also apparent that $(\sigma_f - \sigma_0)$ at the ductile fracture stress is nearly the same as that required for cleavage at the same grain size.

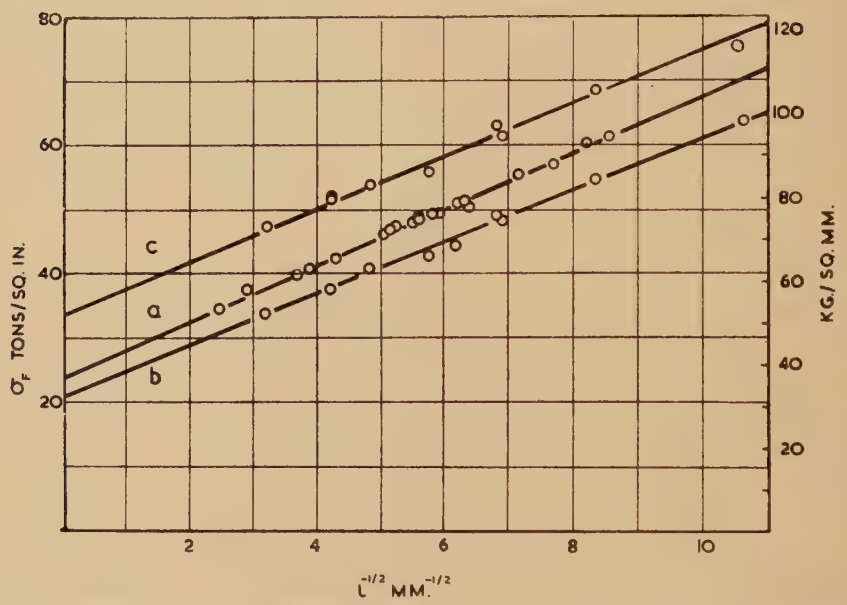

The relationship between fracture stress and grain size for a low-carbon steel at (*a*) −196°C, (*b*) 18°C, (*c*) −115°C.

This is what would be expected from § 1, provided that the dislocation arrays at constant l have the same length and require the same stress ahead of them for the production of cracks at all three temperatures.

This suggestion of the same array length is rather surprising in view of the differences in plastic strain prior to fracture. The dislocation arrays might well be considerably shorter in the ductile fractures and, indeed, the length might become independent of the grain size. But, it follows from the observation that k is constant that the arrays cannot be shorter than in cleavage, unless the stress required ahead of them is also less. The magnitude of this stress will depend on the rigidity modulus and the surface energy, so temperature differences will have only a small effect and the plastic deformation prior to ductile fracture, through the

surface energy will, if anything, probably cause an increase, not a decrease in the stress required. Thus the stress needed ahead of the arrays should not be any less in the ductile fractures. It follows that shorter arrays are improbable.

It is concluded that the ductile fracture stress involves dislocation arrays of nearly the same size and compressed by nearly the same resultant stress as in cleavage at the same grain size. This agrees with the ideas in § 1.

The lack of an effect of plastic deformation on the size of the arrays may indicate that the dislocations in iron are only successfully held up by grain boundaries, or, alternatively, that the size appears unchanged because a number of small arrays produce the same effects as a large one.

The variation of σ_0 in the figure has still to be considered, but this seems readily understandable. Presumably, it represents the change in the stress required to move a dislocation as the temperature is lowered and the iron strain-hardens. The big difference in the strain prior to fracture could explain the smaller value of σ_0 at −196°C than at −115°C.

Since σ_0 varies with strain, there may be some difference between the ductile fracture stress and the applied stress necessary to form the first crack, although there is little difference in the resultant stress on the dislocation arrays.

§ 3. Experimental Details

The mild steel used had the following percentage composition :

C	Si	S	P	Mn	Ni	Cr	N
0·15	0·02	0·05	0·03	0·51	0·08	0·05	0·008

The fracture stress was determined on specimens of 1 in. gauge length and 0·125 in. gauge-length diameter, polished to an 000 emery finish. These were machined from $\frac{5}{16}$ in. diameter cold-drawn rod. The grain size range of 80 to 10 000 grains/mm^2 was principally obtained by holding the specimens *in vacuo* for various times at 900–1200°C and cooling at various rates. The faster rates were all followed by a short anneal at 650°C with subsequent slow cooling. Straining and annealing were used to obtain the very coarse sizes.

In the tensile testing, special care was taken with the axiality of loading and the machine was driven at a cross-head velocity of 0·34 mm/min.

The ductile fracture stress was identified with the value at which there was a sudden discontinuous drop in load, followed almost immediately by fracture. For the specimens that necked, the lack of uniformity of stress had to be considered. Since we are concerned with the stress compressing the dislocation arrays, the measured average tensile stress in the neck was converted by Bridgman's (1943) analysis into the tensile stress that would have been present if uniaxial conditions had persisted.

The required measurements of the diameter of the fracture and the radius of curvature of the neck were made with a projection microscope.

Within each set of measurements there was some variation of the strain at fracture. This produces a variation in σ_0, so the fracture stress figures were corrected to a constant strain at each temperature.

For -196°C, this correction was obtained from a separate experiment in which the effect of strain on the fracture stress was estimated by pre-straining at room temperature and then fracturing at -196°C. This estimate was in close agreement with another made in a different way. Up to grain sizes such that $l^{-1/2} \sim 5{\cdot}5\ \mathrm{mm}^{-1/2}$, there is very little strain prior to fracture, then the strain increases, but again becomes fairly constant for the finer grains (Petch 1953). By plotting the two constant–strain portions of the curve of σ_c against $l^{-1/2}$ without any correction for strain, a determination of the variation of σ_0 with strain can be made.

At 18°C and -115°C a slightly different approach was possible, as described elsewhere (Petch 1955).

Any uncertainty in these corrections does not affect the main conclusion from these measurements, namely that the slope k is nearly independent of temperature. The slope at -196°C is largely fixed by measurements that involve very little strain before fracture, so these do not require any correction. At the other two temperatures, there is little variation of the strain at fracture with grain size, so the corrections required are very small and could be neglected. Also the allowance for necking by the Bridgman analysis is practically constant throughout the grain size range at these temperatures, so any uncertainties in this allowance have little effect on the slope.

Acknowledgment

The author wishes to thank Mr. A. Fillingham for his help with the experimental work.

References

Bridgman, P. W., 1943, *Trans. Amer. Soc. Metals*, **32**, 553.
Greenwood, G. W., and Quarrell, A. G., 1954, *J. Inst. Metals*, **82**, 551.
Koehler, J. S., 1952, *Phys. Rev.*, **85**, 480.
Mott, N. F., 1953, *Proc. Roy. Soc.* A, **220**, 1.
Petch, N. J., 1953, *J. Iron Steel Inst.*, **173**, 25 ; 1954, *Progress in Metal Physics* (London : Pergamon Press), **5**, 1 ; *Phil. Mag.*, in the press.
Stroh, A. N., 1954, *Proc. Roy. Soc.* A, **223**, 404.

XVII. *The Effect of Free Electrons on Lattice Conduction*

By J. M. Ziman
The Cavendish Laboratory, Cambridge University *

[Received September 29, 1955]

Abstract

The scattering of phonons by electrons is calculated, assuming the usual electron–phonon interaction, for a parabolic band whose degeneracy temperature is comparable with the temperature of the lattice. The contribution to the thermal resistance is given by an exact formula, subject only to justifiable assumptions concerning phonon–phonon interactions. With rising temperature the apparent mean free path of the phonons at first decreases as $1/T$ (or, if there are very few electrons, as $\exp(a/T)$), but reaches a minimum and then increases as T^2. Energy and momentum conservation then allow only the tail of the electron distribution to contribute to the scattering. The model is thought to apply to certain observations on p-type germanium, irradiated sapphire and conducting diamond.

The thermal conductivity of a dielectric solid at low temperatures is conveniently expressed by the equation

$$\kappa = \tfrac{1}{3}cvl, \qquad \ldots\ldots\ldots \quad (1)$$

where the specific heat, c, is proportional to T^3 at low temperatures, while the phonon velocity, v, may be taken as constant. Observation of κ thus gives the behaviour, with varying temperature, of l, the phonon 'mean free path'. Without going too deeply into the meaning of this quantity, we may see that, as the phonon distribution at temperature T is heaped up around a fairly high peak at the modes of angular frequency

$$\nu \sim 3kT/\hbar, \qquad \ldots\ldots\ldots \quad (2)$$

the variation of l as a function of T represents, crudely, the variation of the mean free path as a function of ν. For example, if κ is proportional to T^{-1} we conclude that the mean free path of a phonon is proportional to the fourth power of its wavelength—the result characteristic of Rayleigh scattering by obstacles small compared with the wavelength. This argument, combined with a variant of Matthiessen's rule for adding thermal resistances due to distinct scattering processes, can yield useful qualitative information about the types of lattice imperfections present in a given specimen, although it is difficult to justify it in detail (Berman 1953).

---

* Communicated by the Author.

If one thinks of the various possible imperfections—vacancies, interstitials, dislocations, impurities, etc.—one can see that l should always *increase* as the phonon wavelength increases. Only total scattering by the surfaces of the specimen, or by large-angle grain boundaries, could be expected to be independent of the phonon wavelength: even then, the effects of specular reflection cannot be neglected (Berman, Simon and Ziman 1953, Berman, Foster and Ziman 1955). However, recent experiments by Berman, Schneidmesser and Tirmizi (1955) have shown that in certain materials, such as gamma-irradiated artificial sapphire crystals and conducting diamonds, l can be nearly independent of temperature and yet very much smaller than can be explained by boundary scattering alone. Moreover, Rosenberg (1955) has found that in a certain specimen of p-type germanium the thermal conductivity varies as $T^{4\cdot4}$, which is apparently equivalent to l *decreasing* as the phonon wavelength increases.

To explain these anomalies, it was suggested that the phonons might be scattered by electrons (or holes) free to move in some sort of band which is not full at very low temperatures. As will be shown, a simple calculation along well worn tracks leads to unsuspected conclusions when the combined effects of momentum conservation and Fermi degeneracy are allowed for. This calculation is reported here; the detailed interpretation of the experimental results will be presented at a later date.

For the sake of simplicity, we take the most elementary model, in which the phonons have a 'Debye' spectrum with a single constant speed v, independent of their direction and polarization. The electrons will be supposed to lie in a parabolic band with effective mass m^*. By ignoring anisotropy and dispersion we have the advantage that the equations may be solved exactly and involve only these two parameters.

The calculation is a straightforward adaptation of the standard theory of the phonon–electron interaction and has been given already in the limiting case of a typical metal (Sommerfeld and Bethe 1933, Makinson 1938, Wilson 1953): we here consider the slightly more complex case where the temperature is comparable with the Fermi degeneracy temperature of the electron distribution. In brief, we are concerned with processes by which a phonon, of wave vector $\mathbf{p}$, interacts with an electron in the state of wave vector $\mathbf{k}$, which is then scattered into the state $\mathbf{k}'$ whilst the phonon is absorbed. The rate at which this process occurs is given by

$$\frac{\partial N_{\mathbf{p}}}{\partial t} = -\frac{C^2 p N_{\mathbf{p}}}{\rho V \hbar v} n_{\mathbf{k}}(1-n_{\mathbf{k}'})\Omega(E'-E), \qquad . \quad . \quad . \quad (3)$$

where $\Omega(x) \equiv \sin(xt/\hbar)/(x/\hbar)$. E, E' are the initial and final energies of the whole electron–phonon system; $N_{\mathbf{p}}$ is the number of phonons already in the mode $\mathbf{p}$; $n_{\mathbf{k}}$, $n_{\mathbf{k}}'$ are the numbers of electrons in states $\mathbf{k}$, $\mathbf{k}'$; ρ is the mass density of the lattice whose total volume is V. The parameter C has the dimensions of energy (a few electron volts, say) and measures the interaction between electrons and phonons.

Crystal momentum will be conserved in the transition (we are far below the possible limits for Umklapp processes). Hence

$$\mathbf{k}'=\mathbf{k}+\mathbf{p}. \qquad (4)$$

For conservation of energy, we have

$$E'=\frac{\hbar^2k'^2}{2m^*}=E=\frac{\hbar^2k^2}{2m^*}+phv. \qquad (5)$$

Putting these relations into (3), and summing over all possible electronic states, we find that the total rate of change of $N_{\mathbf{p}}$ due to scattering by carriers takes the form

$$\frac{\partial N_{\mathbf{p}}}{\partial t}=-N_{\mathbf{p}}\frac{C^2m^*}{2\pi\rho v\hbar^2}\int_{K_0}^{\infty}n_{\mathbf{k}}(1-n_{\mathbf{k}}')k\,dk, \qquad (6)$$

where k_0 is the minimum value of the modulus of $\mathbf{k}$ which will allow both (4) and (5) to be satisfied, i.e.

$$k_0=\left|\tfrac{1}{2}p-m^*v/\hbar\right|. \qquad (7)$$

If for $n_{\mathbf{k}}$, $n_{\mathbf{k}}'$, we assume the usual Fermi functions, e.g.

$$n_{\mathbf{k}}'=[\exp\{(E'-\zeta)/kT\}+1]^{-1} \qquad (8)$$

then (6) may be integrated exactly in terms of elementary functions. Since (6) is a differential equation representing the exponential decay of the number of phonons in the pth mode, we have at once the relaxation time for that mode, i.e.

$$\frac{1}{\tau_p}=\frac{C^2m^{*3}v}{4\pi\hbar^4\rho}\cdot\left\{\frac{kT}{\tfrac{1}{2}m^*v^2}\right\}\cdot\left\{\frac{z}{1-e^{-z}}\right\}\times\left\{1-\frac{1}{z}\ln\left(\frac{1+\exp\{(\tfrac{1}{2}m^*v^2-\zeta)/kT+z^2kT/8m^*v^2+\tfrac{1}{2}z\}}{1+\exp\{(\tfrac{1}{2}m^*v^2-\zeta)/kT+z^2kT/8m^*v^2-\tfrac{1}{2}z\}}\right)\right\} \qquad (9)$$

where $z=\hbar\nu_p/kT$.

At this point we run into a difficulty which lies deep in the theory of phonon transport and which has not been successfully resolved: how are we to calculate the contribution of this additional scattering process to the thermal resistance of the crystal? One method would be to write down a mean free path

$$l_p=v\tau_p \qquad (10)$$

for each mode, from (9), and to sum over the phonon distribution a series of contributions of the form of (1). Thus we would write

$$\kappa=\tfrac{1}{3}\int c_pvl_p\,dp, \qquad (11)$$

where c_p represents the contribution of the pth mode to the specific heat, i.e.

$$c=\int c_p\,dp. \qquad (12)$$

Unfortunately (11) diverges. To obtain a finite answer it would be necessary to take, in place of l_p, the mean free path for the combined effect of boundary and electron scattering, e.g.

$$l_p'=[l_p^{-1}+D^{-1}]^{-1} \qquad (13)$$

where D is the diameter of the specimen. But the boundary and electron-scattering resistances would then no longer be additive, and the application of Matthiessen's rule would be spurious. This method could be made to yield an answer, but the calculation would be very complicated because of the clumsy form of (13).

The alternative procedure* is to calculate the following average

$$\frac{1}{\bar{l}} = \frac{1}{c}\int \frac{c_p}{l_p}\, dp. \qquad \ldots\ldots (14)$$

This integral always converges, since l_p never tends strictly to zero. If now we write

$$W_e = [\tfrac{1}{3}cv\bar{l}]^{-1}, \qquad \ldots\ldots (15)$$

then this is a thermal resistance which is proportional to the integral in (14), depends only on the electron scattering process, and may legitimately be added to other thermal resistances to give the total resistance of the specimen, according to Matthiessen's rule.

An intuitive argument may be given to justify (14). If we use (11) we are, in effect, assuming that the phonon modes are independent of one another, and carry their separate contributions to the heat current without interference. This assumption is certainly false. There are, between the modes, anharmonic coupling terms which cause three-phonon processes, where a given phonon splits into two others, or two combine to give a third (Peierls 1955). The Umklapp processes, which give rise to the 'intrinsic' thermal resistance of the solid at high temperatures, are certainly frozen out of this calculation ; there are still the other processes, in which momentum is conserved, by which phonons interact strongly, but which give no direct contribution to the thermal resistance.

Now, suppose we have a packet of energy moving through the lattice, concentrated into modes of nearly a single wavelength. As a result of the phonon–phonon interaction, the initial phonons will soon have changed into a variety of others of different wavelengths. There will be a continual exchange of the energy in the packet from one mode to another. If this exchange takes place in a distance short compared with the distance between scattering electrons, the characteristic relaxation time for the packet cannot depend on the wavelength with which it started. Instead, all different values of the electron scattering cross section will be sampled, over all different wavelengths, to yield an average such as (14).

The mathematical justification derives from the general variational principle of transport theory, as applied to the phonon–phonon processes. It can be shown (Ziman, unpublished) that W_e is an upper limit to the excess resistance induced by scattering processes with relaxation time τ_p for phonons in the pth mode. It is assumed that the steady state phonon distribution is dominated by the non-Umklapp processes, but the problem of keeping the long-wave longitudinal phonons in equilibrium (Peierls 1955, Herring 1954) is not considered, and may lead to some error.

* This procedure was used by Berman, Foster and Ziman (1955), on intuitive grounds, before a mathematical justification was found.

The final result of our calculation comes from (9), (10), (12) and (14): the extra thermal resistance due to the scattering of phonons by electrons should appear to be due to a process for which the mean free path at temperature T may be written

$$\bar{l}=l_0\bar{\phi}(T_S/T,\ \zeta/kT), \qquad (16)$$

where

$$l_0=4\pi\hbar^4\rho/C^2m^{*3}. \qquad (17)$$

$$kT_S=\tfrac{1}{2}m^*v^2, \qquad (18)$$

$$\frac{1}{\bar{\phi}}\equiv\frac{T}{T_S}\frac{15}{32\pi^4}\int_0^\infty\frac{z^4\exp(\frac{1}{2}z)}{(\sinh\frac{1}{2}z)^3}$$
$$\times\ln\left\{\frac{\exp(T_S/T-\zeta/kT+z^2T/16T_S)+\exp(\frac{1}{2}z)}{\exp(T_S/T-\zeta/kT+z^2T/16T_S)+\exp(-\frac{1}{2}z)}\right\}dz. \qquad (19)$$

The integration can be carried out numerically with reasonable accuracy. To find $\bar{\phi}$ as an explicit function of temperature one must allow for the variation of the Fermi energy ζ with T. This may be taken from standard tables (e.g. Wilson 1953) once one has decided the degeneracy temperature of the electron distribution, i.e.

$$T_F=(\hbar^2/2m^*k)(3\pi^2n)^{2/3} \qquad (20)$$

if there are n electrons per unit volume.

The dimensionless function $\bar{\phi}$ has been calculated in terms of T/T_S for various values of T_F/T_S. The curves plotted in fig. 1 thus give the expected

Fig. 1

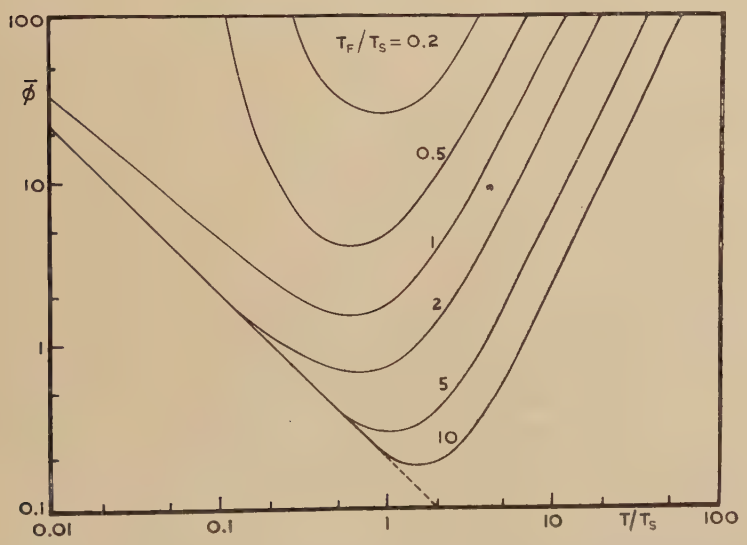

behaviour of the mean free path, suitably scaled, as a function of temperature relative to the scale temperature T_S, for different values of the free electron density. To grasp the behaviour of this function, let us

consider its asymptotic forms. Simple calculations from (19) give the following :

$$(a) \qquad T_F < T_S ; \quad \text{as} \quad T \to 0, \qquad \bar{\phi} \to 0{\cdot}2045 T_S/T. \qquad . \quad . \quad (21)$$

This is the usual result calculated for a metal. At low temperatures the electron distribution is highly degenerate. Only electrons in an energy range of width kT at the Fermi surface can take up the phonon energy and be scattered into empty states. The mean free path comes out inversely proportional to this number, i.e. varies as $1/T$.

$$(b) \qquad T_F < T_S ; \text{ as } T \to 0, \quad \bar{\phi} \to 0{\cdot}0336 (T_S/T) \exp \{(T_S - T_F)/T\}. \qquad (22)$$

The lower limit, k_0, of electron wave vectors is now operating. According to (7), when p is small, as at very low temperatures, only electrons with momentum exceeding m^*v can scatter the phonons. From (18), these have energy kT_S. But, when $T_F < T_S$, there are so few electrons that when the distribution is degenerate the Fermi level lies below kT_S. The number of electrons available for scattering is now reduced by a Boltzmann factor for the energy difference between the Fermi level, kT_F, and the level kT_S : the mean free path increases exponentially as the temperature falls.*

$$(c) \qquad \text{As } T \to \infty, \quad \bar{\phi} \to \frac{\pi^4}{80} \left(\frac{T}{T_F}\right)^{3/2} \left(\frac{T}{T_S}\right)^{1/2} \left[1 + \frac{4}{\sqrt{\pi}} \left(\frac{T_S}{T}\right)^{1/2}\right]^{-1}. \qquad (23)$$

This is the most interesting portion of the curve. If $T \gg T_S$, then most of the phonons have momenta far exceeding m^*v, and the value of k_0 becomes nearly equal to $\frac{1}{2}p$. Let us fix our attention on the ' dominant ' phonons at temperature T, i.e. those of energy around $3kT$. At some temperature the cut-off limit k_0 for these might lie as in fig. 2(*a*), so that most of the electrons can interact with the phonons. But, at twice the temperature, this limit will have moved out, as in fig. 2(*b*), so that only about half the electrons can act. If the temperature is doubled again, although the electron distribution broadens out and spreads to higher energies the limit is so raised that only the tail lies above it. It is this decrease in the number of electrons available for scattering that gives the rise in the mean free path. The asymptotic formula (23) show $\bar{\phi}$ proportional to T^2.

Rosenberg's observations could thus be explained if he were working at temperatures in the region (*c*), i.e. where the mean free path would appear to decrease as the temperature falls. Preliminary quantitative calculations show that T_S and l_0 might have values which would place the measurements on germanium on this part of the curve. In sapphire, and in diamond, the higher velocities of sound would make T_S much

* Professor Gorter has suggested, in private discussion, that the 2nd order perturbation terms (virtual absorption and re-emission of a phonon by an electron) might be important, since the momentum limit would not then apply. Inspection of the matrix elements shows that the probability of such a process is down by several orders of magnitude below the first order terms, and hence would not be observable.

greater, so that we should be in the region of the minimum in $\overline{\phi}$ at helium temperatures. This might well give apparently constant mean free path over a restricted range of temperatures, as in Berman's experiments.

Fig. 2

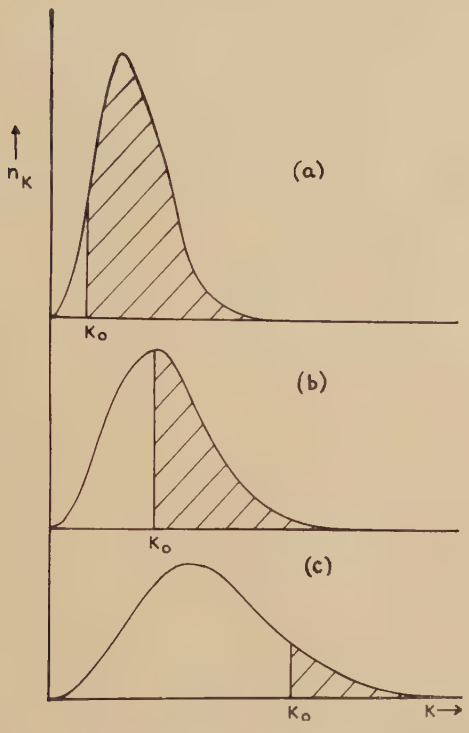

Electron distribution in momentum. Electrons capable of scattering the phonons of energy $3kT$ lie in the shaded regions.
(a) $T/T_S=4$; (b) $T/T_S=8$; (c) $T/T_S=16$.

It may be remarked that in this region the mean free path depends mainly on the electron density, and is almost independent of the value chosen for m^*. It is not to the point here to discuss how it is possible that there should be free electrons in these materials at such low temperatures, although the answer probably lies in the presence of impurity bands. We have seen, however, that from a grossly over-simplified model one can deduce precise formulae which seem to represent, at least qualitatively, the experimental results.

Acknowledgments

This work exists only by virtue of much correspondence and discussion with Drs. Berman, Foster and Rosenberg, to whom the author is gratefully indebted.

References

Berman, R., 1953, *Advances in Physics*, **2**, 103.
Berman, R., Foster, E. L., and Ziman, J. M., 1955, *Proc. Roy. Soc.* A, **231**, 130.
Berman, R., Simon, F. E., and Ziman, J. M., 1953, *Proc. Roy. Soc.* A, **220**, 171.
Berman, R., Schneidmesser, B., and Tirmizi, S. M. A., 1955, *Report of Paris Conference on Low Temperature Physics*.
Herring, C., 1954, *Phys. Rev.*, **95**, 954.
Makinson, R. E. B., 1938, *Proc. Camb. Phil. Soc.*, **34**, 474.
Peierls, R. E., 1955, *Quantum Theory of Solids* (Oxford: University Press).
Rosenberg, H. M., 1955, *Report of Paris Conference on Low Temperature Physics*.
Sommerfeld, A., and Bethe, H., 1933, *Handbuch d. Physik*, **24**/2, 333.
Wilson, A. H., 1953, *The Theory of Metals*, 2nd Ed. (Cambridge: University Press), p. 292.

XVIII. *The Decay of Potassium* 40

By A. McNair, R. N. Glover and H. W. Wilson
Department of Natural Philosophy, The University, Glasgow, W.2*

[Received October 20, 1955]

Abstract

The decay of ^{40}K has been reinvestigated and values of the branching ratio, defined as the ratio of gamma or electron capture to beta transitions, have been determined by two methods, giving the values $0{\cdot}124 \pm 0{\cdot}002$ and $0{\cdot}121 \pm 0{\cdot}004$ respectively. The absolute beta and gamma decay rates and the half-life have been measured, the value of the latter being $1{\cdot}28 \pm 0{\cdot}02 \times 10^9$ years. A fresh determination of the gamma energy is described, and evidence as to the mode of decay is discussed. Finally, the results are given of experiments on the reflection of electrons by solid source supports.

§ 1. Introduction

The decay of Potassium 40 has been the subject of many investigations in the past and it is now fairly well established that the decay is according to the scheme shown in fig. 1, first suggested in a slightly modified form by Suess, 1948. The experiments about to be described were undertaken to elucidate several uncertain results, in particular the branching ratio of the decay which will be defined here as the ratio of the gamma or electron capture transition rate to the beta transition rate. This ratio may be determined by two methods :—

(1) By direct counting methods and the application of suitable corrections for solid angle, efficiency etc.

(2) By measurement of the amount of argon or calcium, or both, in a potassium-bearing mineral of known geological age (the geological method).

The results obtained by method (1) show a certain variation, but in general tend towards a value of the ratio of 0·12. (Sawyer and Wiedenbeck 1949, 1950, Houtermans *et al.* 1950, Ceccarelli *et al.* 1950, Spiers 1950, and others.) The results of some investigators are not quite independent since they measured only the gamma or beta activity and relied on the results of others to derive the ratio. The results obtained by method (2) show a greater variation and the values obtained range from 0·05 to 0·12, more recent results being in the region of 0·09 (Shillibeer and Russell 1954, Wasserburg and Hayden 1954) to 0·12 (Inghram *et al.*

* Communicated by the Authors.

1950). The fact that the geological method tends to give a lower value is of considerable importance since the reverse process of measuring the ^{40}K–^{40}A ratio is of value in the determination of the age of minerals. Two reasons for arriving at a lower ratio which one might suspect are, firstly, loss of argon from the mineral during geological times and, secondly, incomplete removal of argon from the mineral sample. That the latter can happen has been proved by re-examination of the minerals used by Russell *et al.* (who got a value of 0·06, Russell *et al.* 1953) by Wasserburg and Hayden (1954) and by Shillibeer *et al.* (1954) the results of the last two investigations yielding a value of about 0·090 due to more efficient argon extraction. In view of the discrepancies, it was felt well worthwhile making, as carefully as possible, another determination of the branching ratio by the counting method. At the same time fresh estimations were made of the absolute beta and gamma decay rates (and, hence, of the half-life) and the energy of the gamma transition while further experimental evidence for the decay scheme of fig. 1 was sought. In order to arrive at absolute values of the beta decay rates, experiments on the back-scattering of electrons were made, and are reported here.

Fig. 1

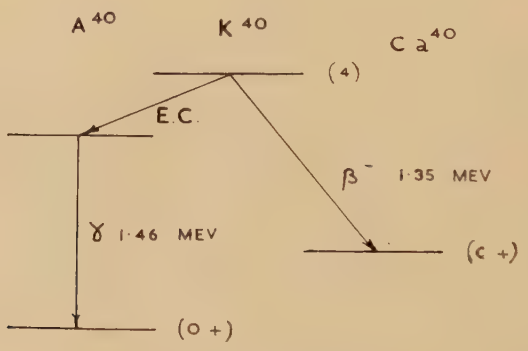

Decay scheme of ^{40}K.

§ 2. The Measurement of the Branching Ratio

Two methods were employed to measure the branching ratio. In both methods, it was assumed that the decay scheme of fig. 1 was correct and that the ratio of the absolute rates of emission of gamma rays to beta particles yielded the branching ratio.

First Method

In the first method, difficult and uncertain calculation of the beta and gamma detector overall efficiencies was avoided, to a first order, by comparing the known gamma–beta ratio of ^{60}Co to that of ^{40}K. The energies of the gamma transitions of ^{60}Co (1·17 and 1·33 Mev) are fairly close to the ^{40}K gamma energy (1·46 Mev). Had the gamma ray energies,

the maximum beta ray energies and the beta spectrum shapes been identical, it is easy to show that the branching ratio for ^{40}K, R say, would have been given by

$$R = 2\frac{\gamma_K}{\beta_K}\frac{\beta_{Co}}{\gamma_{Co}}$$

where γ_K, β_K are the gamma and beta counting rates of a known ratio of amounts of ^{40}K and γ_{Co}, β_{Co} are the corresponding rates for the *same* ratio of quantities of ^{60}Co. As the gamma and beta spectra were not identical corrections had to be made. These will be described later.

The gamma detector is shown in fig. 2. A NaI crystal, thallium activated, 2 in. long and $\frac{3}{4}$ in. diameter, is surrounded coaxially by a cylindrical vessel of capacity 186 cm^3 which was filled to a mark A with the solutions which were measured. The crystal, which was surrounded by sufficient absorber to absorb all beta particles, was mounted

Fig. 2

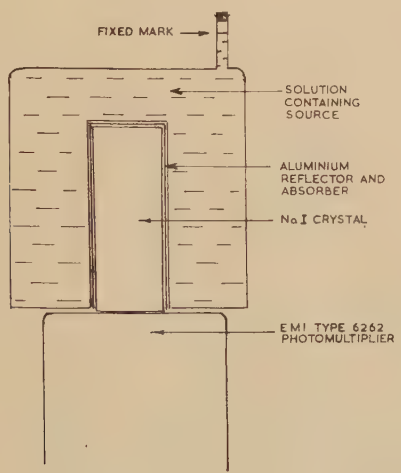

Gamma ray detection apparatus. Lead shielding not shown.

on an EMI type 6262 photomultiplier and the whole encased by 4 in. of lead. The pulses were amplified, passed through a discriminator and recorded by a scaler. The solutions used were, (i) water containing a known aliquot of a standard $^{60}CoCl_2$ solution and (ii) an aqueous solution of potassium hydroxide (493 g K/litre), the latter giving 700 c.p.m. above background (87 c.p.m.). It was found that the background with water, carbon tetrachloride or aqueous solutions of calcium chloride or sodium chloride in the vessel was slightly higher than when it was empty, the actual rate being independent, within experimental error, of which liquid was employed. Hence the background rate was always checked with water in the vessel. Integral bias curves were obtained for the test solutions between the energies of 10–100 kev. Calibration

was effected by the 46·7 kev gamma ray of RaD. The results for potassium with and without background subtracted are shown in fig. 3 (*a*) and fig. 3 (*b*). Figure 3 (*c*) is the curve obtained after correcting for bremsstrahlung as will be described later. Figure 4 is the corresponding curve for ^{60}Co. The counting rates γ_K, γ_{C_o} to be substituted in the formula were obtained by extrapolating the curves to zero energy and making the necessary corrections to the values thus obtained.

Fig. 3

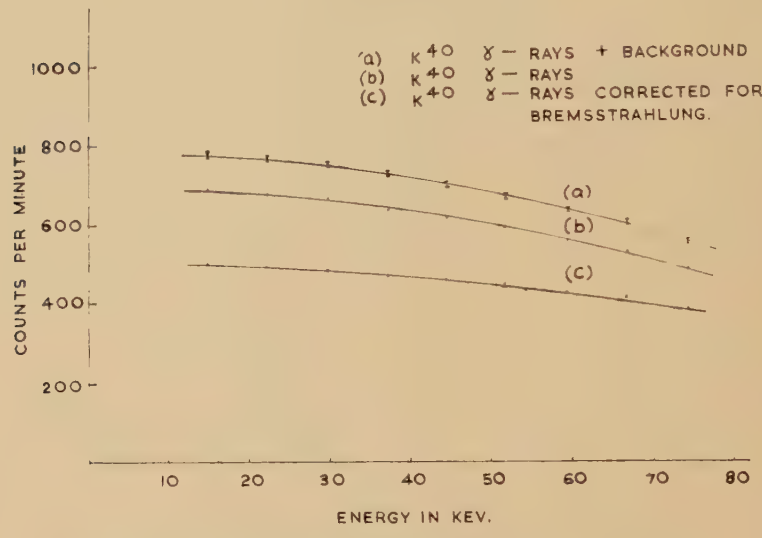

Discriminator bias curves for ^{40}K gamma rays.

The beta detector was a cylindrical, end-corrected proportional counter filled with argon and methane to a total pressure of one atmosphere. The source was spread uniformly over an area of $\sim$1000 cm^2 on a thick stainless steel foil pressed against the wall of the counter. The large surface area ensured reasonable counting rates from thin sources of ^{40}K($\sim$1 mg/cm^2). In order to reduce the background, the counter was surrounded by a double layer of G–M counters in anti-coincidence and the whole, in turn, by 4 in. of lead on all sides. The anti-coincidence arrangement was not used in the measurement of the ^{60}Co beta emission rate as a reduction in counting rate of $\sim$4% was found due to coincident detection of the gammas in cascade with the betas. Integral bias curves were taken from 0·2–10·0 kev.

§ 3. Corrections

In calculating the branching ratio from these results corrections must be made for (i) absorption and scattering of ^{40}K gamma rays by the dense and relatively high Z potassium hydroxide solution ; (ii) the slight

difference in the crystal efficiency for ^{40}K and ^{60}Co gammas ; (iii) gamma detector counts due to bremsstrahlung, especially in the case of ^{40}K ; (iv) coincident detection in the crystal of both ^{60}Co gamma rays. A separate series of experiments, described later, showed that the fraction of electrons reflected by the stainless steel source support was the same for ^{60}Co and ^{40}K so that no correction for this effect was necessary in determining the branching ratio.

Fig. 4

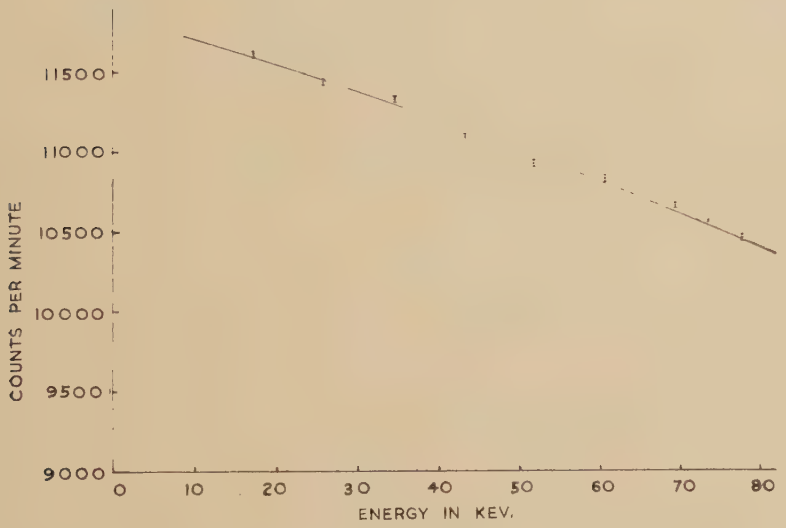

Discriminator bias curve for ^{60}Co gamma rays.

The correction for absorption and scattering of ^{40}K gamma radiation was determined by adding a known small volume of $^{60}CoCl_2$ solution to the potassium hydroxide solution and comparing the increase in counting rate with that due to the same quantity of $^{60}CoCl_2$ solution diluted with water to fill the vessel. It was found that the effect of the potassium hydroxide solution was to increase the counting rate slightly showing that the absorption of the gamma rays was more than compensated for by their being scattered into the crystal, in the geometry employed. A correction to the gamma counting rate of about 6% had to be applied to allow for this effect.

The correction for the slight difference in detection efficiency for ^{60}Co and ^{40}K gammas was determined by postulating an average path length in the crystal, X say, which the gammas have to traverse. Then it can be shown that the ratio of the true count rates, I_{Co}, I_K say, is given, for our experimental arrangement, by the expression

$$\frac{I_{Co}}{I_K} = 1{\cdot}015 \frac{\rho_K}{\rho_{Co}} \frac{\gamma_{Co}}{\gamma_K}$$

where ρ_K, ρ_{Co} are the absorption coefficients of NaI for the ^{40}K and ^{60}Co gamma rays and γ_K, γ_{Co} are the measured count rates.

It is necessary to make a correction to the ^{40}K gamma counting rate for the effect of bremsstrahlung. This effect is much more important for the case of ^{40}K than for ^{60}Co since (*a*) the ratio of betas to gammas is $\sim$16 times greater, (*b*) the ^{60}Co beta spectrum is softer, (*c*) the ^{60}Co betas pass through a solution of lower density and of lower atomic number. The effect was estimated by examining, as a function of discriminator voltage, the counting rate in the gamma detector due to the addition of a solution of ^{32}P which emits only electrons. The strength of the solution was monitored by measuring the beta rays, using the proportional counter. Figure 3 (*c*) shows the ^{40}K spectrum corrected for bremsstrahlung.

A small correction was made to the ^{60}Co gamma rate to allow for the probability of coincident detection of the two gammas which are emitted in cascade by this source.

Result by the First Method

The value of the branching ratio obtained by this method was

$$R = 0{\cdot}124 \pm 0{\cdot}002$$

or $11{\cdot}0 \pm 0{\cdot}2\%$ of the decays are to ^{40}A, $89{\cdot}0 \pm 0{\cdot}2\%$ to ^{40}Ca.

Second Method

This method eliminated many of the corrections necessary in the first. It made use of the fact that ^{24}Na possesses a gamma transition very close in energy to that of ^{40}K (1·38 Mev and 1·46 Mev respectively) while the beta ray energies are almost identical (1·39 Mev and 1·36 Mev resepctively). In principle, the areas under the photo-electric peaks of the gamma rays as observed by a large NaI(Tl) crystal were compared, the sources being monitored by their beta emission. ^{24}Na emits also a 2·76 Mev gamma ray which precluded its use in the first experiment.

The gamma spectrum of ^{40}K was examined by placing a shallow cylindrical glass vessel (1 in. high $\times$ 2 in. diameter), filled with a concentrated solution of potassium hydroxide, on top of a large (2 in. long $\times$ 2 in. diameter) NaI(Tl) crystal which was mounted, in turn, on a Dumont Type 6292 photomultiplier, the whole being surrounded by lead. The pulses were analysed by means of a 100-channel kicksorter of the Hutchinson–Scarrott type. A very small quantity of $^{24}NaCl$ solution was mixed with the potassium hydroxide solution and a second spectrum taken. By subtraction and knowing the form of the background spectrum, the spectra, corrected for background, were obtained (figs. 5 and 6). The areas under the photo-electric peaks, corrected in the case of ^{24}Na for the small contribution from the Compton electrons due to the 2·76 Mev gamma ray, gave a relative measurement of the gamma ray

intensities. The beta rates were found for the potassium hydroxide solution and for the mixed solution, by examination in the proportional counter used previously. The result was corrected for the decay of the ^{24}Na.

Figs. 5 and 6

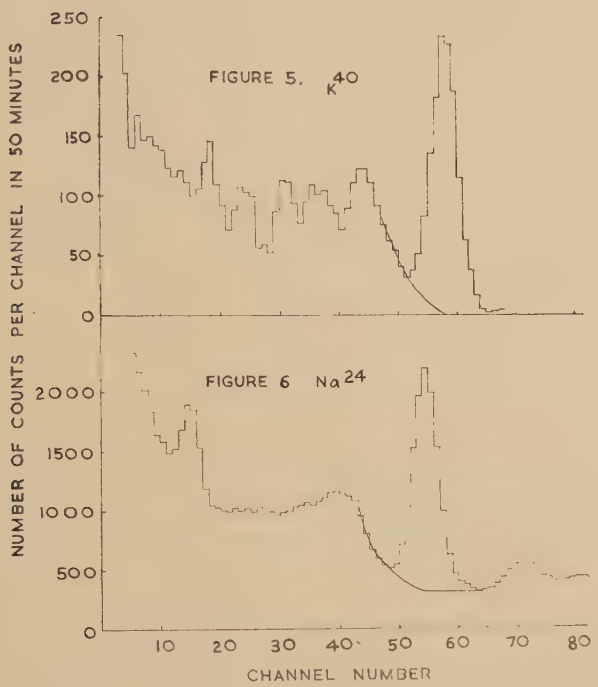

The gamma ray spectra of ^{40}K and ^{60}Co.

The branching ratio is now given by the expression

$$R = \frac{\gamma_K}{\beta_K} \frac{\beta_{Na}}{\gamma_{Na}}$$

where γ_K, β_K and γ_{Na}, β_{Na} refer to the gamma and beta counting rates of potassium and ^{24}Na respectively.

As the beta ray energies were practically the same, no correction for reflection of electrons by the source and source support was necessary. (This experiment was devised before completion of the reflection experiments which showed no change in the back scattering factor over an energy range which included ^{60}Co and ^{40}K beta ray energies). Since the ^{24}NaCl was added to the potassium hydroxide solution, no correction for absorption and scattering of ^{40}K was necessary. The use of a mixed source in the proportional counter meant that no correction for source thickness was necessary since it was effectively the same for both the ^{40}K and the ^{24}Na measurements. Bremsstrahlung from the beta rays

did not affect the magnitude of the peaks since the maximum beta ray energies are close to the gamma ray energies.

Corrections were made for (*a*) the probability of coincident detection of the 1·38 and the 2·76 Mev gamma rays in the ^{24}Na measurement. (*b*) the slight difference in the scintillation detector efficiency for 1·38 Mev and 1·46 Mev gamma rays and (*c*) the dead time of the kicksorter, which was 0·75 milliseconds. The first was calculated by estimating the actual disintegration rate from a knowledge of the beta counting rate and assuming a backscattering coefficient of 0·45 for the stainless steel support. The efficiency of the crystal for 1·38 and for 2·76 Mev gamma rays was calculated and the error introduced due to coincident detection found to be $\sim$7%. Note that the assumption of a particular value of a back scattering factor here does not introduce any appreciable error, since the value of the correction is small. The second correction was calculated as described earlier for the first method.

Result by the Second Method

The value of the branching ratio is

$$R=0\cdot121\pm0\cdot004$$

or $10\cdot8\pm0\cdot4$% of the decays are to ^{40}A, $89\cdot2\pm0\cdot4$% to ^{40}Ca, in good agreement with the value obtained by the first method.

The Absolute Decay Rates and the Half-life of ^{40}K

Assuming a backscattering factor of $0\cdot450\pm0\cdot015$ for ^{40}K beta rays, we calculate the disintegration rate for the decay to ^{40}Ca to be

$$1650\pm15 \text{ betas/gram/minute}$$

and for the decay to ^{40}A to be

$$204\cdot5\pm3\cdot8 \text{ gammas/gram/minute.}$$

This figure, of course, does not include argon x-rays resulting from electron capture. These values give a total half-life of

$$1\cdot28\pm0\cdot02\times10^{8} \text{ years}$$

assuming Nier's value of $0\cdot0119\pm0\cdot001$% for the abundance of the ^{40}K isotope in potassium (Nier 1950).

§ 4. The Energy of the Gamma Ray

The gamma ray spectrum emitted by $\sim$330 g of pure potassium chloride was examined using the crystal and kicksorter which were employed in the measurement of the branching ratio by the second method. Comparison with the gamma radiation of ^{22}Na (1·277 Mev) and ^{24}Na

(1·38 MeV) gave an energy for the ^{40}K gamma ray of 1·46±0·01 MeV in agreement with values obtained by other investigators (Bell and Cassidy 1950 b, Good 1951 a). The gamma spectrum is shown in fig. 7.

Fig. 7

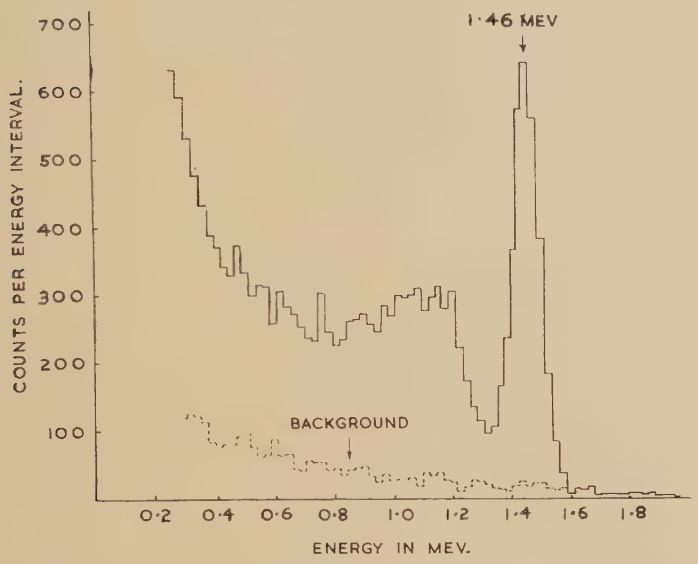

^{40}K gamma ray spectrum.

§ 5. The Evidence for the Mode of Decay of ^{40}K

There is a large body of evidence favouring the decay scheme of fig. 1, although much of it is not altogether convincing, due to the difficulty of carrying out coincidence experiments with the very low specific activities involved. Perhaps the most satisfying proof is that of Johnson (1952) who showed by measurement of the masses of ^{40}A, ^{40}K and ^{40}Ca that the energies available for the decay to ^{40}A and to ^{40}Ca are 1·30±0·07 MeV and 1·49±0·07 MeV respectively. The first value is in good agreement with the maximum beta energy (1·35 MeV) and examination of the spectrum shape fails to reveal the presence of softer beta spectra. Also the energy available is less than the energy of the gamma ray which must therefore be associated with the decay to ^{40}A. Sawyer and Wiedenbeck (1950) report that the electron capture disintegration rate approximately equals the gamma emission rate. Thus, the probability of electron capture to the ground state of ^{40}A is fairly small, a result supported theoretically by Morrison (1951). The absence of 0·511 MeV gamma rays (Bell and Cassidy 1950 a, 1950 b, Good 1951 b) and of 180° coincidences (Colgate 1951) show that the probability of decay by positron emission is very small, $<0·06\%$ according to Colgate and $<0·10\%$ according to Good. Morrison's theoretical investigation confirms these results.

An examination of fig. 7 shows no evidence of a lower energy gamma transition which shows that decay to an excited state of ^{40}A below 1·46 MeV is not probable ; nor has any such level been found by particle excitation experiments (Endt and Kluyver 1954).

Johnson's results make it most unlikely that there should be two gamma transitions in cascade unless one were very soft. Nevertheless direct experimental evidence is desirable. Figure 8 (*a*) shows the ^{40}K

Fig. 8

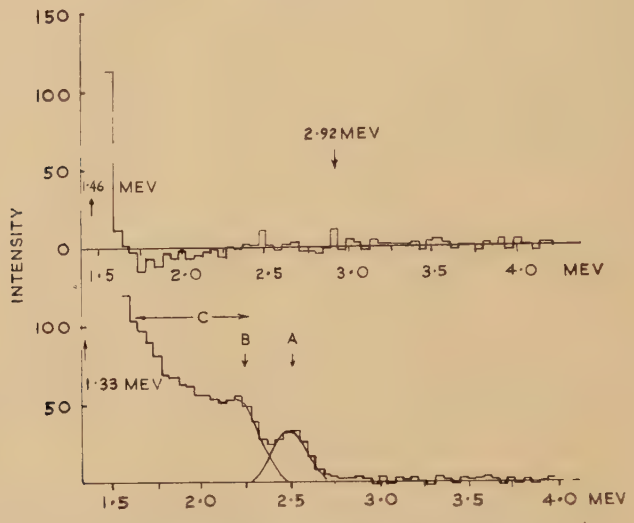

(*a*) ^{40}K gamma spectrum above 1·46 MeV.
(*b*) ^{60}Co gamma spectrum above 1·33 MeV.

gamma spectrum above 1·46 MeV while fig. 8 (*b*) shows the corresponding region for ^{60}Co. In this case there is a fairly well defined peak A at 2·50 MeV due to the coincident detection of the 1·17 and 1·33 MeV gamma rays. B represents the Compton edge of one gamma ray carried forward by the coincident photo-electric capture of the other. The region C is due to the integration of the two Compton distributions. No such effect is observed in fig. 8 (*a*) and from this graph we believe that fewer than 10% of the gamma transitions are in coincidence. A separate gamma gamma coincidence experiment was carried out to investigate this point further. A NaI detector was placed against the side of the vessel shown in fig. 2 and the coincidence rate observed as the vessel was filled in turn with water, potassium hydroxide solution and ^{60}CoCl$_2$ solution. However, the overall efficiency of the system was very low and, on the basis of this experiment, we can say only that fewer than one in five gamma rays were in coincidence.

Although Johnson's figures do not permit of the possibility of a gamma of energy equal to, or greater than, 1·35 MeV being involved in the decay

to ^{40}Ca, and Endt and Kluyver report no energy level in ^{40}Ca lower than 3·35 MeV, several searches for beta–gamma coincidences have been made (Meyer *et al.* 1947, Houtermans *et al.* 1950). No beta–gamma coincidences were detected. We also carried out a search for beta–gamma coincidences using a source of enriched potassium. Enriched potassium chloride (60 mg) was placed on a 1 mil aluminium foil and covered with a thin plastic sheet and a 50 mil sheet of steel to absorb the beta rays. On top of this was placed a 1 in. cube of NaI to detect the gammas while on the other side the beta detector consisted of a $2\frac{1}{2}$ in. diameter plastic phosphor (1·5% 1 : 1 : 4 : 4 tetraphenyl 1 : 3 butadiene dissolved in polystyrene). The whole system was surrounded by 4 in. of lead. The pulses were amplified, passed through discriminators and then into a coincidence circuit, the resolving time of the circuit being $6{\cdot}2\times10^{-7}$ seconds. The beta, gamma and beta–gamma coincidence rates were recorded as a function of beta discriminator voltage. The enriched potassium chloride was found to be only $\sim$0·57% ^{40}K whereas a degree of enrichment of approximately 150 had been anticipated. Consequently the counting rates were lower than had been expected when the experiment was planned. With the source in position the coincidence rate increased by $1{\cdot}43\pm0{\cdot}20\times10^{-3}$ coincidences per beta detected. Since some of this could have been due to bremsstrahlung, ^{32}P was substituted and gave an increase of $1{\cdot}040\pm0{\cdot}016\times10^{-3}$ coincidences per beta, i.e. a somewhat smaller increase than in the case of ^{40}K. However, in view of the low counting rates involved the authors do not attach too much importance to this difference. It is hoped that, at a future date, the use of larger quantities of more highly enriched potassium and bigger crystals will permit more significant measurements to be made.

§ 6. The Backscattering of Electrons

Two methods of measuring backscattering were employed. In the first, a thin beta emitting source was deposited on a thin nylon film, which effectively formed part of the cathode of a cylindrical proportional counter. That the film caused negligible backscattering was shown by reversing it, this giving no detectable decrease in count rate. A saturation thickness of steel or aluminium was placed behind and in contact with the film. The backscattering factor was then given by the ratio of the increase in count rate with the backing to the rate without backing.

A second method was evolved to meet the criticism of Jaffe (1950) that a source having a film of nylon between it and the backing is not necessarily equivalent to a source deposited directly on the backing. Sources emitting both gamma and beta radiation were employed and the count rates of sources deposited on nylon and directly on the backing material were compared, the relative source strengths being obtained from the gamma emission rate. Essentially the same results were obtained

by both methods and there was no suggestion of a systematic variation of backscattering factor with the method employed.

For the first method, ^{60}Co, ^{22}Na, ^{24}Na, ^{89}Sr, and ^{32}P were employed, but ^{89}Sr and ^{32}P were unsuitable for the second method. The results are shown in fig. 9 where the points indicate, in most cases, the average

Fig. 9

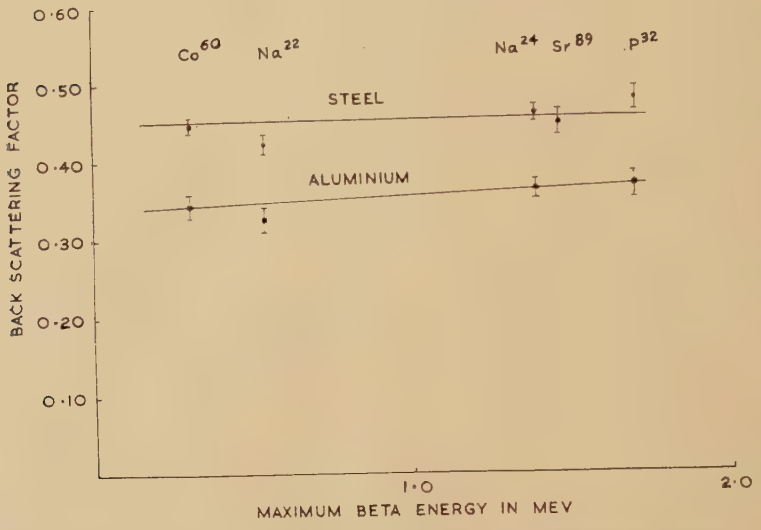

Backscattering of electrons by steel and aluminium source supports. Circles and squares indicate results for steel and aluminium respectively.

of several determinations by both methods. The errors take into account the scatter of the individual results and are larger than those due to the statistics of counting alone. In the case of steel, there appears to be no significant energy dependence, in the region investigated, though there may be a slow increase with energy for aluminium. There appears to be some slight justification for believing that the backscattering factors for positrons (^{22}Na) are somewhat lower than for negatrons. Assuming no energy dependence for steel and aluminium the average values obtained are

Steel .. .. $0{\cdot}449 \pm 0{\cdot}009$

Aluminium .. $0{\cdot}348 \pm 0{\cdot}075$.

In calculating the absolute decay rates, a value for steel of $0{\cdot}450 \pm 0{\cdot}015$ was taken.

§ 7. Conclusion

The experiments described here yielded values for the branching ratio, absolute decay rates and half-life of ^{40}K. The gamma and beta ray energies appear to be well established and the form of the beta spectrum has been carefully studied by several investigators. At present, however,

the evidence for the mode of the decay is somewhat indirect or lacking in precision and it is felt that it would be worthwhile carrying out further experiments to verify the presently accepted decay scheme.

Acknowledgments

We wish to thank Dr. S. C. Curran, F.R.S., for many helpful comments and discussions, and Professor P. I. Dee, F.R.S., for his interest and encouragement. Two of us (A. McN. and R. N. G.) wish to record our indebtedness to D.S.I.R. for the award of research grants.

References

Balfour, J. G., 1954, *J. Sci. Inst.*, **31,** 395.
Bell, P. R., and Cassidy, J. M., 1950 a, *Phys. Rev.*, **77,** 409 ; 1950 b, *Ibid.*, **79,** 173.
Ceccarelli, M., Quareni, G., and Rostagni, A., 1950, *Phys. Rev.*, **80,** 909.
Colgate, S. A., 1951, *Phys. Rev.*, **81,** 1063.
Endt, P. M., and Kluyver, J. C., 1954, *Rev. Mod. Phys.*, **26,** 147.
Good, M. L., 1951 a, *Phys. Rev.*, **81,** 891 ; 1951 b, *Ibid.*, **81,** 1058.
Houtermans, F. G., Haxel, O., and Heintze, J., 1950, *Z. Physik*, **128,** 657.
Inghram, M. G., Brown, H., Patterson, C., and Hess, D. C., 1950, *Phys. Rev.*, **80,** 916.
Johnson, W. H., 1952, *Phys. Rev.*, **88,** 1213.
Meyer, H. A., Schwachhiem, G., and de Souza Santos, M. D., 1947, *Phys. Rev.*, **71,** 908.
Morrison, P., 1951, *Phys. Rev.*, **82,** 209.
Nier, A. O., 1950, *Phys. Rev.*, **77,** 789.
Russell, R. D., Shillibeer, H. A., Farquhar, R. M., and Mousuf, A. K., 1953, *Phys. Rev.*, **91,** 1223.
Sawyer, G. A., and Wiedenbeck, M. L., 1949, *Phys. Rev.*, **76,** 1535 ; 1950, *Ibid.*, **79,** 490.
Shillibeer, H. A., and Russell, R. D., 1954, *Can. J. Phys.*, **32,** 681.
Shillibeer, H. A., Russell, R. D., Farquhar, R. M., and Jones, E. A. W., 1954, *Phys. Rev.*, **94,** 1793.
Spiers, F. W., 1950, *Nature, Lond.*, **165,** 356.
Suess, H. E., 1948, *Phys. Rev.*, **73,** 1209.
Wasserburg, G. J., and Hayden, R. J., 1954, *Phys. Rev.*, **93,** 645.
Yaffe, L., October, 1950, Prelim. Report No. 8, *Nuclear Science Series.*

XIX. *Multiple Scattering of Electrons and Positrons in Nuclear Emulsions*

By F. F. Heymann and W. F. Williams
Department of Physics, University College, London*

[Received August 8, 1955]

§ 1. Introduction

The work described below was performed in the Physics Laboratories at University College, in order to add to the available experimental information on the multiple scattering of electrons and positrons in nuclear emulsions in the range of energies between 1 and 3 Mev. Where it was found possible, plates were exposed under nearly identical conditions to electrons and positrons of the same energy, in order to enable close comparison between the behaviour of the two types of particle to be made.

§ 2. Exposure of Plates

The observations were made on six plates chosen from a series which were exposed to nearly mono-energetic electrons and positrons obtained from radio active sources.

Plates No. 1 and No. 2, (2 in. × 2 in., Kodak NT4), were irradiated in a flat magnetic spectrometer. The magnet was one which had been designed for a microtron (Henderson *et al.* 1953) and was utilized for the present purpose prior to completion of this machine. The magnetic field distribution of this magnet is uniform to better than $\pm 0{\cdot}05\%$ over the region used for the present experiments, and its absolute calibration at the time of use is known to better than $\pm 0{\cdot}5\%$.

The vacuum chamber of the spectrometer was designed such that the radioactive source and the centre of the photographic plate respectively were at the 180° points of particle trajectories with a mean radius of 10·5 cm.

Baffles were inserted between the source and the plate-holder such as to limit the direction of entry of electrons to $\pm 6°$ from the mean direction.

The plate holder was designed to allow the electrons to enter the emulsion at a glancing angle of incidence of 8°.

Because of the finite size of the plates, the incident energy of the electrons varied by $\pm 6\%$ over the area scanned. The tracks were found to be distributed uniformly enough over the scanned area to enable a simple correction for this energy spread to be made.

Plates No. 3, No. 4, No. 5 and No. 6, (3 in. × 1 in. Ilford G5), were exposed to radioactive sources in a lens spectrometer which has been fully described elsewhere (Rundle *et al.* 1954). This spectrometer had been equipped with

* Communicated by Professor H. S. W. Massey, F.R.S.

a helical baffle system such that either electrons or positrons could be focused on to the photographic plate by a reversal of the magnetic field direction.

The absolute calibration of this spectrometer is known to better than $\pm 0{\cdot}5\%$, and the scanned area of the plates was chosen such as to keep the total spread in energy to less than $\pm 3\%$.

The plates were exposed as shown in table 1.

Table 1

Plate No.	1	2	3	4	5	6
Plate type	NT4	NT4	G5	G5	G5	G5
Particles	Electron	Electron	Positron	Positron	Electron	Positron
Approx. energy in MEV	1·0	1·5	1·0	1·5	2·5	2·5

§ 3. Observations

The plates were scanned on Cooke M 4005 microscopes, using $45\times$ oil-immersion objectives and $15\times$ eyepieces.

In all cases an area less than 1 in. $\times \frac{1}{4}$ in. near the centre of the plate was scanned, in order to exclude tracks in the possibly distorted emulsion at the edges of the plates as well as to minimize the energy spread of the particles.

Only tracks with an initial direction within $\pm 6^\circ$ of the expected mean direction were taken into account. A subsidiary experiment indicated that this angular range would exclude the bulk of the background tracks.

At the relatively low energies involved in these experiments, the tracks deviate so much from linearity that the coordinate method of making multiple scattering measurements due to Fowler is not feasible unless inordinately small cell lengths (< 5 microns) are used. Accordingly, the observations were recorded in terms of the projected angles between successive chords measured by means of an ocular protractor. Again, because of the large scattering angles observed, no correction for microscope noise was necessary. A chord length of 50 microns was used in all six cases.

The number of observations made on each plate varied from 672 to 1102. In the plates exposed to 1·5 MEV and 2·5 MEV particles, measurements were made on no more than four 50-micron chords on each track. No correction for energy loss was made. On the two plates exposed to 1·0 MEV particles, because of the considerable difficulty in finding tracks not scattered out of the emulsion, readings were made (where it was possible) on up to ten 50-micron chords ; in consequence a correction for energy loss was essential. This was done by calculating the theoretical rate of loss of energy for electrons at 1·0 MEV (Ross and Zajac 1949) and assuming the rate to vary little over the range, calculating the mean energy over the total length of track under observation.

§ 4. Results

The angular distribution on each plate was examined and found to be approximately Gaussian. The number of readings on each plate (approx. 800) was insufficient to enable more exact comparison with the theoretical shape of the distribution curve to be made. However a composite distribution of scattering on all plates was obtained by summing the distribution in intervals of one-quarter of their separate r.m.s. scattering angles. This is shown in fig. 1 compared with a Gaussian of the same r.m.s. angle and

Fig. 1

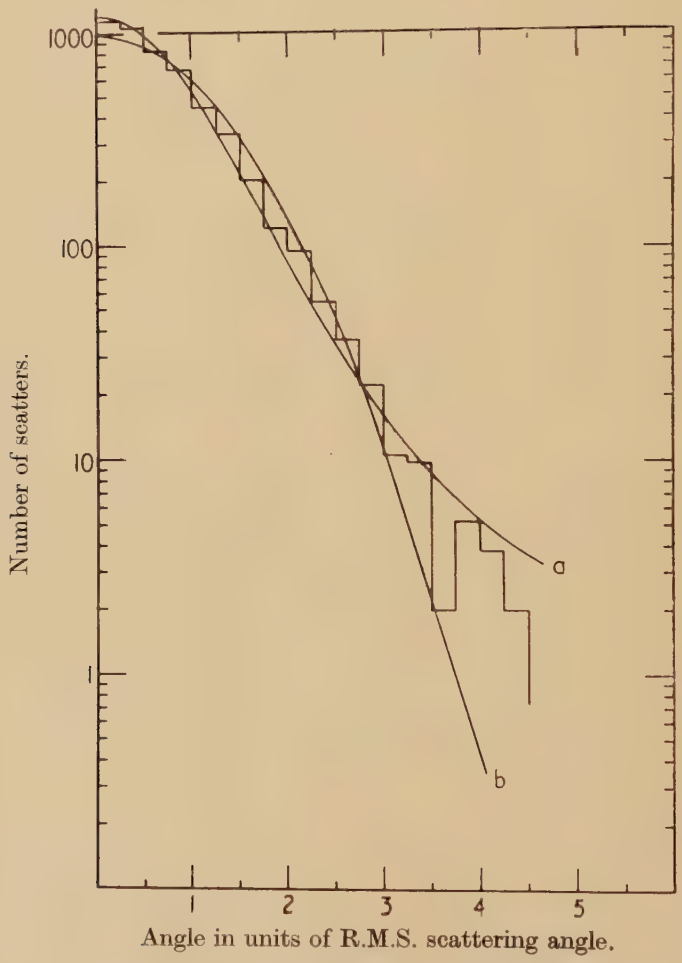

Composite histogram of all electrons and positrons.
(a) Molière distribution. (b) Gaussian distribution.

with a Molière distribution with the same mean scattering angle. Similar composite histograms are shown for electrons and positrons separately in figs. 2 and 3 respectively.

The values of the scattering constants with and without cut-off have been calculated for the readings on each plate and are shown compared with the values predicted by Williams and by Molière in table 2. $K_{\text{Molière}}$ was calculated directly from information supplied by the makers of the respective emulsions, by the method described by Molière (1948), and the method of smoothing in converting from tangent to chord angles described by Menon *et al.* (1951).

Fig. 2

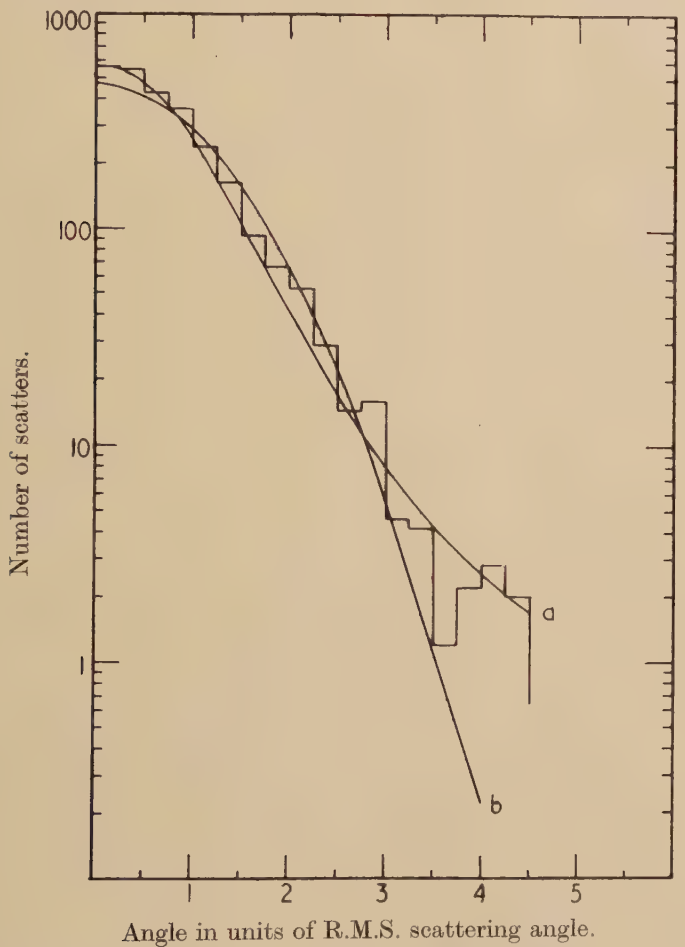

Composite histogram of all electrons.
(a) Molière distribution. (b) Gaussian distribution.

All the values shown, both theoretical and experimental are for 50-micron chord lengths. At both 1 and 1·5 Mev, the experimental positron-electron differences are largely caused by the different emulsions used ;

Fig. 3

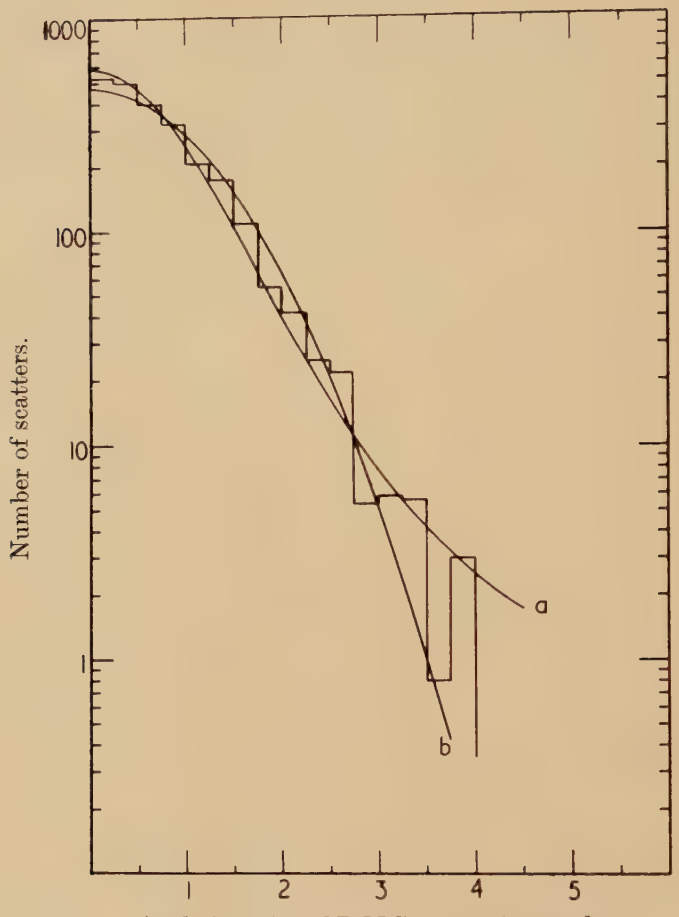

Composite histogram of all positrons.
(a) Molière distribution. (b) Gaussian distribution.

Table 2. Experimental and Theoretical Values of the Scattering Constant

Energy in MeV	0·95	1·01	1·45	1·53	2·50
K_{exp-}		20·4±0·6		20·0±0·4	25·9±0·6
K_{exp+}	18·8±0·15		19·1±0·5		22·2±0·5
$_{co}K_{exp-}$		19·9±0·6		19·1±0·4	24·1±0·6
$_{co}K_{exp+}$	18·6±0·5		18·3±0·5		21·0±0·5
$K_{Williams}$	24·5	25·2	24·4	25·1	24·3
$K_{Molière}$	24·2	24·9	24·1	24·8	24·0
$_{co}K_{Molière}$	21·8	22·5	21·7	22·4	21·6

NT4 and G5 respectively. No calculation of the effect of different charge has been included in the theoretical calculations of $K_{\text{Molière}}$.

These results show two features of interest. The experimental scattering constants appear to decrease with decreasing energy to values appreciably lower than those predicted theoretically. This has been earlier remarked by Hisdal (1952) and by Överös (1954) and the graph of the results of many workers (fig. 4) shows a possibility that this may be

Fig. 4

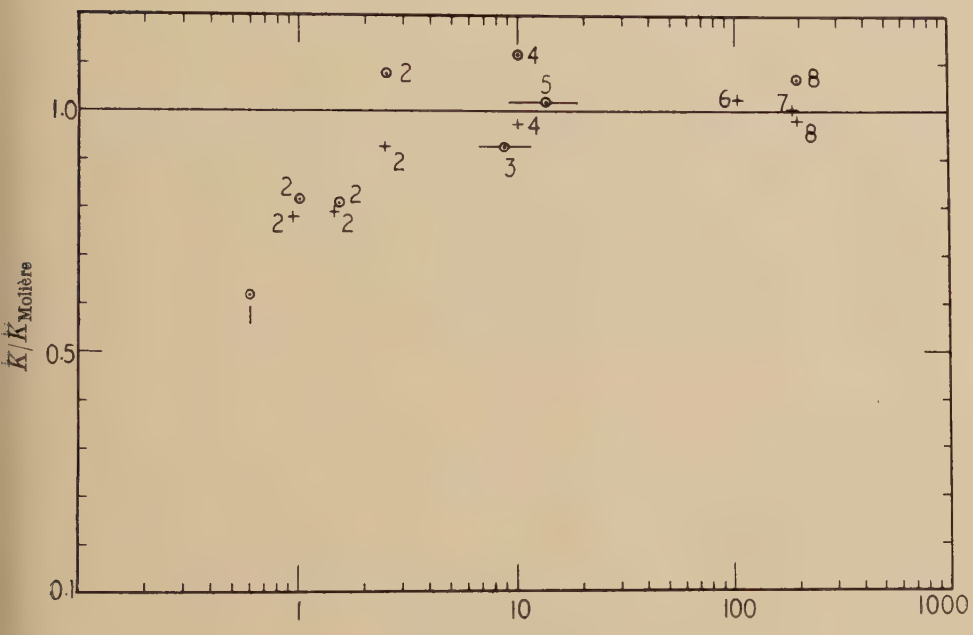

Variation of relative scattering constant with energy.
Results of many workers.
Ringed points, electrons. Crossed points, positrons.

1. Hisdal (1952)
2. Present work
3. Husain (1955)
4. Bosley and Hughes (1955)
5. Bosley and Muirhead (1953)
6. Gottstein *et al.* (1951)
7. Menon *et al.* (1951)
8. Corson (1951)

a real effect. However this impression given by fig. 4 rests largely on the results of the present workers and of Hisdal and Överös in all of which the low values may be caused by a combination of the 'thin chamber' effect discussed by Molière and the difficulty of following the more heavily scattered tracks biassing the results towards low values of the scattering constant. These considerations should not however affect the readings at 2·5 MeV where the absolute mean scattering angle was only of the order

of 4°. The second feature of interest arises from the comparison of the scattering of positrons and electrons shown in table 3.

Table 3. Electron : Positron Ratio of Scattering Constants

Energy in MeV	1·0	1·5	2·5
K_-/K_+	$1{\cdot}08 \pm 0{\cdot}04$	$1{\cdot}05 \pm 0{\cdot}04$	$1{\cdot}17 \pm 0{\cdot}04$
${}_{\text{co}}K_-/{}_{\text{co}}K_+$	$1{\cdot}08 \pm 0{\cdot}04$	$1{\cdot}04 \pm 0{\cdot}04$	$1{\cdot}14 \pm 0{\cdot}04$

The apparent difference at 1 and 1·5 MeV is largely attributable to the different emulsions used. This and other differences in conditions at these energies caused by availability of equipment made accurate comparisons invalid at these energies. At 2·5 MeV however considerable care was taken to obtain similar conditions and G5 emulsions were used for both particles. The difference found here is considerable and of similar order to those reported by other workers (Bosley and Hughes 1955, Corson 1951, Groetzinger, Humphrey and Ribe 1952). Furthermore as is shown by the ratio of cut-off scattering constants and by the separate histograms of the positron and electron distributions—fig. 5—this

Fig. 5

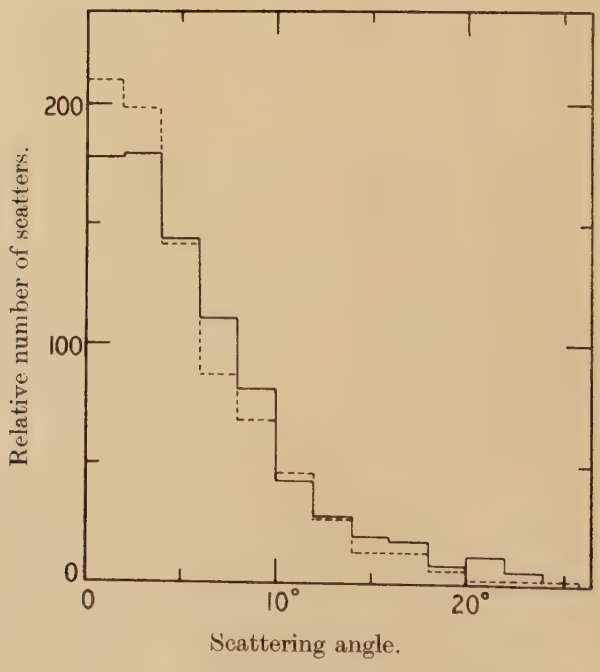

Histograms for 2·5 MeV particles.
Full line, electrons. Dotted line, positrons.

difference is not caused primarily by the increased frequency of large angle scatters in the case of electrons. At these energies single scatters of the order of 20° or more are easily visually observed and if these are ignored in calculating the scattering constants the same difference remains.

In addition to the readings recorded and discussed above a reading was taken of the angle between the tangent to each track and a 50-micron chord. The absolute mean value of this angle was found to be one-half of the absolute mean value of the angle between successive 50-micron chords within the statistical error. The ratio between the absolute mean values of this angle for electrons and positrons at 2·5 MEV was found to be $1{\cdot}15 \pm 0{\cdot}08$.

§ 5. Conclusions

The present work shows a larger difference between the multiple scattering of electrons and that of positrons at 2·5 MEV than is predicted by theory (Mohr 1954). Both the electron–positron difference at lower energies and the falling off of the scattering constant at low energies (for which $\beta^2 \ll 1$) require further investigation and it is hoped to examine both these points and to bridge the gap between the present work and that of Hisdal (1952) and of Överös (1954) by making measurements on both positron and electron plates exposed and developed under similar conditions to 0·75 MEV and 1·5 MEV particles.

Acknowledgments

The authors wish to acknowledge their indebtedness to Professor H. S. W. Massey, F.R.S., and Dr. E. H. S. Burhop for continued interest in the work described here. Thanks are due to the Microtron and Lens Spectrometer Groups in this department for the use of equipment and to Dr. A. A. Ahmed for the loan of two photographic plates.

The prior author wishes to point out that his contribution to this work was limited almost entirely to help with the exposure, processing and analysis of plates No. 1 and No. 2.

The latter author is indebted to Mr. H. S. Barlow, Head of the Physics and Mathematics Department, S.E. Essex Technical College, without whose assistance and encouragement this work would have been impossible.

References

Bosley, W., and Hughes, I. S., 1955, *Phil. Mag.*, **46**, 1281.
Bosley, W., and Muirhead, H., 1952, *Phil. Mag.*, **43**, 63.
Corson, D. R., 1951, *Phys. Rev.*, **84**, 605.
Fowler, P. H., 1950, *Phil. Mag.*, **41**, 169.
Gottstein, K., Menon, M. G. K., Mulvey, J. H., O'Ceallaigh, C., and Rochat, O., 1951, *Phil. Mag.*, **42**, 708.
Groetzinger, G., Humphrey, W., and Ribe, F. L., 1952, *Phys. Rev.*, **85**, 78.
Henderson, C., Heymann, F. F., and Jennings, R. E., 1953, *Proc. Phys. Soc.* B, **66**, 654.

Hisdal, E., 1952, *Phil. Mag.*, **43,** 790.
Husain, A., 1955, *Proc. Phys. Soc.* A, **68,** 45.
Menon, M. G. K., O'Ceallaigh, C., and Rochat, O., 1951, *Phil. Mag.*, **42,** 932.
Mohr, C. B. O., 1954, *Proc. Phys. Soc.* A, **67,** 730.
Molière, G., 1948, *Z. Naturforschung*, **3***A*, 78.
Överös, H., 1954, *Phil. Mag.*, **45,** 158.
Ross, M. A. S., and Zajac, B., 1949, *Nature, Lond.*, **164,** 311.
Rundle, G. P., Ellis, J., Griffith, T. C., and Tomlinson, H. S., 1954, *Proc. Phys. Soc.* B, **67,** 52.

XX. REVIEWS OF BOOKS

Proceedings of the International Conference of Theoretical Physics, Kyoto and Tokyo, 1953. (Tokyo : Science Council of Japan, 1954.) [Pp. xxviii+942.] $10.

This volume records the first purely scientific international conference to be held in Japan. Over one hundred speakers contributed with original papers or informal reviews of current fields of interest. The following topics were discussed :—

Field theory ; cosmic rays ; pions ; intermediate and strong coupling theory ; nuclear forces ; nuclear reactions ; shell structure and beta-decay ; polymers ; liquids ; transport phenomena ; irreversible processes ; general methods in statistical mechanics ; crystal dislocation ; molecules ; metals ; electron theory of intrinsic magnetization ; antiferro- and ferromagnetism ; magnetic resonance ; dielectrics ; colour centres ; liquid helium ; superconductivity.

J.M.Z.

Determination of Organic Structures by Physical Methods. Edited by E. A. Braude and F. C. Nachod. 22 Contributors. (New York : Academic Press Inc. ; London : Academic Books Ltd.) [Pp. xiii+810.] Price £5 7*s*. 0*d*.

This book should be warmly welcomed by organic chemists and by those physicists and physical chemists who specialize in the application of physical methods to the determination of the structures of molecules. The majority of such methods were originally developed by physicists for their own interest, and were only subsequently applied to organic compounds, and although often described individually in text-books, there was, until the appearance of this volume, no collective review of the principles involved in their application.

Part I contains two chapters dealing with methods based on the phase properties of molecules, and which are of importance in the determination of molecular size. Part II consists of five chapters describing the application of optical and magnetic measurements to the determination of general structural features. The third and longest part contains nine chapters dealing with methods which have contributed information about the fine structure of molecules, especially details of stereochemistry and electron distribution. The sixteen topics treated thus range from ' Phase Properties of Small Molecules ' through ' Optical Rotation ' and ' X-ray Diffraction ' to (somewhat surprisingly) ' Wave-Mechanical Theory '.

A glance at the list of contributors shows the authors' remark that " each is an active and acknowledged leader of research in the field he surveys " to be justified. The book contains nearly 2000 references to publications, and is well produced but expensive.

W. C.

Quantum Mechanics. Second edition. By L. I. Schiff. (McGraw-Hill Book Company, Inc.) [Pp. xii+417.] Price 47*s*.

The second edition of Professor Schiff's well-known book on quantum mechanics is welcome as this is one of the most useful books for introducing a serious student to the subject. The book is substantially the same as the first edition though several minor changes have been made improving the presentation and in places bringing it up to date.

The Laws of Nature. By R. E. Peierls. (George Allen and Unwin.) [Pp. 284.] Price 21 $.

Professor Peierls was led to write this book from recent experience in lecturing to various audiences on atomic energy. Among his listeners he found some who were infected with the same scientific curiosity that scientists possess, but who were without the background of knowledge that a quite general scientific training would have given them.

In this book, under its self explanatory title the author sets out to provide information for intelligent non specialists. He is right in thinking that the reading of it will come more easily to those who possess some elementary knowledge of Physics. But he is to be congratulated on the success of his labours. Indeed professional physicists will find in the book modes of presentation of well-known topics which may be useful also to them if they instruct the young in the class-room or find themselves like Professor Peierls facing a wider public. A. M. T.

BOOK NOTICES

Principles and Applications of Physics. By O. Blüh and J. D. Elder. (Harvard: University Press.) [Pp. 866.] Price 45*s*.

Progress in Biophysics and Biophysical Chemistry. Vol. 5. By J. A. V. Butler and J. T. Randall. (Pergamon Press.) [Pp. 231.] Price 55*s*.

Classical Electricity and Magnetism. By W. K. H. Panofsky and Melba Phillips. (Cambridge, Mass.: Addison-Wesley Publishing Co.) [Pp. 400.] Price $8.50.

Linear Feedback Analysis. By J. G. Thomason. (Pergamon Press.) [Pp. 355.] Price 55*s*.

Introduction to Electronic Analogue Computers. By C. A. A. Wass. (Pergamon Press.) [Pp. 231.] Price 22*s*.

The Unified System Concept of Nature. By S. T. Bornemisza. (New York: Vantage Press Inc.) [Pp. viii+137.] Price $3.

The Elements of Probability Theory and some of its Applications. By Harald Cramer. (London: Chapman and Hall.) [Pp. 281.] Price 56*s*.

Theories of Perception and the Concept of Structure. By F. H. Allport. (London: Chapman and Hall.) [Pp. xxii+709.] Price 64*s*.

University Physics. By F. W. Sears and M. W. Zemansky. (Cambridge, Mass.: Addison-Wesley Publishing Co., Inc.) [Pp. viii+1031.] Price $10.

[*The Editors do not hold themselves responsible for the views expressed by their correspondents.*]

Fig. 3

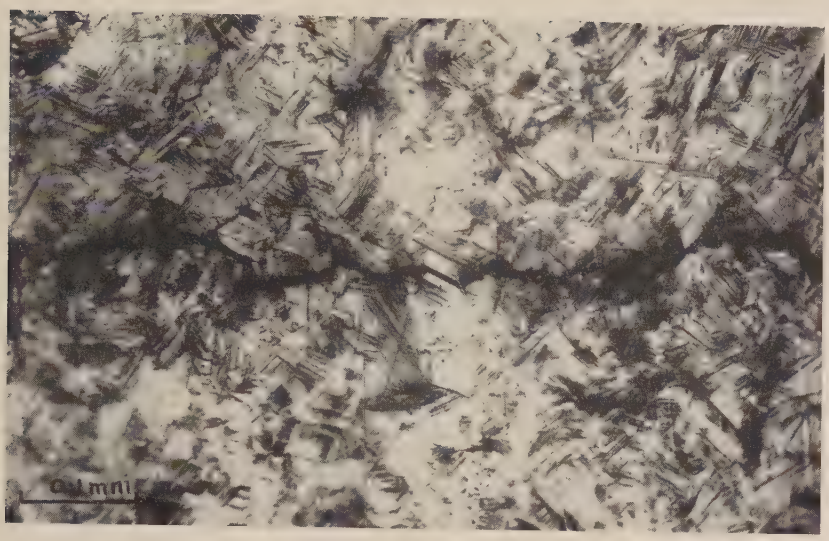

Centre of fatigue crack.

Fig. 4

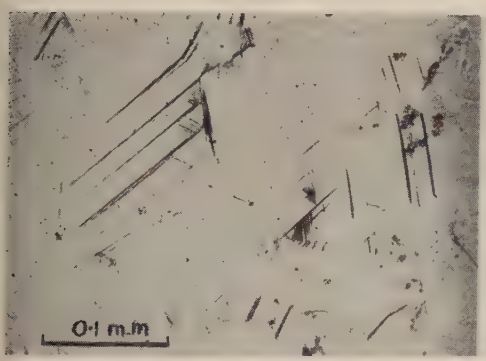

Fig. 5

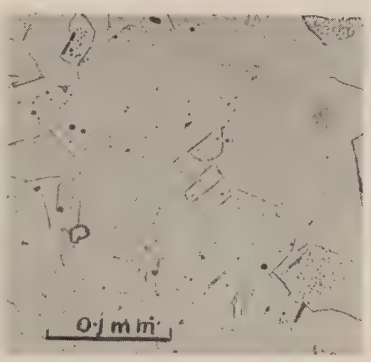

Fig. 6

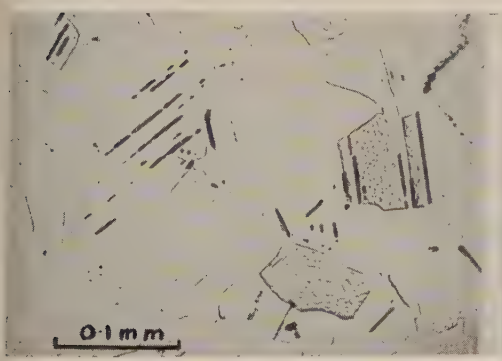

Fig. 7

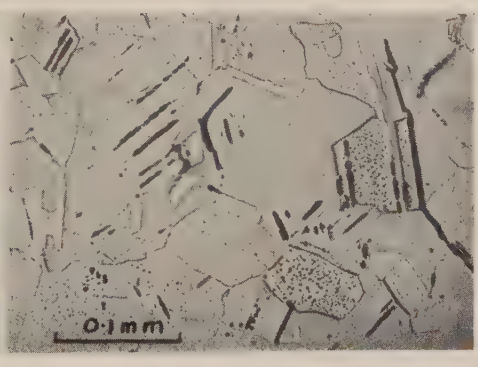

Figs. 4–7: Development of fatigue crack.
(4), after 7½% of life; (5), as (4), electropolished; (6). after 42% of life, electropolished; (7), after 77% of life, electropolished.

Fig. 8

Fig. 9

Fig. 10

Figs. 8–10: Another part of the same specimen.
(8), after 42%, electropolished; (9), after 77%, electropolished;
(10), at conclusion of test ($3{\cdot}6\times10^6$ cycles), not polished.

Fig. 11

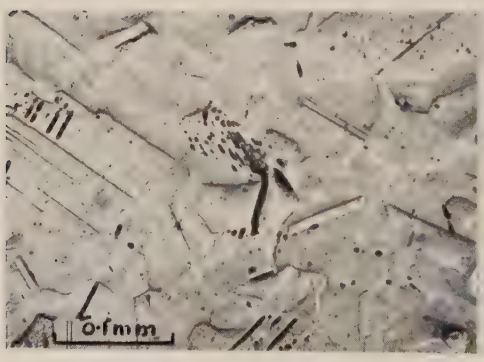

Fig. 12

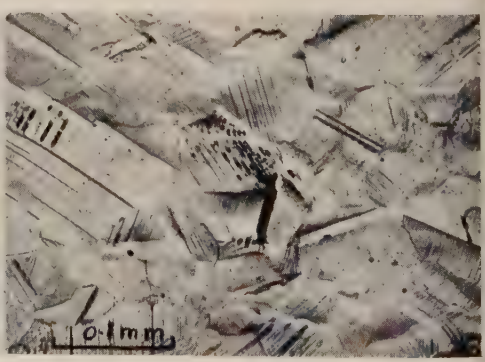

Figs. 11 and 12: Partially fatigued specimen, electropolished, before (11) and after (12) 5% tensile strain.

Fig. 13

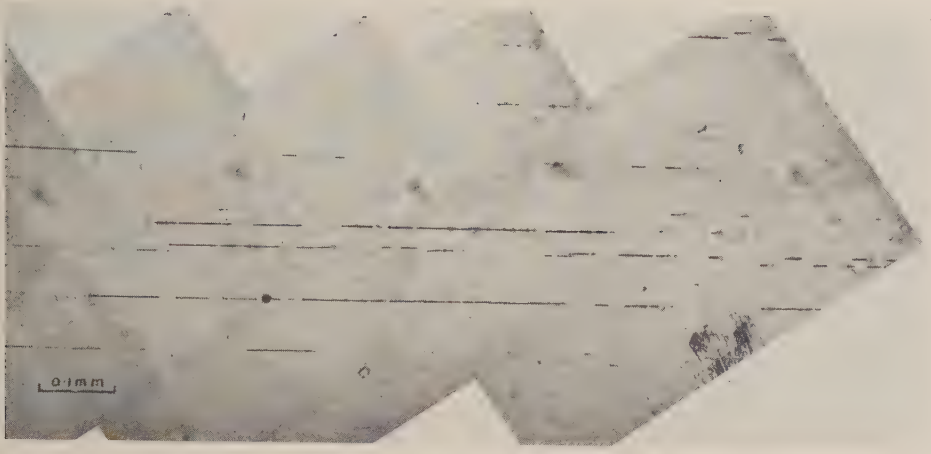

Fig. 14

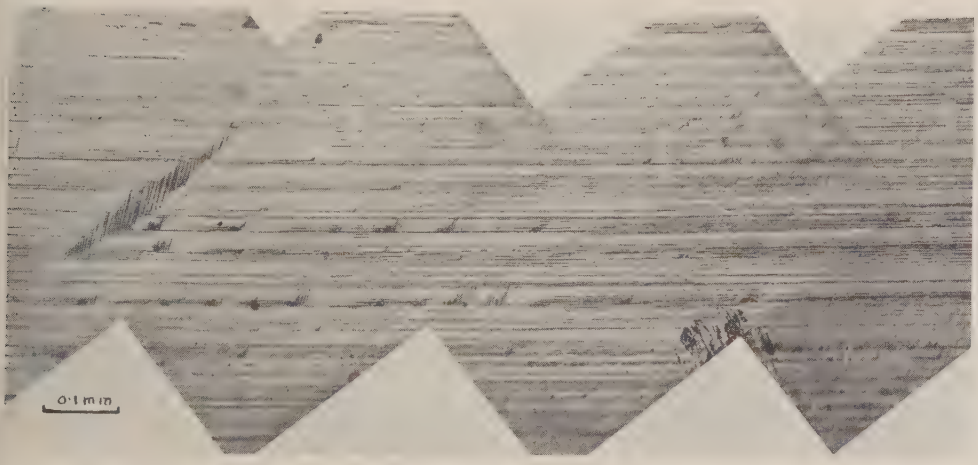

Fig. 15

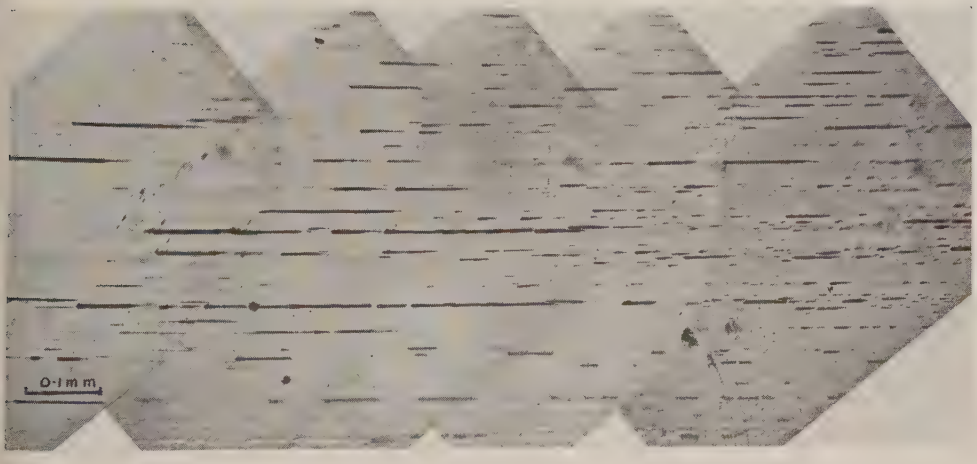

Figs. 13–15: Development of fatigue crack in single crystal.
(13), after 18%, electropolished; (14), after 36%; (15) as (14), but electropolished.

Fig. 16

Fig. 17

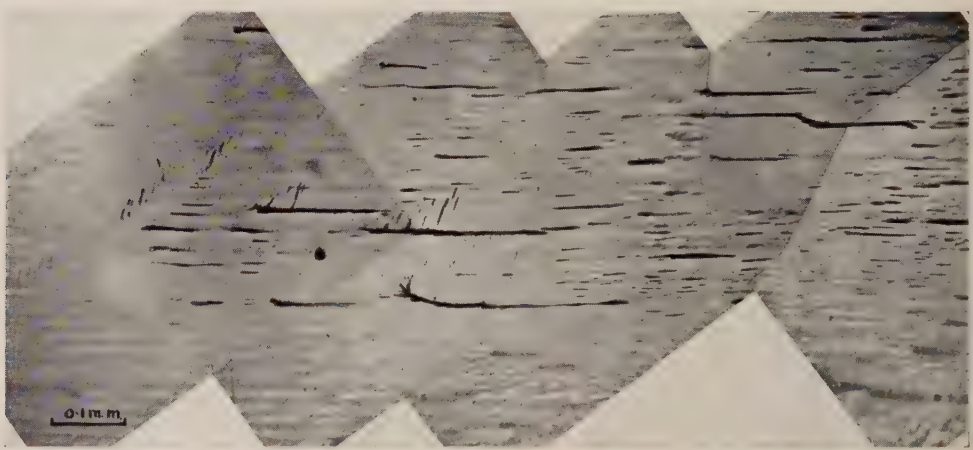

Fig. 18

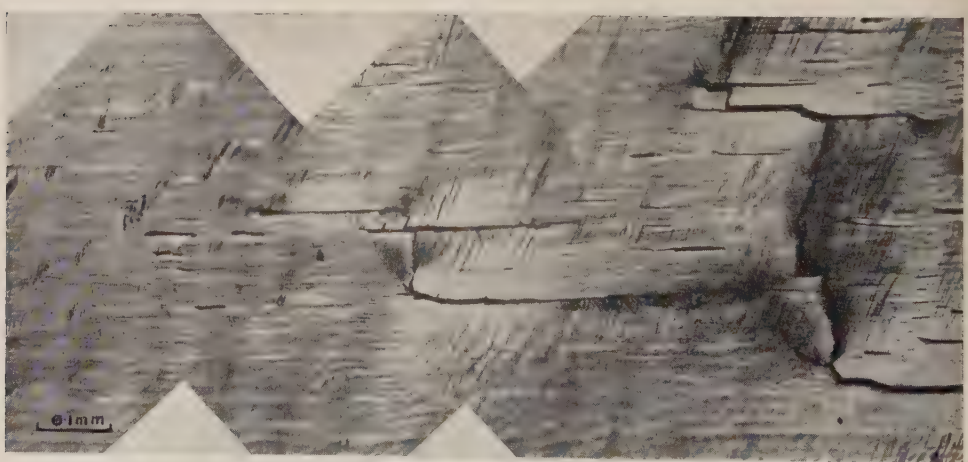

Figs. 16–18: Development of fatigue crack in single crystal. (16), after 54%, electropolished; (17), after 90%, electropolished; (18), at conclusion of test (10^6 cycles).

Fig. 19

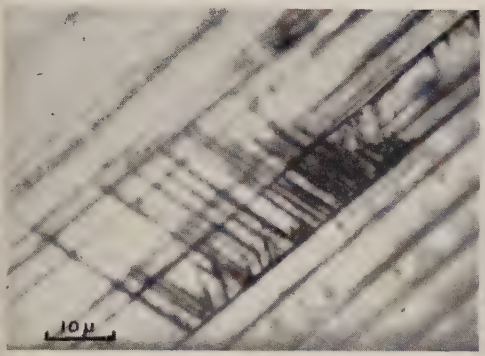

Fig. 20

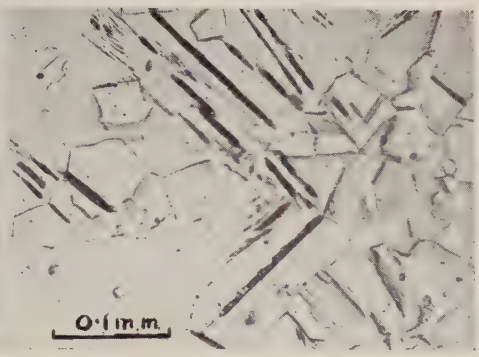

Fig. 21

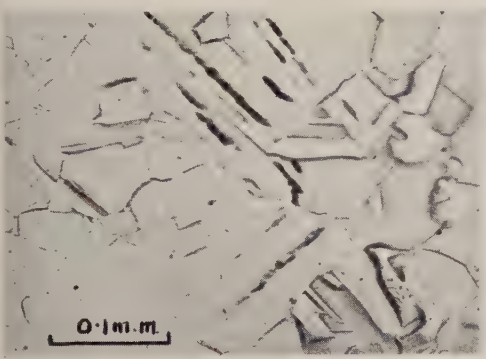

Fig. 22

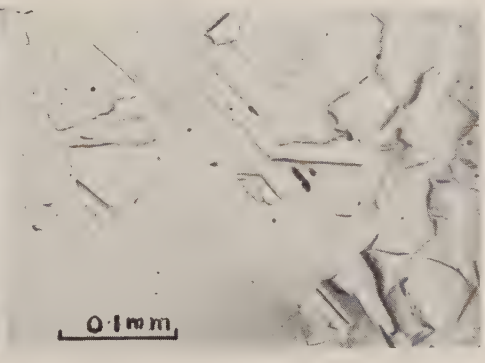

Fig. 23

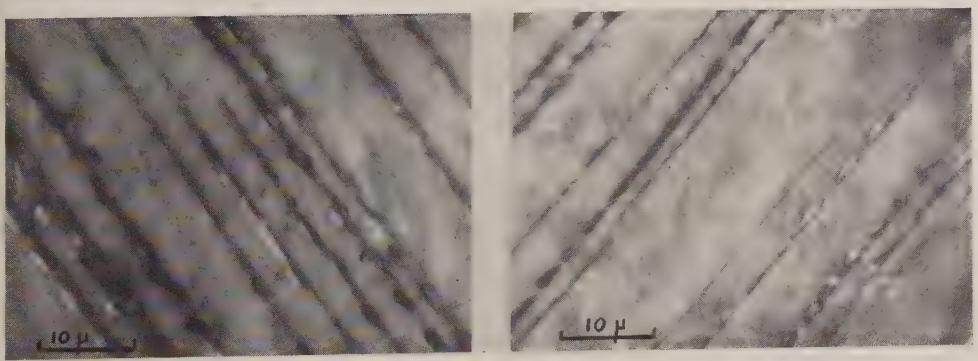

(*a*) (*b*)

Fig. 19: Slip on three planes: single crystal.

Figs. 20–22: Effect of deep electropolish on persistent slip bands.
(20), after removing 2μ from surface; (21), after removing 10μ; (22), after removing 18μ.

Figs. 23 (*a*) and (*b*): Material extruded from slip bands of fatigued single crystal.

Fig. 24

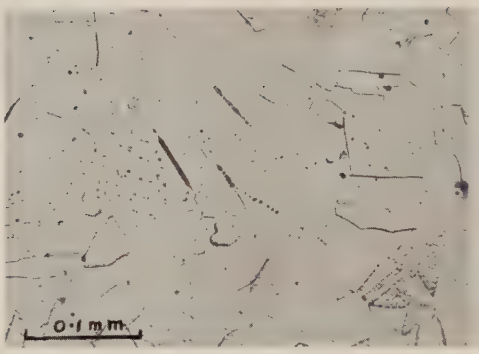

Fig. 25

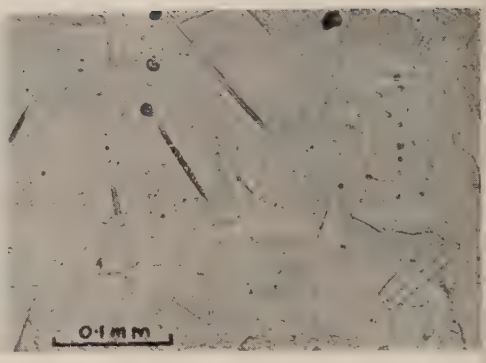

Fig. 26

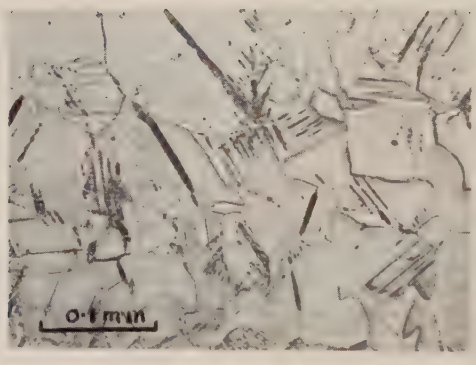

Fig. 27

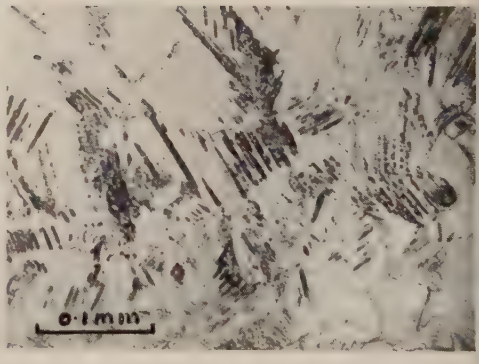

Figs. 24–27: Development of fatigue crack in specimen tested in nitrogen. (24), after about 1% of life in nitrogen: electropolished; (25), after 7½%, electropolished; (26), after 30%, electropolished; (27), after 73%, electropolished.

Fig. 3

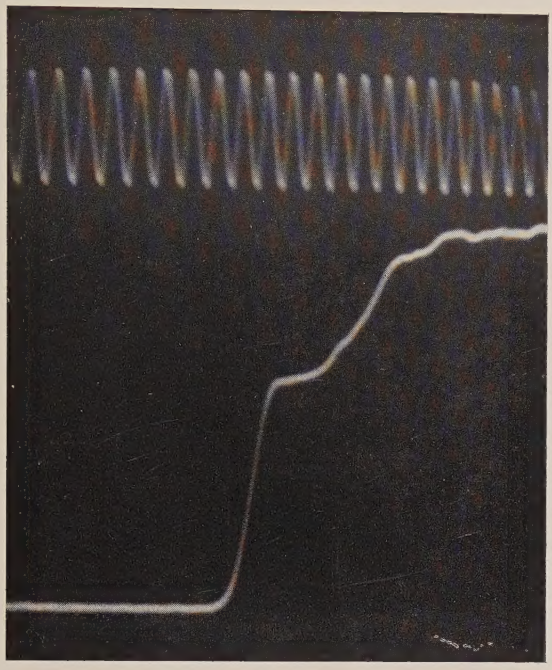

(*a*)

Oscillogram of a compression pulse in water. Upper trace: 100 kc/s timing wave. Lower trace: amplified voltage output from condenser microphone.

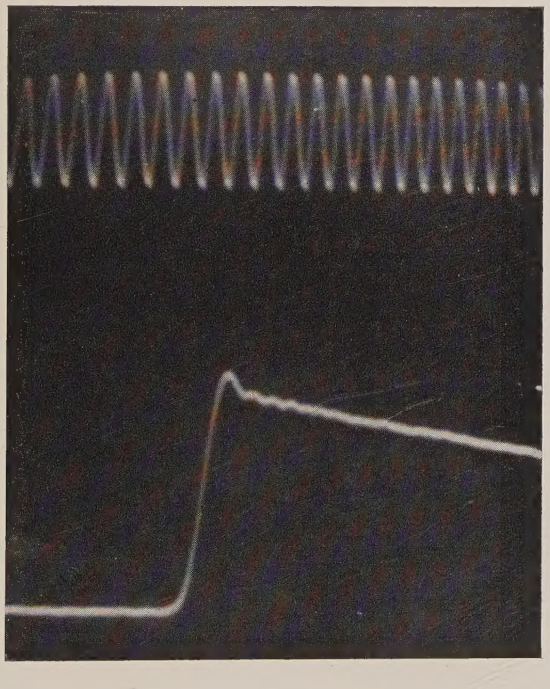

(*b*)

Oscillogram of pressure changes 1 cm below a free water surface during reflection of a compression pulse. Upper trace: 100 kc/s timing wave. Lower trace: amplified voltage output from condenser microphone.

Fig. 5

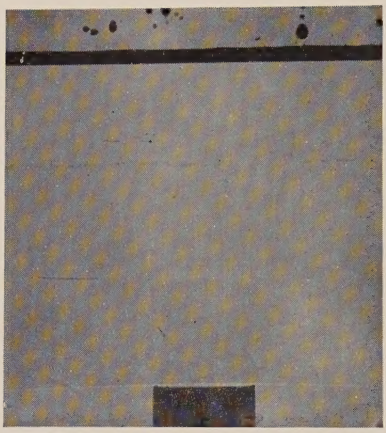

537 μsec

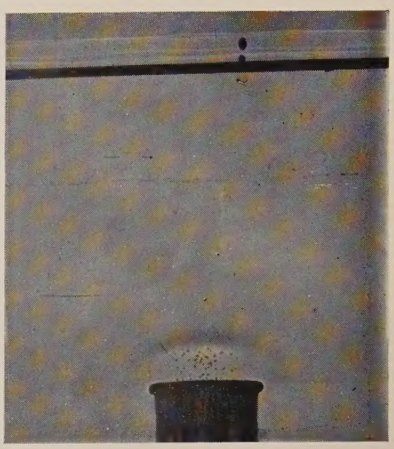

575 μsec

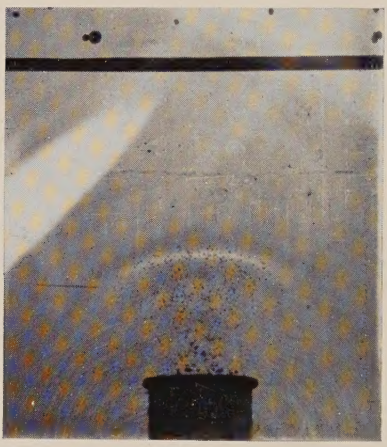

592 μsec

611 μsec

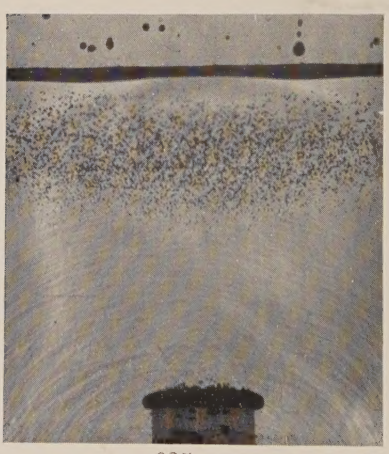

625 μsec

Spark shadowgraph of cavitation in water. The times shown below each photograph indicate the interval between the firing of the detonator and the emission of light from the spark gap.

Fig. 6

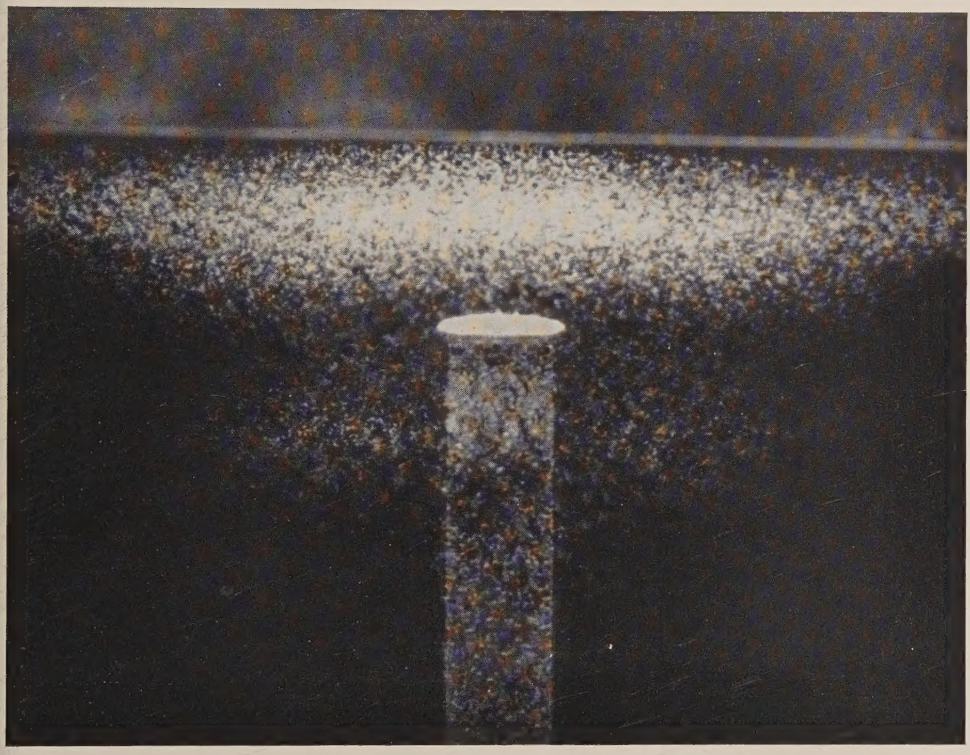

Cavitated zone produced in water by reflection of a compression wave at the free surface.